A BASIC STUDY OF THE IGNITION OF HYPERGOLIC LIQUID PROPELLANTS

FINAL REPORT - CONTRACT NAS7-438

BY

L. B. ZUNG AND B. P. BREEN

DYNAMIC SCIENCE, A DIVISION
OF MARSHALL INDUSTRIES
2400 MICHELSON DRIVE
IRVINE, CALIFORNIA

FEBRUARY 1970

NATIONAL AERONAUTICS AND SPACE ADMINISTRATION

A BASIC STUDY OF THE IGNITION OF HYPERGOLIC LIQUID PROPELLANTS

Final Report - Contract NAS7-438

February 12, 1970

By: L. B. Zung and B. P. Breen
DYNAMIC SCIENCE, a Division
of Marshall Industries
2400 Michelson Drive
Irvine, California 92664

For:

Jet Propulsion Laboratories
California Institute of Technology
4800 Oak Grove Drive
Pasadena, California 91103

NATIONAL AERONAUTICS AND SPACE ADMINISTRATION

FOREWORD

This report documents the work performed at Dynamic Science, a Division of Marshall Industries, under NASA Contract NAS7-438. This report details the work performed during the period 5 May 1968 - 5 May 1969.

Dr. Robert Levine of Office of Advanced Research and Technology (OART) was the program manager. Dr. Raymond Kushida of Jet Propulsion Laboratory was the Technical Manager.

The Quantitative Analysis of Reaction Products was performed by Aerojet General Analytical Laboratories, Azusa, California. Dr. D. L. Quick was the Chief Investigator.

NOTICE

SUMMARY

A research program covering three years has been conducted by Dynamic Science to study ignition of hypergolic liquid propellants. The published reports and presentations are:

Effect of Additives on the Ignition Delay Time of Hypergolic Propellants, by Stevens, M.R., Fisher, H.D., Weiss, H.G., and Breen, B.P.

A Basic Study on the Ignition of Hypergolic Liquid Propellants, Interim Final Report by Zung, L.B., Tkachenko, E. A., and Breen, B.P.

A Basic Study on the Ignition of Hypergolic Liquid Propellants, Final Report by Zung, L. B., and Breen, B. P.

Effect of Additives on the Ignition Delay Time of Hypergolic Propellants, by Stevens, M.R., Fisher, H.D., Weiss, H.G., and Breen, B.P. WSCI-67-22, presented at Western States/ Combustion Institute.

A Basic Study of Ignition of Hypergolic Liquid Propellants, by Zung, L.B., Breen, B. P. and Kushida, R., WSCI-68-43, presented at Western States/ Combustion Institute.

NASA/OART Space Storable Propulsion Technology Review, Lewis Research Center, June 1968.

Ignition studies of hydrazine and nitrogen tetroxide were first conducted with hydrazine at 0°C and -30°C. Experiments were conducted by first introducing hydrazine into the test cell. When hydrazine was at thermal equilibrium with its immediate environment, the test cell was evacuated to the limiting vapor pressure of hydrazine followed by the admission of vapor nitrogen tetroxide. Minimum oxidizer ignition threshold pressures and ignition delay times were measured for various oxidizer temperatures. It was found that solidification of the oxidizer inhibited the ignition process. The effect of additives were also evaluated. Hydrazine nitrate greatly decreased the minimum oxidizer ignition threshold pressure and the presence of a halogen increased the threshold pressures.

One of the drawbacks of these ignition studies is the certain amount of randomness exhibited by ignition delay measurements. This is partly due to the inability to control experimentally species diffusion and flow conditions when nitrogen

tetroxide is first admitted into the test cell. In order to remedy this difficulty an ignition burner based on the stagnation flow field was developed. Minimum concentrations of nitrogen dioxide that induce ignition were measured as a function of hydrazine temperature. Effects of flow Reynolds number, burner pressure, oxidizer temperature, and hydrazine water content were evaluated. For a 30% increase in flow velocity, it was observed that the threshold concentration of nitrogen dioxide increases by about 20%.

It was found that for hydrazine temperature under approximately $310^{o}K$, the vapor pressure of hydrazine was not high enough to sustain a vapor phase ignition. Reactions between nitrogen dioxide and liquid hydrazine were significant as evidenced by foaming and bubbling observed on the liquid surface. Heat release associated with these reactions gradually raised the hydrazine temperature which in turn led to a vapor phase ignition. Measurements also show that for hydrazine temperatures below $310^{o}K$, the threshold nitrogen dioxide concentration assumed a constant value. This could be partly explained by the fact that the rate of diffusion of nitrogen dioxide played a more dominant factor in the vapor-liquid phase reaction. Foaming and bubbling on the liquid surface were less significant at higher temperatures. For hydrazine near its boiling point, it was observed that ignition could take place before the introduction of nitrogen dioxide mixture. This could be due either to hydrazine autodecomposition on the stainless surfaces or reaction with the residual atmospheric oxygen in the burner.

Based on similar experimental techniques, ignition of liquid diborane and diluted (with helium) oxygen difluoride were studied. The results were less successful because of the difficulties encountered to maintain sufficient liquid diborane within the diborane cup.

A theoretical study to understand the ignition of liquid fuel was carried out. Based on the stagnation flow field, the governing partial differential equations were reduced to a set of ordinary differential equations. The species concentrations and temperature profiles of the nonreactive flows were used to describe the rate of reaction prior to ignition. Information based on the effect of liquid temperature on the reaction rate can indicate more meaningful temperature ranges where liquid surface reaction is important.

Highly diluted vapor phase reactions of nitrogen tetroxide with hydrazine unsymmetrical dimethylhydrazine and monomethylhydrazine clarify the formation of certain explosive solid intermediates. Reaction products of hydrazine/nitrogen tetroxide and monomethylhydrazine/nitrogen tetroxide both show that an excess of oxidizer favors ammonium nitrate formation while an excess fuel favors the formation of hydrazinium nitrate and monomethylhydrazinium nitrate respectively. In the case of unsymmetrical dimethylhydrazine, both fuel-rich and oxidizer-rich conditions gave the same salt, ammonium nitrate. Main gaseous products were found to be N_2O, NO, N_2, and H_2O.

TABLE OF CONTENTS

INTRODUCTION

Experience (Ref. 1 & 2) with altitude ignition of hypergolic bipropellants shows that, on occasion, damaging high amplitude pressure waves develop. A sufficient understanding of the ignition processes for these propellant combinations must be gained in order to eliminate or suppress large transient overpressures. Research work covering various phases of the hypergolic propellant phenomena has been carried out. Emphasis has been placed on hydrazine/nitrogen tetroxide* systems.

The first phase of this research program was to qualitively determine chemical interactions during the transient preignition period (Ref. 3 & 4). Specifically, reaction characteristics between solid and vapor phases were sought. Experiments were carried out during this phase to define ignition thresholds, ignition delay times, and intermediate reaction characteristics of condensed phase reactants. These experiments were qualitative in nature and were intended to establish orders of importance of preignition chemical effects. The first series of experiments determined the ignition characteristics of solid hydrazine at 0°C and -30°C, with nitrogen tetroxide vapor at temperature ranging from 25°C to 100°C. The second series of experiments characterized the reaction when the oxidizer was initially at the low temperature (-30°C).

The chemistry of nitrogen tetroxide/hydrazine base (N_2H_4, MMH, UDMH, A-50) fuels is undoubtedly complex both from the standpoint of kinetics and of the diversity of reaction products. In addition, the reaction rates in the gaseous or liquid phase are very rapid (ignition delay times of the order of microseconds (Ref. 5) to milliseconds (Ref. 6) depending on the method of measurements.) Preignition reactions in the vapor phase yield gaseous as well as condensed reaction products (Ref. 7) and it was concluded by the same authors that the ignition process proceeds by a thermal rather than a free radical mechanism. Reaction products were also studied with propellant temperatures initially at the triple point of nitrogen tetroxide (-11.2°C) and at room temperature (21°C) (Ref. 8). MMH nitrates and hydrazine nitrate were observed to be the major residue component for MMH/nitrogen tetroxide and hydrazine or A-50/nitrogen tetroxide reactions. Hydrazoic acid and ozides were identified by Dauerman and coworkers (Ref. 9) when mixture of nitrogen

*In the text, nitrogen tetroxide or nitrogen dioxide represents the equilibrium mixture of nitrogen tetroxide and nitrogen dioxide.

tetroxide condensed (at liquid nitrogen temperatures) onto hydrazine or vice versa and were allowed to warm up slowly. It is noteworthy that the temperatures prevalent in this work are far below those to be expected at rocket engine space start conditions (Ref. 1). Experiments were also carried out with nitrogen tetroxide/hydrazine system using a two-dimensional plastic combustion chamber (Ref. 10). Residue accumulated on the chamber wall was in sufficient quantity to make possible chemical analysis. By means of infrared method, the major residue component was identified as hydrazine nitrate. Based on thermochemical determinations, it appears that the reaction intermediates play an important role in severe ignition pressure spiking (Ref. 11).

Under this research program work concerning preignition stoichiometry for nitrogen/tetroxide hydrazine base fuels have also been studied, (Ref. 12 & 13). Gas phase reactions at low temperatures and low concentrations (diluted with helium so as to produce an isothermal environment) clarified whether explosive solid intermediates such as NH_4, NO_3, and $N_2H_5NO_3$ were formed. Further monitoring the hydrazine/nitrogen tetroxide reactions, it has helped to resolve the question of the conditions under which either the NH_4NO_3 or the $N_2H_5NO_3$ has been the predominant solid intermediate. Quantitative results from these preignition chemistry studies have also been used as inputs to a certain mathematical space start model(Ref.14). The reason for this is that any clarification of the paths of formation of detonable and sensitizing substances, together with the associated preignition heat release and gas formation, will help predict chamber pressurization and the chemical species present in the chamber at ignition. Similar studies have also been carried out for unsymmetrical dimethyl-hydrazine/nitrogen tetroxide and monomethyl-hydrazine/nitrogen tetroxide. The results of these highly diluted vapor phase reactions are discussed in detail in the following section of this report.

Hypergolic propellant ignition involves a complex interrelationship of chemical and physical phenomena. During rocket engine ignition the rates of preignition reactions, the chemical nature of preignition products, and the associated heat release are closely coupled with physical transport properties such as heat and mass transfer. In order to help unravel the relative significance of these basic processes on hypergolic ignition, it becomes necessary

to isolate, and study separately and under controlled conditions, important physical factors.

One of the drawbacks of the ignition studies conducted during the first phase of this research program (Ref. 3 & 4)was certain randomness exhibited by ignition delay measurements. This was partly due to the inability to control, experimentally species diffusion and flow conditions when nitrogen tetroxide was first admitted into the test cell. In order to remedy this difficulty, an ignition burner based on the stagnation flow field was developed. By introducing the oxidizer gas to flow over liquid fuel in a direction perpendicular to the fuel surface, the uncertainties of fluid dynamics are removed and each of the transport rate processes leading to ignition were studied individually, so as to integrate combustion theory with that of chemical kinetics. Based on this technique, experimental parameters which are easily controlled are (i) fuel temperature, (ii) oxidizer temperature, (iii) oxidizer concentration, (iv) burner pressure, and (v) oxidizer flow velocity. Ignition of liquid hydrazine and vapor nitrogen tetroxide was studied using such a burner (Ref. 13, 14, 15). In addition to evaluating the significance of physical transport properties, reactions between nitrogen tetroxide on the liquid hydrazine surface were also characterized. This vapor-liquid reaction has significant effects on engine starts and engine problems. The bubbles and foaming on the liquid surface formed a diffusion barrier which greatly reduced the rate of fuel vaporization and thus has a much longer ignition delay time. This can cause unexpected difficulties associated with space start problems. The reaction intermediates formed on the surface dissolved in the fuel droplets which in turn can serve as sources for detonation waves.

Similar experimental technique has also been used to study the ignition mechanisms of liquid diborane and vapor oxygen difluoride. This study, which is discussed in this report, was less successful due to the cryogenic nature of the propellant.

To understand the ignition phenomena in more detail, an analytical study has been carried out based on the stagnation flow field. The purpose of this study is to define propellant temperature ranges where vapor phase reaction is dominant. Based on the similarity flow field, the governing partial

equations were reduced to a set of ordinary differential equations. Realizing the fact that prior to ignition the species concentrations and gas temperatures do not vary much from the nonreactive flows, the nonreactive solutions were used to describe the rate of reaction. Information based on the effect of liquid temperature on the reaction rate can indicate more meaningful temperature ranges where liquid surface reaction is important.

QUANTITATIVE ANALYSIS OF VAPOR PHASE REACTION PRODUCTS OF UNSYMMETRICAL DIMETHYLHYDRAZINE AND MONOMETHYLHYDRAZINE WITH NITROGEN DIOXIDE

Introduction

The complexity of a hypergolic propellant in general, and that of the nitrogen dioxide/hydrazine base fuels in particular, necessitates the study of preignition products of such systems. Distribution of the products are required in order to assess the importance of various possible reactions. In order to examine products formed under preignition conditions, dilute mixtures of fuel and oxidizer were introduced into a batch reactor. The main reason for the dilution was to keep the temperature rise small and hence obtain a nearly isothermal reaction. The reactor and sampling systems were designed and built to provide (i) inert surfaces, (ii) rapid mixing of reactants, and (iii) demountable vacuum tight fittings for easy removal of solid or gaseous reaction products. Reactions of hydrazine and nitrogen dioxide were previously studied (Ref. 1) at various mole ratios. Reactions of unsymmetrical dimethylhydrazine and monomethylhydrazine with nitrogen dioxide, at various mole ratios, were carried out at 25°C.

Experimental Apparatus

Reaction and Sampling System. - The reaction chamber, trap, and holding bulb (Fig. 1 and 2) used in this study were fabricated of pyrex glass. A glass system was used in preference to metal because of the known catalytic effects of certain metals (e.g., Fe^{+++}, Cr^{+++}, Al^{+++}, Cu^{++}, Ni^{++}) upon hydrazine family derivatives. All control valves were Fisher and Porter 4mm quick opening Teflon plug and glass seats. Connections between reaction system elements were of glass and butyl O-ring vacuum connections. The relative volumes of the holding bulbs and the reaction chamber allowed a one to seven expansion and mixing of the reactants in the reaction chamber.

A CEC 21-130 mass spectrometer was used for all gas analysis. One feature of this instrument is a low volume fractionation and sample introduction system placed in parallel with the conventional sampling inlet system. The low volume inlet, because of its low surface area ($\approx$ 1/100 of that of the conventional system) and adjustable leak into ion source, is invaluable when surface effects, temperature, or minute sample size preclude the conventional approach.

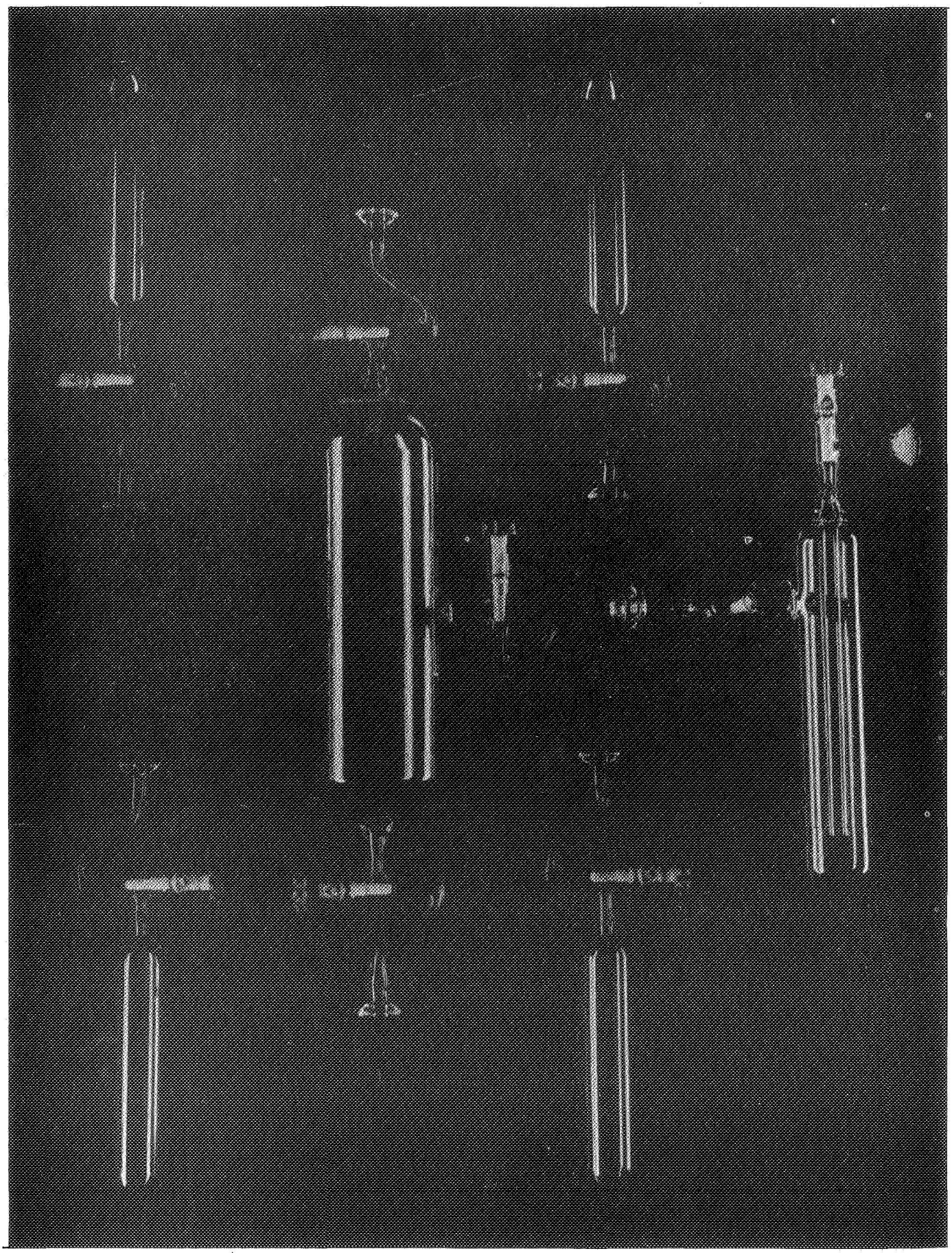

Figure 1. Reaction Chamber, Trap, and Holding Bulb.

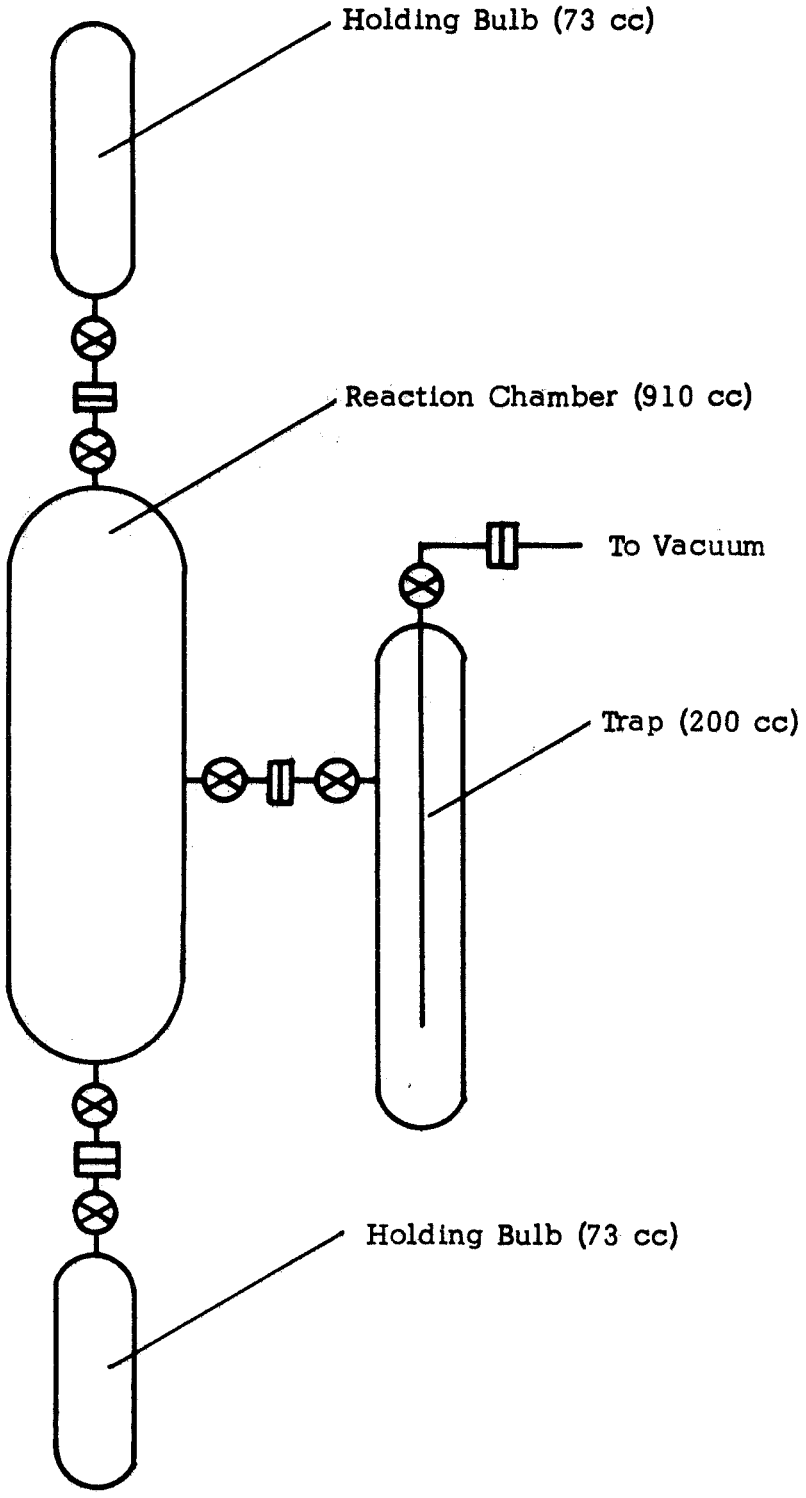

Note: Volume between bulbs = 7.5 ml

Figure 2. Reactor Assembly.

Infrared analysis of solid and gaseous products were studied using a Beckman IR-4 and PE 237 instrument. Vapor spectra were obtained using a 10 cm gas cell fitted with silver chloride windows. Infrared spectra of the solid products, labeled 1 through 10 with each representing five replicas, were taken in the form of KBr pellets.

Experimental Procedures

Known quantities of liquid UDMH (unsymmetrical dimethylhydrazine) or MMH (monomethylhydrazine) fuel were measured by a microliter MicroTek vacuum pipet and cryogenically transferred into a holding bulb. Nitrogen dioxide was blended by a pressure-volume relationship at pressure below 22 mm using a Wallace & Tiernan Model FA 145 differential gauge (calibrated in 0.2 mm div). A correction was calculated for $N_2O_4 \rightleftarrows 2\ NO_2$ dissociation at 25°C for example:

2 mm pressure - 96.7 % dissociated
4 mm pressure - 93.8 % dissociated
6 mm pressure - 91.1 % dissociated
8 mm pressure - 88.6 % dissociated
10 mm pressure - 86.3 % dissociated
12 mm pressure - 84.2 % dissociated
14 mm pressure - 82.2 % dissociated
16 mm pressure - 80.4 % dissociated
18 mm pressure - 78.7 % dissociated

Holding bulbs containing the reactants were pressurized to 600 mm with helium, yielding concentrations of from 0.4 to 2.5 mole-%. After equilibrating at 25°C, the reactants were expanded into the evacuated reaction chamber maintained at 25°C.

The runs were divided into sets of five; each run of a set had the same fuel-to-oxidizer ratio. Five replicas of each reaction served to (i) check repeatability of reaction product concentration, and (ii) accumulate solid residue for infrared analysis. At time (t), a gas aliquot of the reaction product was measured and transferred to the mass spectrometer for analysis. Gaseous reaction products were also analyzed by infrared spectrophotometry.

Solid residue from each set of reactions was accumulated by solvent extraction (absolute methanol) and weighed before submitting for infrared analysis. The ratios of fuel-to-oxidizer provide a basis for comparing the data for respective runs. The following series of tests were performed during this study.

Fuel	Oxidizer	Fuel/Oxidizer Mole Ratio
UDMH	NO_2	1/6
UDMH	"	1/2
UDMH	"	1/1
UDMH	"	5/2
UDMH	"	2/1
MMH	"	1/5
MMH	"	5/8
MMH	"	5/4
MMH	"	5/2
MMH	"	15/8

Results and Discussions

Fifty low pressure nonignition vapor phase reactions of UDMH and MMH with NO_2 at 25°C were effected. The absolute weight and the mole percent of the reactants are summarized in Table I.

Infrared Analysis. -

Solids from UDMH/NO_2 Reactions: The infrared spectra of solids #1*, #2, and #3 (Figs. 12, 13, 14) were obtained from reactions in which the oxidizer was very rich, rich, and equimolar. Spectra are complicated by heavy background absorption in the 8 to 10 μ region, indicating varieties of C - O and N - O possibilities. A heavy NH_4 band at 7.1 μ indicates the principal constituent is ammonium nitrate.

In both the fuel very rich (solid #10) and fuel rich (solid #7) reactions (Figs. 15, 16, 17, 18) ammonium nitrate appears to be the major constituent.

*The IR spectrum of #1 is not included. It was of poor quality with little absorption discernible above background noise.

TABLE I

NON-IGNITION VAPOR PHASE REACTIONS OF UNSYMMETRICAL DIMETHYLHYDRAZINE AND MONOMETHYLHYDRAZINE WITH NITROGEN DIOXIDE AT 25° C

Run No.	Reactants (mg)			Reactants (mole-%)*		
	NO_2	UDMH	MMH	NO_2	UDMH	MMH
1	5.3	1.0	-	2.5	0.4	-
2	5.3	1.0	-	2.5	0.4	-
3	5.3	1.0	-	2.5	0.4	-
4	5.1	1.0	-	2.4	0.4	-
5	5.1	1.0	-	2.4	0.4	-
6	1.7	1.0	-	0.8	0.4	-
7	1.7	1.0	-	0.8	0.4	-
8	1.7	1.0	-	0.8	0.4	-
9	1.7	1.0	-	0.8	0.4	-
10	1.7	1.0	-	0.8	0.4	-
11	1.7	2.0	-	0.8	0.8	-
12	1.7	2.0	-	0.8	0.8	-
13	1.7	2.0	-	0.8	0.8	-
14	1.7	2.0	-	0.8	0.8	-
15	1.7	2.0	-	0.8	0.8	-
16	5.3	-	1.0	2.5	-	0.5
17	5.3	-	1.0	2.5	-	0.5
18	5.3	-	1.0	2.5	-	0.5
19	5.1	-	1.0	2.4	-	0.5
20	5.1	-	1.0	2.4	-	0.5
21	1.7	-	1.0	0.8	-	0.5
22	1.7	-	1.0	0.8	-	0.5
23	1.7	-	1.0	0.8	-	0.5
24	1.7	-	1.0	0.8	-	0.5
25	1.7	-	1.0	0.8	-	0.5
26	1.7	-	2.0	0.8	-	1.0
27	1.7	-	2.0	0.8	-	1.0
28	1.7	-	2.0	0.8	-	1.0

*Diluted with helium

TABLE I (Continued)

Run No.	Reactants (mg)			Reactants (mole-%)*		
	NO_2	UDMH	MMH	NO_2	UDMH	MMH
29	1.7	-	2.0	0.8	-	1.0
30	1.7	-	2.0	0.8	-	1.0
31	1.7	4.0	-	0.8	1.6	-
32	1.7	4.0	-	0.8	1.6	-
33	1.7	4.0	-	0.8	1.6	-
34	1.7	4.0	-	0.8	1.6	-
35	1.7	4.0	-	0.8	1.6	-
36	1.7	-	3.0	0.8	-	1.5
37	1.7	-	3.0	0.8	-	1.5
38	1.7	-	3.0	0.8	-	1.5
39	1.7	-	3.0	0.8	-	1.5
40	1.7	-	3.0	0.8	-	1.5
41	1.7	-	4.0	0.8	-	2.0
42	1.7	-	4.0	0.8	-	2.0
43	1.7	-	4.0	0.8	-	2.0
44	1.7	-	4.0	0.8	-	2.0
45	1.7	-	4.0	0.8	-	2.0
46	1.7	5.0	-	0.8	2.0	-
47	1.7	5.0	-	0.8	2.0	-
48	1.7	5.0	-	0.8	2.0	-
49	1.7	5.0	-	0.8	2.0	-
50	1.7	5.0	-	0.8	2.0	-

*Diluted with helium

Additional sharp singlets (solid #7) appearing between 3.48 and 3.52 μ indicate minor amounts of CH-bearing constituents which do not contain the NO_2 group. Unsymmetrical dimethylhydrazine nitrate was not detected in any of the UDMH/NO_2 solid reaction products.

Solids from MMH/NO_2 Reactions: The IR spectra of solids #4, #5, and #6 (Fig. 19-24) were obtained from oxidizer very rich, oxidizer rich, and equimolar reactions. The spectra are all quite similar. They are significantly different than monomethylhydrazine nitrate reference spectra owing to the absence of four characteristic singlets between 9 and 11μ. Comparisons with reference spectra suggest that solids #4, #5, and #6 are mixtures of ammonium nitrate and methyl ammonium nitrate, $CH_3NH_3NO_3$.

Solid #8 (Figs. 25 & 26) fuel rich reaction is very similar to solids #4, #5, and #6. However, spectra from solid #9 (Figs. 27 and 28 fuel very rich) compares very well with that of a reference standard of monomethyl hydrazine nitrate, $CH_3NHNH_3\ NO_3^{\theta}$. It is in combination with another constituent indicated by a sharp singlet at 6.28 μ, which exhibits a less intense shoulder at 6.33 μ. These latter signals are as yet unidentified but probably indicate minor amounts of a covalent nitrite (R-O-NO), nitrate (R-O-NO_2), or imine (R=N-).

Gaseous Products from UDMH/NO_2 Reactions: Spectrum #1 (Figs. 29 and 30, oxidizer very rich) indicates 2 $NO_2 \rightleftarrows N_2O_4$ (6.16 and 6.27 μ) as the principle constituent. Minor amounts of N_2O are apparent at 4.47 and 4.53 μ. The spectrum is complicated by the appearance of a broadened band at 9.31 μ, which exhibits a shoulder at 9.8μ. A sharp, less intense singlet at 10.20 μ appears related. These bands have not been assigned although they appear in the general region of C-O and C-N stretch vibrations.

For spectrum #2 (Figs. 31 and 32 oxidizer rich) and #7 (Figs. 33 and 34 fuel rich) N_2O is the only constituent indicated positively (N-N stretch at 4.50 and 4.55 μ). The spectrum of #3 (Figs. 35 and 36) indicates N_2O as principle constituent (4.49 and 4.54 μ) with $NO_2 \rightleftarrows N_2O_4$ suggested as a minor, about 1/4 the concentration of NO_2 (N-O stretch vibrations 6.16 and 6.27 μ).

Gaseous Products from MMH/NO_2 Reactions: Spectrum #4 (Figs. 37 and 38, oxidizer very rich) indicates N_2O is a major constituent (4.49 and 4.54 μ) as is 2 $NO_2 \rightleftarrows N_2O_4$ (6.16 and 6.27 μ). More intense bands, attributable to another principal constituent, appear as follows: 3.4 to 3.5 μ multiplet with

dominant singlet at 3.44 μ ; 5.99, 6.60 μ singlets; 7.73 μ sharp singlet; 9.7 to 9.9 μ multiplet with dominant singlet at 9.80 μ; 11.6 to 11.9 μ multiplet with dominant singlet at 11.69 μ. These data compare well with the spectrum of methyl nitrate, CH_3ONO_2.

Spectra #5 (Figs. 39 and 40 oxidizer rich) and #8 (Figs. 41 and 42 fuel rich) show N_2O as the only constituent indicated positively. In spectrum #8 a broadened band at 3.38 μ and two minute sharp singlets at 3.54 and 3.61 μ suggest a minor constituent, as yet not identified.

The spectrum of #6 (Figs. 43 and 44) exhibited no discernable signals above background noise that are attributable to reaction products. A broad unresolved band is evident at 7.8 μ, but its profile is not characteristic of any vapor species. Consequently it is attributed to a residue on the AgCl cell windows and appears to some extent in all vapor spectra.

Examination of the IR spectral data indicates the reaction products from the low pressure nonignition vapor phase reaction of UDMH, MMH, and NO_2 were for the most part oxides of nitrogen and nitrates (i.e., N_2O, NO, NO_3). Reaction products from MMH/NO_2 were similar to those obtained previously (Ref. 12). (Reaction of N_2H_4 with NO_2). An excess of fuel favored $N_2H_5NO_3$ formation:

$$3\ N_2H_4(\text{excess}) + 2\ N_2O_4 \rightarrow 2\ N_2H_5NO_3 + H_2O + N_2O + N_2,$$

while an excess of oxidizer favored NH_4NO_3 formation:

$$N_2H_4 + N_2O_4(\text{excess} \rightarrow NH_4NO_3.$$

In a similar manner an excess of MMH favored formation of salt, $N_2H_4CH_3NO_3$, while an excess of oxidizer favored production of ammonium nitrate and methyl ammonium nitrate. In the case of UDMH, both fuel rich and oxidizer rich conditions gave the same salt, ammonium nitrate.

The mass spectral data of gaseous reaction products is consistent with the infrared interpretations. The major components detected by mass spectrometer gaseous reaction products with both UDMH and MMH were various nitrogen oxides.

As the stoichiometry with UDMH becomes more and more fuel-rich, the predominant species in the gas phase shift from NO_2 to NO to N_2O. At the fuel

TABLE II

GASEOUS AND SOLID REACTION PRODUCTS FROM NON-IGNITION VAPOR PHASE REACTIONS OF UDMH With NO_2

Run Series	#1 to #5	#6 to #10	#11 to #15
Gaseous Products Milligram per Run			
NO_2	1.50	0.09	0.01
N_2O	0.03	0.03	0.25
CO_2	0.02	0.02	0.02
Methane	0.0	0.0	0.0
NO	0.89	0.51	1.16
N_2	-	-	0.06
H_2O	0.03	0.03	0.82
Total Milligrams of Gaseous Products Recovered per Run	2.47	0.68	2.32
Solid Products Milligram per	0.76	0.66	0.58
Reactants, mg			
NO_2	5.2	1.7	1.7
UDMH	1.0	1.0	2.0
Total Reactants, mg	6.2	2.7	3.7
Total Products	3.2	1.4	2.9
Loss	3.0	1.3	0.8

TABLE II (Continued)

Run Series	#31 to #35		#46 to #50
Gaseous Products P. Milligram per Run			
NO_2	0.03		0.02
N_2O	0.84		1.87
CO_2	0.03		0.07
Methane	0.0		0.0
NO	0.11		0.17
N_2	0.08		0.40
H_2O	0.01		0.03
Formaldehyde dimethyl hydrazine	trace		0.60
Total Milligrams of Gaseous Products Recovered per Run	1.10		3.16
Solid Products Milligram per Run	0.36		0.36
Reactants, mg			
NO_2	1.7		1.7
UDMH	4.0		5.0
Total Reactants, mg	5.7		6.7
Total Products	1.5		3.2
Loss	4.2		3.5

rich composition there are traces of compounds that could be nitromethane, methyl nitrate, and unreacted UDMH. Significant amounts of a compound that give a mass spectrum attributed to formaldehyde dimethyl hydrazine, $CH_2 = N\text{-}N\text{-}(CH_3)_2$, appear in the reaction with highest fuel content.

As the stoichiometry with MMH becomes more fuel rich, the predominant species in the gas phase changes from NO_2 to N_2O and N_2. Large amounts of NO were not observed to appear, as was the case with UDMH.

It seems unlikely that NO_2 would appear to any extent at high fuel ratios with MMH. The small amounts of gas appearing at molecular weight 46 in the mass spectra and attributed to NO_2, could possibly be part of the cracking pattern of methyl nitrate. This pattern cannot be unambiguously resolved in the presence of large amounts of nitrogen oxides and MMH.

TABLE III

GASEOUS AND SOLID REACTION PRODUCTS FROM NONIGNITION VAPOR PHASE REACTIONS OF MMH WITH NO_2

Reaction Series	#16 to #20	#21 to #25	#26 to #30	#36 to #40	#41 to #45
Gaseous Reaction Products Milligram per Reaction					
NO_2	0.83*	0.55	0.11	0.10	0.10*
N_2O	0.12	0.10	0.19	0.08	0.20
CO_2	0.01	0.03	0.06	0.00	0.01
Methane	0.00	0.00	0.08	0.02	0.14
NO	0.00	0.00	0.54	0.00	0.00
N_2	0.04	0.04	0.65	0.20	1.53
H_2O	-	-	0.01	0.00	0.02
Total Milligrams of Gaseous Products Recovered per Reaction	1.0*	0.72	1.64	0.40	2.0
Solid Reaction Products Milligram per Reaction	0.28	0.40	0.30	0.50	0.46
Reactants, mg					
NO_2	5.2	1.7	1.7	1.7	1.7
MMH	1.0	1.0	2.0	3.0	4.0
Total Reactants, mg	6.2	2.7	3.7	4.7	5.7
Total Reaction Products	*	1.1	1.9	0.9	2.0
Loss	*	1.6	1.8	3.8	3.7

*A measurement of the total amount of gaseous reaction products was not obtained The values given are weight percent.

IGNITION STUDIES OF OXYGEN DIFLUORIDE AND LIQUID DIBORANE

Introduction

Potter and Butler (Ref. 16)were able to investigate the extinguishment of diffusion flames by metering fuel and oxidant flow rates through two opposed jets. In terms of an apparent flame strength, a more detailed study on the flame blow-off for various fuel-oxidant combinations has been carried out by Potter, Heimal, and Butler (Ref.17) and propane-oxygen flames at low pressure by Anagnostou and Butler, (Ref.18) Based on this principle of employing directly opposed flows of reactants, Pandya and Weinberg (Ref. 19)were able to stabilize a one-dimensional diffusion flame. Flow patterns were studied and a one-dimensional temperature distribution was obtained. The thermal structures were analyzed to yield the distribution of the rate of heat release per unit volume. The flame structure was analyzed by Kushida (Ref.20) who also used such a counter-flow burner to study ethylene oxygen flames.

The experimental technique can also be used to great advantage for studying ignition phenomena. The burner permits experimentation with known steady state conditions in terms of reactant concentrations, gas temperatures, and burner pressures. For fuel-oxidant systems involving two different phases, as ignition of liquid or solid fuels by an oxidizing gas, the burner can be modified by employing a stagnation flow field. The oxidizing gases are led to flow over the fuel in the direction normal to the fuel surfaces. Based on this stagnation flow field, the uncertainties of fluid dynamics are removed and a one-dimensional gas temperature and reactant concentrations, varying in the direction perpendicular to the fuel surface can be obtained. Effects of physical transport properties and quantitative evaluation of thermal reactions leading to ignition can be studied.

Experimental Apparatus

Ignition studies were conducted by introducing a stream of oxygen difluoride/helium gas mixture to flow over a dish of liquid diborane in a direction perpendicular to the liquid surface. Based on this stagnation flow field, a cylindrical burner was constructed. The details of the burner cross-section is shown in Figure 3. A schematic of the propellants' flow system is shown in Figure 4. A five pound capacity tank furnished by Callery Chemical Corporation where diborane was purchased was used as the diborane supply tank. The tank was enclosed within a fifty-five gallon drum, and dry ice was packed inside

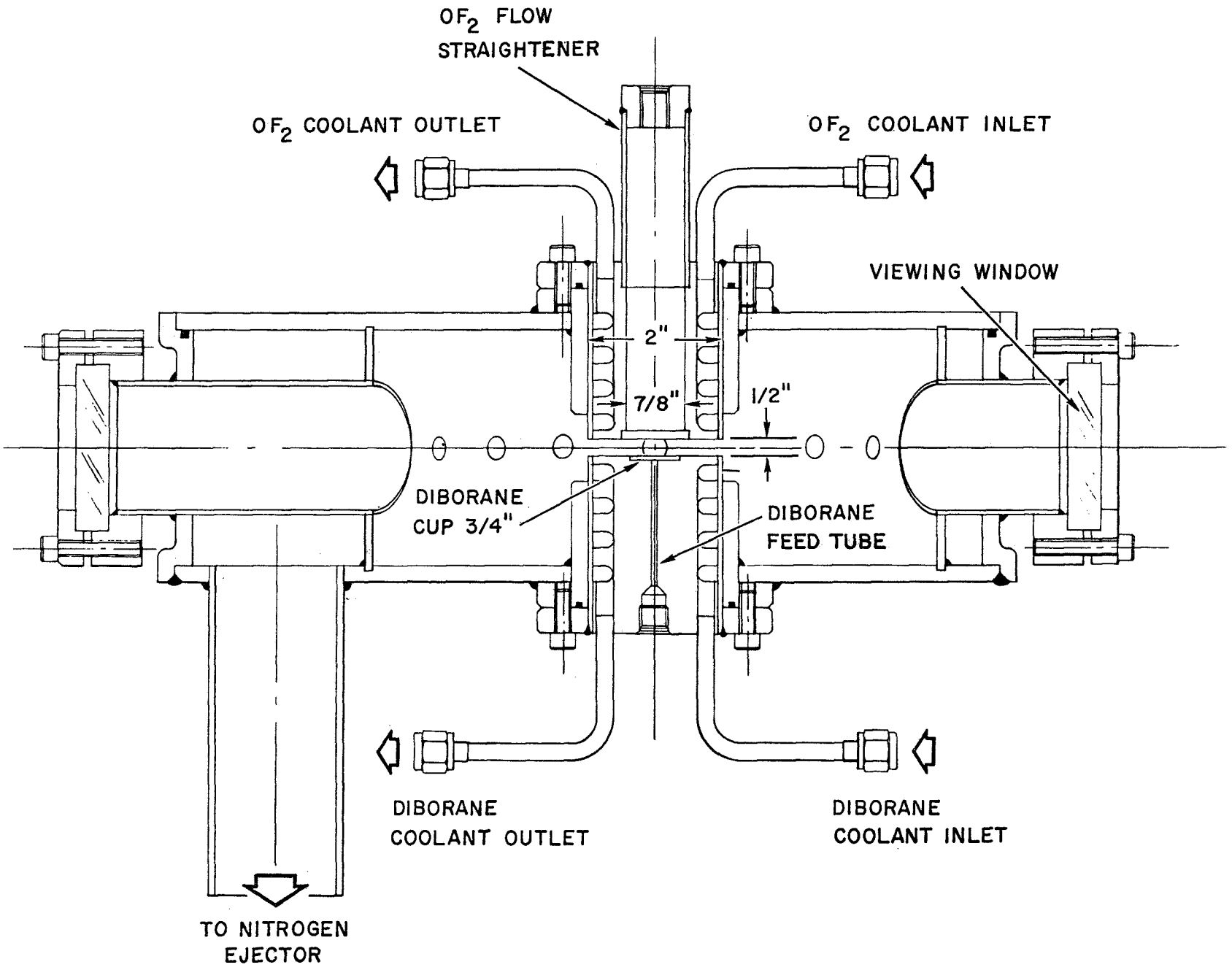

Figure 3. Stagnation Burner.

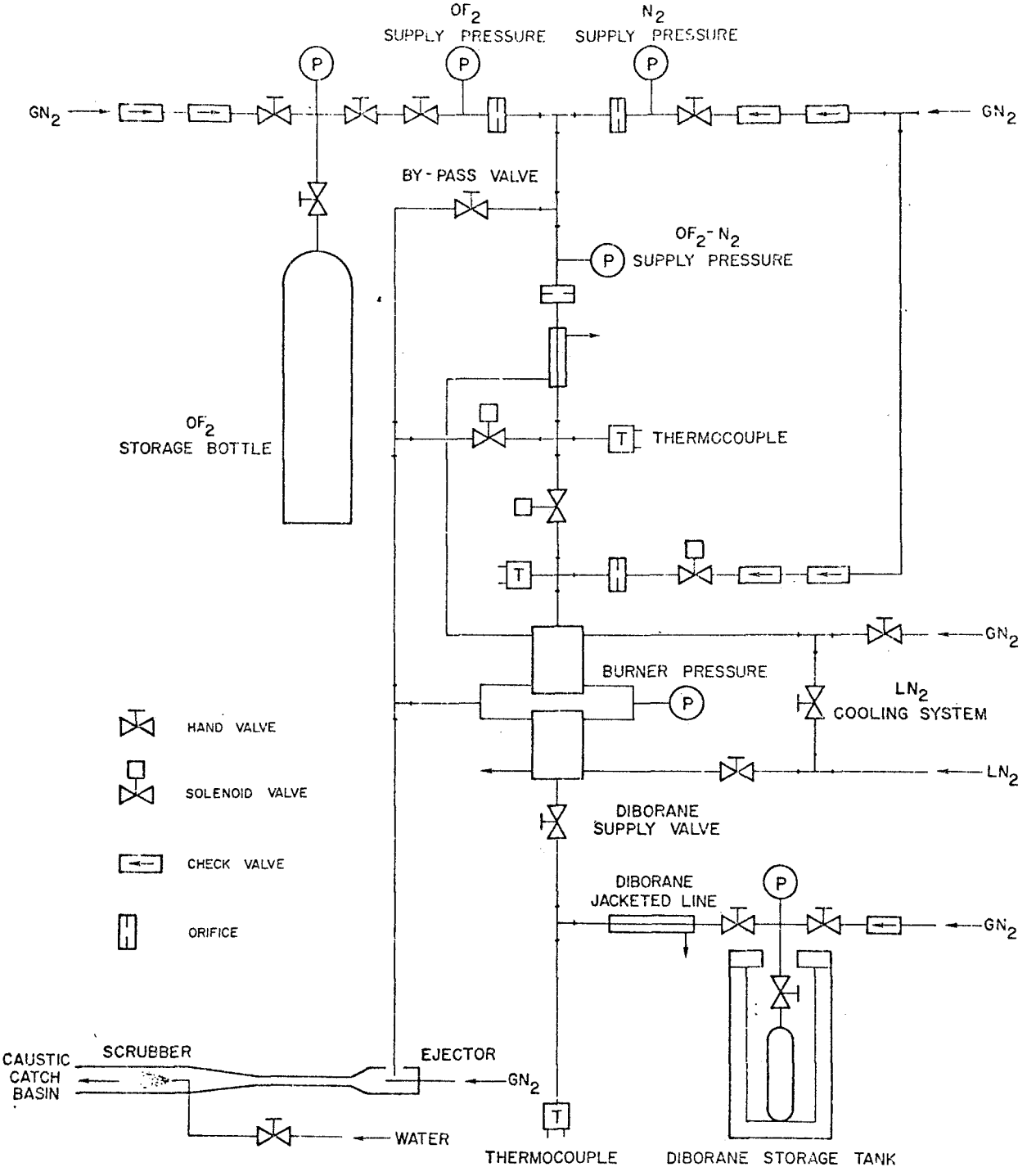

Figure 4. Schematic Diagram of the Burner.

the drum to always maintain diborane at approximately 190°K corresponding to a diborane vapor pressure of 2 atm. Liquid nitrogen was used as a coolant. The fuel supply systems consisted mainly of coaxial lines with liquid nitrogen as the coolant. The supply line was led from the storage tank into the diborane feed tube (Fig. 3) which ran through the center of a copper diborane holder of 2" diameter, terminating into a cup of 3/4" diameter, recessed 1/16" into the holder. The temperature of diborane inside the cup was controlled by the liquid nitrogen passages through the holder. A thermocouple, coaxial with the diborane feed tube was used to record preignition diborane temperatures. A gas nitrogen purging system was used throughout the diborane supply system.

The flow rates of oxygen difluoride and helium were metered by two sonic orifices. Gas flow rates through the sonic orifices were calibrated with nitrogen at 20°C. Flow rates of oxygen difluoride and helium were corrected for molecular wt difference and temperature effects. The gas mixture was led to two separate lines, one leading into the burner and a bypass line to the exhaust. Two calibrated sonic orifices were installed along these lines to control the net gas flow rate into the burner. Prior to each test, the gas mixture was first introduced to flow through the bypass line until the desired and constant flow velocity and gas temperatures were attained. The gas mixture was then introduced through the top of the burner consisting of a 1" diameter stainless steel tubing filled with stainless steel wool and temperature controlled by liquid nitrogen. The oxygen difluoride-helium gas mixture was then led into a flow straightener 7/8" diameter to flow over liquid diborane in a direction normal to the liquid surface. The open end of the straightener was fitted with a porous disc. The straightener was partly embedded in a copper holder which was also temperature controlled by liquid nitrogen or liquid and gas nitrogen mixtures. Two thermocouples, one installed immediately above the porous disc and one immediately following the oxygen difluoride-nitrogen cooling system, were used to record the preignition gas mixture temperature. Three solenoid valves were used to minimize possible transient flow errors. A nitrogen gas purging system was used throughout the oxidizer supply system. The gap spacing between the porous disc and the diborane surface could be varied from 1/16" to 3/8".

The burner was enclosed within two nonconcentric stainless steel cylinders 3 3/4" high and diameters of 11 3/4" and 8 3/4" respectively (Fig. 3). A nitrogen ejector system was fitted to the spacing between the two cylinders to control the

burner pressure. Ten sonic orifices were installed along the centerline of the inner cylinder so as to maintain a cylindrically symmetric flow field. Two viewing windows were provided for visual observation. The entire flow system and the burner were first cleaned to specification MIL 5002. Oxygen difluoride passivation of the system was carried out after the system was assembled.

Figure 5 is a front view of the burner before it was installed in the test base. The entire test program was conducted at Wyle Laboratory at their Norco test facility. Figure 6 is a side view of the burner after it was installed in the test base. All transfer operations and testing were performed remotely with either pneumatic Nupro bellow valves or manually operated valves with stems through steel protective shields. Experiments were conducted from the other side of the shield provided with viewing windows as shown in Figure 7. Figure 8 shows the valves that controlled the oxygen difluoride transfer operations.

The vent gas of the flow system was neutralized with a charcoal reactor before being exhausted into the atmosphere. Combustion products from the test chamber were aspirated with nitrogen gas, scrubbed with water and periodically neutralized in the disposal posposal ponds.

Experimental Work and Discussion

The hydrodynamic flow field of the burner was studied. Smoke particles were introduced immediately above the flow straightener for flow visualization. The diborane holder was removed and a 2" diameter pyrex glass tubing with a 2" diameter pyrex glass disc attached to one of the open ends was fitted into the burner. The gas mixtures with smoke particles were introduced to flow over the pyrex disc in a direction normal to the disc. Ten sonic orifices were fitted over the ten 3/8" diameter openings along the midpoint of the inner cylinder of the burner. By observing the flow field through the viewing windows of the burner and through the 2" diameter pyrex glass disc, the sizes of the sonic orifices were adjusted until a laminar, steady, axial-symmetric flow field was obtained. Attempts were made to photograph the flow field through the pyrex disc and the viewing windows. Because of the fineness of the smoke particles, the quality of the pictures was unsatisfactory. No major effort was devoted to developing the photographic technique of obtaining satisfactory pictures, however, visual observations indicated that a satisfactorily uniform flow field had been obtained.

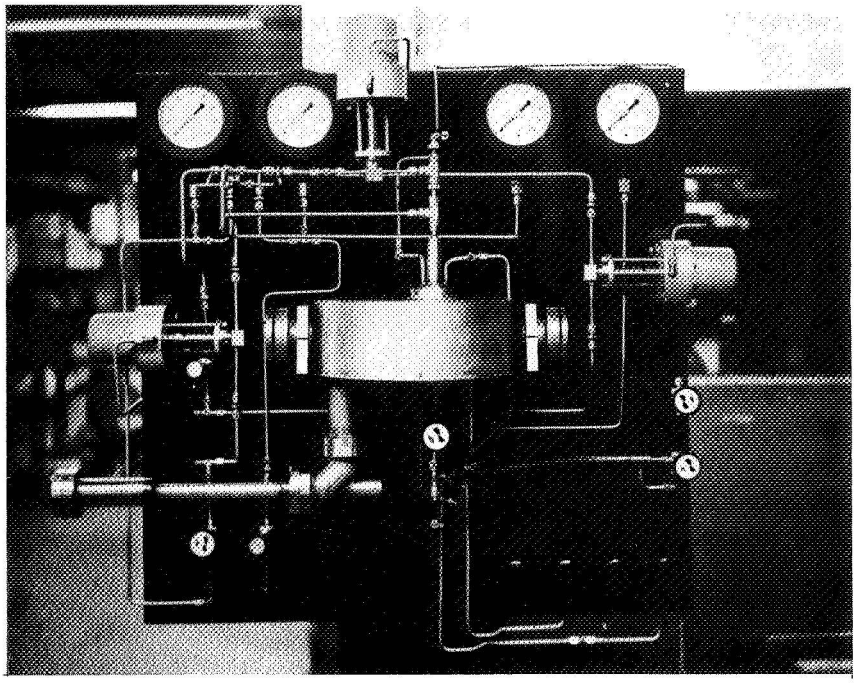

Figure 5. Front View of the Stagnation Burner.

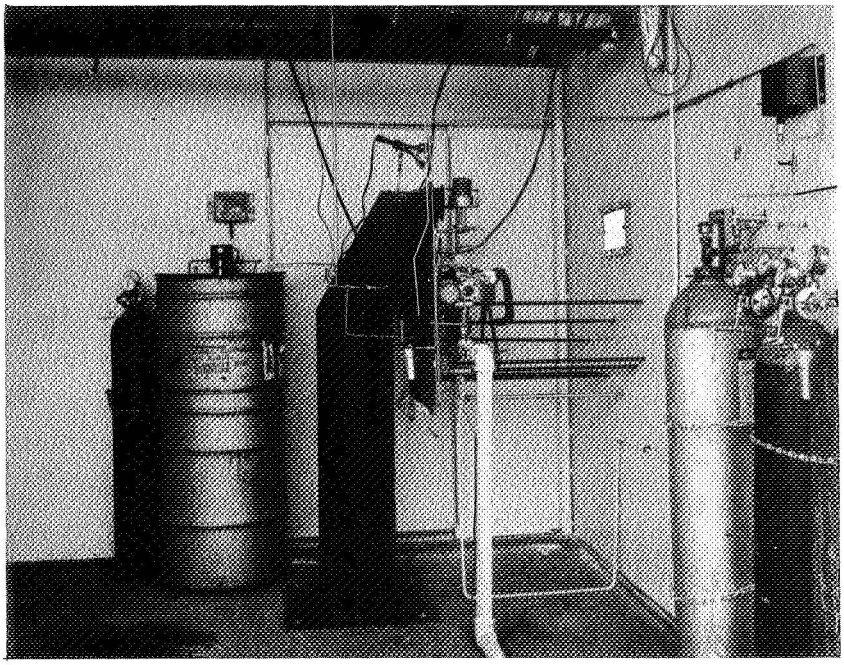

Figure 6. Side of the Burner After Installation.

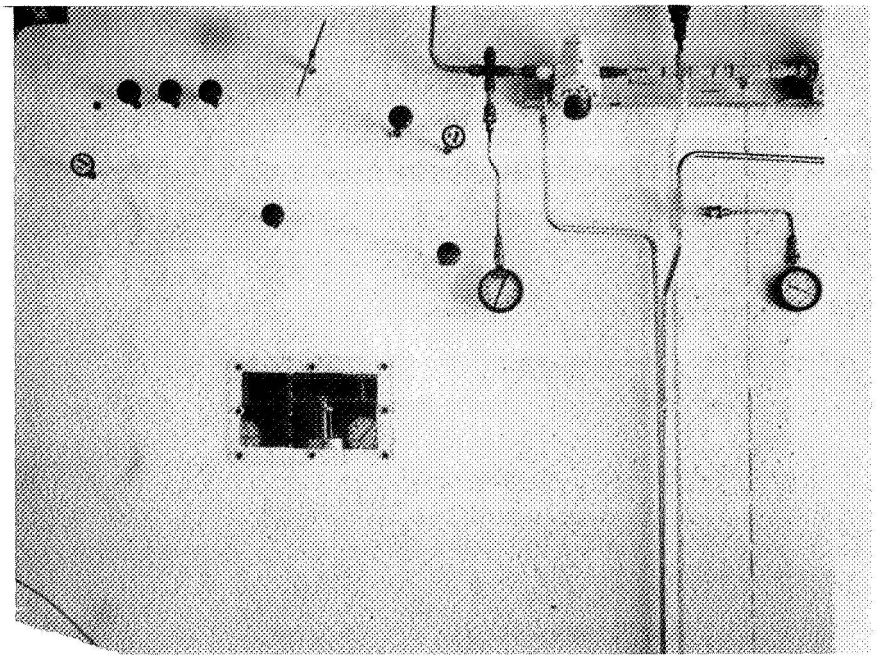

Figure 7. Viewing Window with Extended Valves.

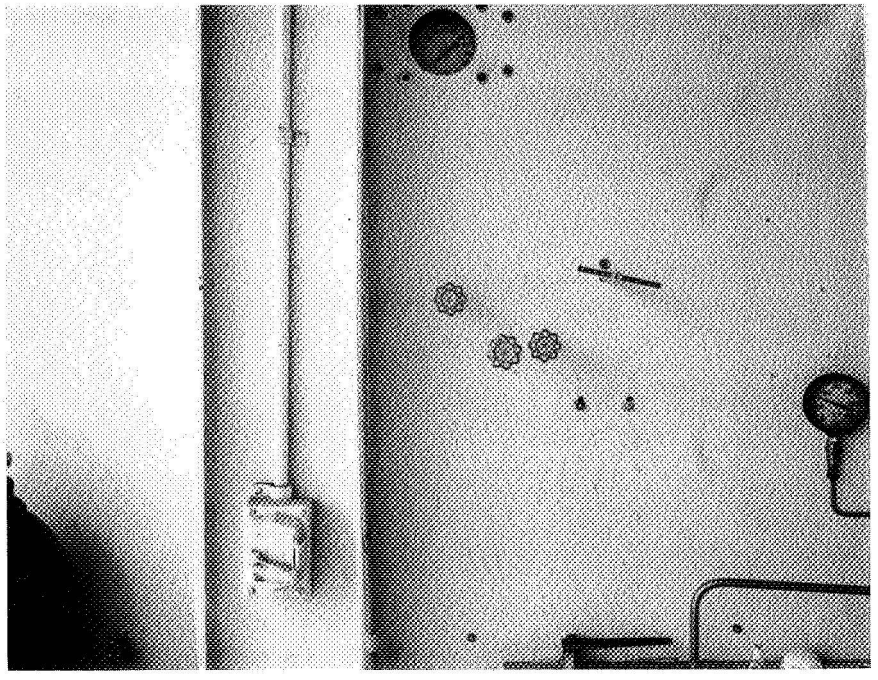

Figure 8. Control of OF_2 Supply System.

One of the problems in the initial phase of the experiment was to achieve a proper vacuum system of the entire flow lines. It was particularly difficult to properly seal the fuel supply system. It was finally realized that the diborane tank valve which was supplied by Callery Chemical only sealed when it was totally open or totally closed. Most of the problems pertaining to the leakage of gas diborane from the system were due to the fact that under experimental conditions the diborane tank valve was only partially open rather than fully open.

The experimental conditions for ignition studies were:

B_2H_6 temperature	$-270^{\circ}F$ - $-100^{\circ}F$
OF_2 temperature	$-150^{\circ}F$ - $0^{\circ}F$
OF_2 concentration	0% - 100%
Burner pressure	2 psia - atm pressure.

Initial tests were conducted with the burner pressure equal to 10 psia and the diborane cup at $-140^{\circ}F$. Rate of evaporation of diborane under these conditions (diborane boiling point is $-134.5^{\circ}F$) was very rapid and it was not possible to maintain any significant amount of liquid diborane within the diborane cup. No significant changes were observed when diborane cup was at $-160^{\circ}F$ and $-180^{\circ}F$. In order to maintain significant amount of liquid diborane within the cup, it appeared necessary to reduce the temperature of the entire burner. The system was modified by exhausting the liquid nitrogen, which was used to control the temperature of the diborane cup and the oxygen difluoride flow straightener, to flow over the entire burner. Experiments were repeated with the diborane cup temperature at approximately $-230^{\circ}F$. Oxygen difluoride/ helium mixture with equal molar concentrations of oxygen difluoride and helium at $-30^{\circ}F$ was introduced to flow over liquid diborane. No ignition was observed. Tests were repeated by reintroducing diborane and simultaneously increasing the oxygen difluoride concentrations. No ignitions were observed with oxygen difluoride molar concentration at 0.6 and 0.8. When pure oxygen difluoride was finally introduced to flow over liquid diborane an explosion was observed. The resulting overpressure bent the top plate where two C-clamps were used to hold the top plate onto the burner. This overpressure corresponds to a minimum of 200 psia. Figure 9 shows the burner after the explosion. Damage to the burner was minor

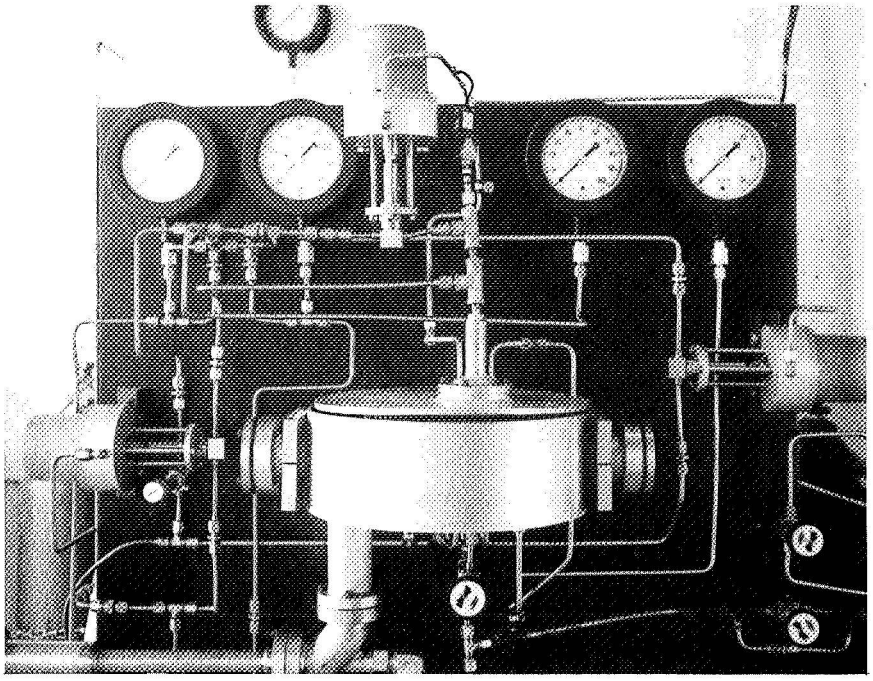

Figure 9. Burner After Explosion.

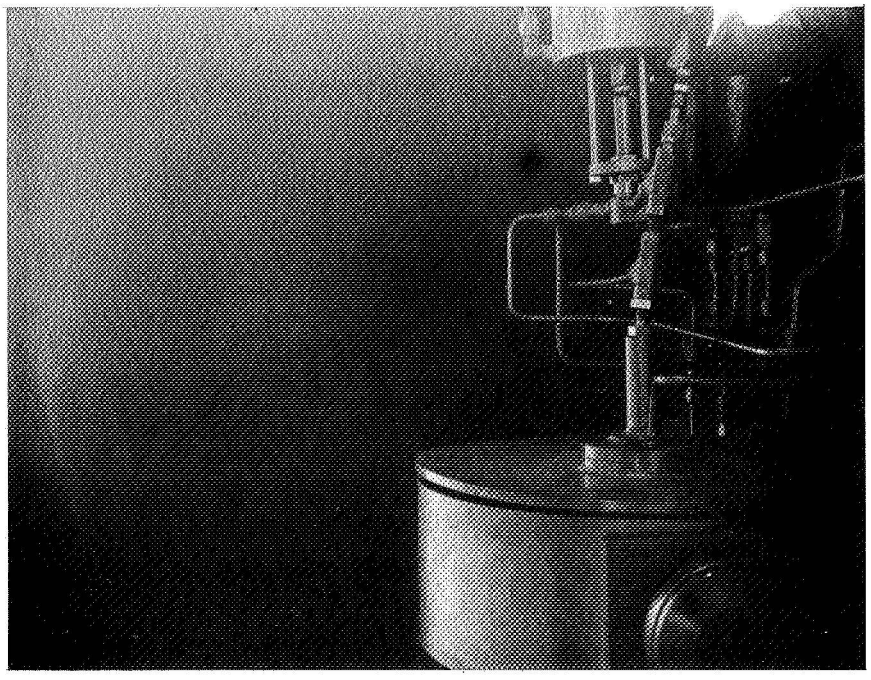

Figure 10. Close View of Burner After Explosion.

as compared with that of Figure 5. The side view of the burner is shown in Figure 10 where part of the supply line is also bent.

The burner was repaired and additional ignition experiments were repeated at higher diborane temperatures. In order to maintain a significant amount of liquid diborane within the diborane cup, low temperature nitrogen gas was introduced into the burner. Liquid diborane was observed with the diborane cup temperature at $-170^{\circ}F$. The nitrogen gas greatly reduced the propellant concentrations within the burner and meaningful results were difficult to obtain.

To summarize, for liquid diborane at low temperatures (diborane cup temperature equal to $-230^{\circ}F$) detonation-like ignition phenomena were observed. This could cause engine stability problems with very damaging results. One of the major problems encountered in this experiment was to maintain a sufficient amount of liquid diborane within the diborane cup at higher diborane temperatures. The gas inside the burner was at a much higher temperature than the boiling point of diborane. Without reducing the temperature of the surrounding gas, the rate of evaporation of liquid diborane was very rapid due to the heat transfer between the liquid fuel and the surrounding gas. To conduct ignition studies of liquid diborane, with diborane temperature varying between its boiling and melting point, it is necessary to control the temperature of the surrounding gas. This can be accomplished by first completely sealing the burner system and by metering the flow rate of nitrogen gas at a desired temperature (i.e., $-150^{\circ}F$) into the burner. The nitrogen flow rates must be such that the fuel concentrations within the spacing between the liquid diborane and the oxygen difluoride exit are not significantly altered. If these experimental conditions were obtained, it is believed that liquid diborane could be maintained between its boiling and melting point.

THEORETICAL ANALYSIS OF IGNITION MECHANISMS

Introduction

Ignition mechanisms of liquid hydrazine and vapor nitrogen tetroxide has been previously studied under this program (Ref. 12, 13, 15). The experimental technique was based on introducing vapor nitrogen tetroxide (diluted with nitrogen) to flow over liquid hydrazine in a direction perpendicular to the liquid surface. Based on this technique, the experimental parameters, such as fuel temperature, oxidizer temperature, oxidizer concentrations, flow velocities and burner pressures were well controlled and constantly monitored throughout the entire experiment. Thus the important experimental conditions were prescribed prior to ignition. Experimental measured ignition limits were expressed in terms of these parameters.

A theoretical correlation of the experimental findings have been attempted. The governing equations were formulated based on the stagnation flow field with the above mentioned experimental parameters appropriately incorporated as boundary conditions. Solutions to the steady state governing equations were reached for various different boundary conditions corresponding to the temperature ranges of the experimental study. The significant feature of this approach was that it allowed correction of the experimental findings without requiring the investigation of a set of time dependent equations.

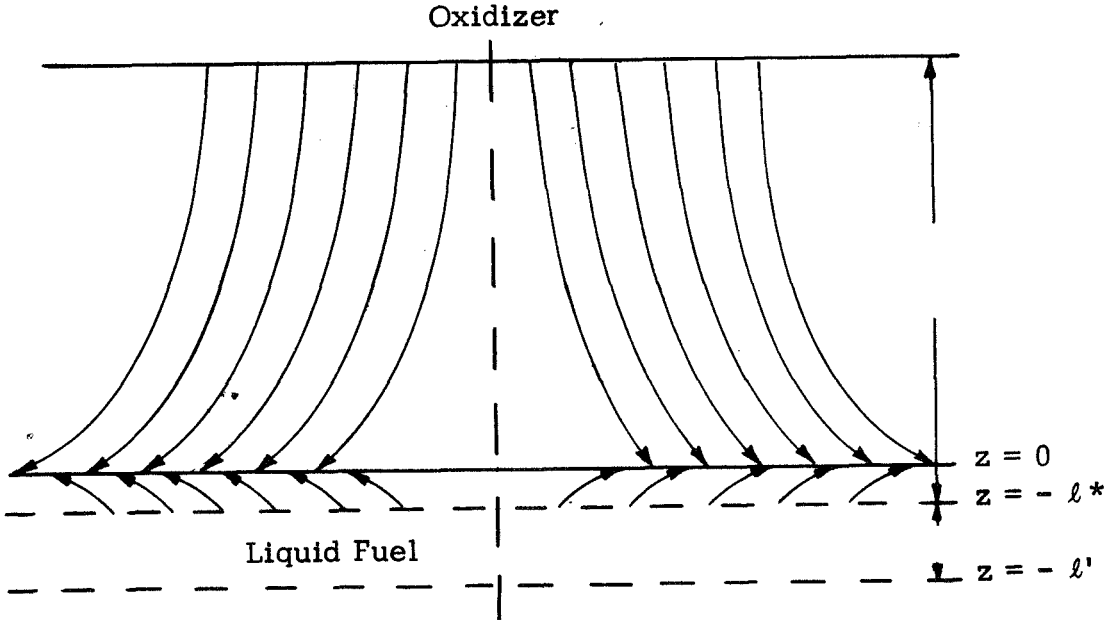

Figure 11. Stagnation Flow Field.

Based on the flow configuration, it is evident that the velocity in the tangential direction θ as well as $\partial/\partial\theta$ are identically equal to zero. Denote u' and w' as the velocity components in the radial and axial directions and ρ' as the gas mixture density, the continuity equation can be written as

$$\frac{\partial}{\partial r'}(\rho' u' r') + \frac{\partial}{\partial z'}(\rho' w' r') = 0. \tag{1}$$

The momentum equations in the r' and z' directions are respectively:

$$\rho' u' \frac{\partial u'}{\partial r'} + \rho' w' \frac{\partial u'}{\partial z'} = -\frac{\partial P'}{\partial r'} + \frac{\partial}{\partial r'}(\tau'_{rr}) + \frac{\partial}{\partial z'}(\tau'_{rz}) + \frac{2\mu'}{r'}\left(\frac{\partial u'}{\partial r'} - \frac{u'}{r'}\right) \tag{2}$$

$$\rho' u' \frac{\partial w'}{\partial r'} + \rho' w' \frac{\partial w'}{\partial z'} = -\frac{\partial P'}{\partial z'} + \frac{1}{r'}\frac{\partial}{\partial r'}(r'\tau'_{rz}) + \frac{\partial}{\partial z'}(\tau'_{zz}) \tag{3}$$

P' and μ' are the local gas mixture pressure and viscosity. The stress terms are defined as

$$\left.\begin{aligned} \tau'_{rr} &= 2\mu' \frac{\partial u'}{\partial r'} - \frac{2\mu'}{3}\left(\frac{1}{r'}\frac{\partial}{\partial r'}(r'u') + \frac{\partial w'}{\partial z'}\right) \\ \tau'_{rz} &= \mu'\left(\frac{\partial u'}{\partial z'} + \frac{\partial w'}{\partial r'}\right) \\ \tau'_{zz} &= 2\mu' \frac{\partial w'}{\partial z'} - \frac{2\mu'}{3}\left(\frac{1}{r'}\frac{\partial}{\partial r'}(r'u') + \frac{\partial w'}{\partial z'}\right) \end{aligned}\right\} \tag{4}$$

Using equation (4), the momentum equations read as follows:

$$\rho' u' \frac{\partial u'}{\partial r'} + \rho' w' \frac{\partial u'}{\partial z'} = -\frac{\partial P'}{\partial r'} + \frac{\partial}{\partial r'}\left[2\mu' \frac{\partial u'}{\partial r'} - \frac{2\mu'}{3}\left(\frac{1}{r'}\frac{\partial}{\partial r'} r'u' + \frac{\partial w'}{\partial z'}\right)\right] + \frac{\partial}{\partial z'}\left[\mu'\left(\frac{\partial u'}{\partial z'} + \frac{\partial w'}{\partial r'}\right)\right] + \frac{2\mu'}{r'}\left(\frac{\partial u'}{\partial r'} - \frac{u'}{r'}\right) \tag{5}$$

$$\rho' u' \frac{\partial w'}{\partial r'} + \rho' w' \frac{\partial w'}{\partial z'} = -\frac{\partial P'}{\partial z'} + \frac{1}{r'} \frac{\partial}{\partial r'} r' \left[\mu' \left(\frac{\partial u'}{\partial z'} + \frac{\partial w'}{\partial r'} \right) \right]$$

$$+ \frac{\partial}{\partial z'} \left[2\mu' \frac{\partial w'}{\partial z'} - \frac{2\mu'}{3} \left(\frac{1}{r'} \frac{\partial}{\partial r'} r' u' + \frac{\partial w'}{\partial z'} \right) \right] \tag{6}$$

$\varkappa_i$ is defined as the local concentration of the gas species i, and

$$\sum_i \varkappa_i = 1 \tag{7}$$

The local gas density ρ_i' of species i is related to ρ' as

$$\rho_i' = \rho' \varkappa_i \tag{8}$$

Define U_i' and W_i' as the diffusion velocities of species i in the radial and axial directions, the continuity equations for species i can be written as

$$\frac{1}{r'} \frac{\partial}{\partial r'} [r' \rho' \varkappa_i (u' + U_i')] + \frac{\partial}{\partial z'} [\rho' \varkappa_i (w' + W_i')] = \omega_i' \tag{9}$$

ω_i' is the rate of mass production or mass consumption of species i. For the simplified case where the coefficients of diffusion of all molecular species are approximately equal, or for a binary gas mixture, the diffusion velocities can be approximated by

$$\left.\begin{aligned} \rho' \varkappa_i U_i' &= -\rho' D' \frac{\partial \varkappa_i}{\partial r'} \\ \rho' \varkappa_i W_i' &= -\rho' D' \frac{\partial \varkappa_i}{\partial z'} \end{aligned}\right\} \tag{10}$$

where D' is the diffusion coefficient. Equation (1) further assumes that the thermal diffusion terms are negligible. The validity of equation (10) will be further investigated. Using eqn. (10), equation (9) can be written as

$$\rho' u' \frac{\partial \varkappa_i}{\partial r'} + \rho' w' \frac{\partial \varkappa_i}{\partial z'} = \omega_i' + \frac{1}{r'} \frac{\partial}{\partial r'} \left[r' \rho' D' \frac{\partial \varkappa_i}{\partial r'} \right]$$

$$+ \frac{\partial}{\partial z'} \left[\rho' D' \frac{\partial \varkappa_i}{\partial z'} \right] . \tag{11}$$

The enthalpy of the i^{th} species h'_i can be defined in terms of the specific heat C_{pi} and gas mixture temperature T'.

$$h'_i = \int_{T_o}^{T'} C_{pi}\, dT' + h_i^o \tag{12}$$

h_i^o is some reference enthalpy at temperature $T' = T_o$. The enthalpy of the gas mixture h' can thus be defined as

$$h' = \sum_i \varkappa_i\, h'_i \tag{13}$$

In terms of gas enthalpy, the energy equation can be written as

$$\rho' u' \frac{\partial h'}{\partial r'} + \rho' w' \frac{\partial h'}{\partial z'} = \frac{1}{r'} \frac{\partial}{\partial r'} \left[r' \left(k' \frac{\partial T'}{\partial r'} + \sum_i \rho' D' h'_i \frac{\partial \varkappa_i}{\partial r'} \right) \right]$$

$$+ \frac{\partial}{\partial z'} \left[k' \frac{\partial T'}{\partial z'} + \sum_i \rho' D' h'_i \frac{\partial \varkappa_i}{\partial z'} \right] \tag{14}$$

where k' is the coefficient of thermal conductivity of the gas mixture. Equation (14) also assumes that the kinetic energy of the gas mixture, as well as viscous dissipation terms and radiative effects are negligible.

For a mixture of ideal gases, the equation of state is

$$P' = \rho' \bar{R} T' \tag{15}$$

where $\bar{R} = \sum \frac{R}{M_i} \varkappa_i$, M_i being the molecular weight of species i.

Define nondimensionalized quantities as

$$u = u'/u_o$$

$$w = w'/u_o$$

$$\rho = \rho'/\rho_o$$

$$p = p'/\rho_o u^2{}_o$$

$$\rho_i = \rho'_i/\rho_o$$

$$U_i = U'_i/u_o$$

$$W_i = W'_i/u_o$$

$$T = T'/T_o$$

$$r = r'/L$$

$$z = z'/L$$

$$\omega_i = \omega'_i/(\rho_o u_o/L)$$

$$D = D'/D_o$$

$$\mu = \mu'/\mu_o$$

$$k = k'/k_o$$

$$h_i = h'_i/C_p T_o$$

$$h = h'/C_p T_o$$

The governing equations can be expressed as:

$$\frac{\partial}{\partial r}(\rho u r) + \frac{\partial}{\partial z}(\rho w r) = 0 \tag{16}$$

$$\rho u \frac{\partial u}{\partial r} + \rho w \frac{\partial u}{\partial z} = -\frac{\partial p}{\partial r} + \frac{1}{Re}\left\{\frac{\partial}{\partial r}\left[2\mu\frac{\partial u}{\partial r} - \frac{2\mu}{3}\left(\frac{1}{r}\frac{\partial}{\partial r}ru + \frac{\partial w}{\partial z}\right)\right]\right.$$

$$\left. + \frac{\partial}{\partial z}\left[\mu\left(\frac{\partial u}{\partial z} + \frac{\partial w}{\partial r}\right) + \frac{2\mu}{r}\left(\frac{\partial u}{\partial r} - \frac{u}{r}\right)\right]\right\} \tag{17}$$

$$\rho u \frac{\partial w}{\partial r} + \rho w \frac{\partial w}{\partial z} = -\frac{\partial p}{\partial z} + \frac{1}{Re}\left\{\left[\frac{1}{r}\frac{\partial}{\partial r}r\left(\mu\frac{\partial u}{\partial z} + \mu\frac{\partial w}{\partial r}\right)\right]\right.$$

$$\left. + \frac{\partial}{\partial z}\left[2\mu\frac{\partial w}{\partial z} - \frac{2\mu}{3}\left(\frac{1}{r}\frac{\partial}{\partial r}ru + \frac{\partial w}{\partial z}\right)\right]\right\} \tag{18}$$

$$\rho u \frac{\partial \chi_i}{\partial r} + \rho w \frac{\partial \chi_i}{\partial z} = \omega_i + \frac{1}{ReSc}\left[\frac{1}{r}\frac{\partial}{\partial r}\rho D r \frac{\partial \chi_i}{\partial r} + \frac{\partial}{\partial z}\rho D \frac{\partial \chi_i}{\partial z}\right] \tag{19}$$

$$\rho u \frac{\partial h}{\partial r} + \rho w \frac{\partial h}{\partial z} = \frac{1}{Re}\frac{1}{r}\frac{\partial}{\partial r}\left[r\left(\frac{1}{Pr}k\frac{\partial T}{\partial r} + \frac{1}{Sc}\sum_1 \rho D h_i \frac{\partial \chi_i}{\partial r}\right)\right]$$

$$+ \frac{1}{Re}\frac{\partial}{\partial z}\left[\frac{1}{Pr}k\frac{\partial T}{\partial z} + \frac{1}{Sc}\sum_1 \rho D h_i \frac{\partial \chi_i}{\partial r}\right] \tag{20}$$

$$p = \rho T \frac{1}{\gamma M^2} \sum \frac{\chi_i}{M_i} \tag{21}$$

The dimensionless groups are defined as

$$\left.\begin{aligned} &\text{Reynolds number} && Re = \frac{u_o \rho_o L}{\mu_o} \\ &\text{Prandtl number} && Pr = \frac{\mu_o c_p}{k_o} \\ &\text{Schmidt number} && Sc = \frac{\mu_o}{\rho_o D_o} \\ &\text{Mach number} && M = \frac{u_o}{a_o} \end{aligned}\right\} \tag{22}$$

The governing equations for the liquid fuel can be similarly obtained. Since the liquid is stationary, the convective velocities are not present. Define T_ℓ as the nondimensionalized liquid temperature, the energy equation is

$$\frac{1}{Pr_\ell}\left[\frac{1}{r}\frac{\partial}{\partial r}\, rk_\ell \frac{\partial T_\ell}{\partial r} + \frac{\partial}{\partial z}\, k_\ell \frac{\partial T_\ell}{\partial z}\right] = \theta_\ell \tag{23}$$

θ_ℓ being the heat of reaction. Pr_ℓ and k_ℓ are the liquid Prandtl number and the coefficient of thermal conductivity of the liquid fuel. The diffusion of oxidizer species through the liquid is described by

$$\frac{1}{ReSc_\ell}\left[\frac{1}{r}\frac{\partial}{\partial r}\, \rho_\ell D_\ell r \frac{\partial \chi_i}{\partial r} + \frac{\partial}{\partial z}\, \rho_\ell D_\ell \frac{\partial \chi_i}{\partial z}\right] = -\Omega_i \tag{24}$$

where Sc_ℓ, D_ℓ, and ρ_ℓ are the liquid Schmidt number, coefficient of liquid diffusion and the density of the liquid. Ω_i is the rate of mass consumption due to liquid phase reactions.

Similarity Solution

Karman first investigated the stagnation flow field over an infinitely large rotating disc (Ref. 8). A similarity variable proportional to z is introduced to reduce the set of governing partial differential equations to a set of ordinary differential equations. The same technique has been also applied to two-phase flow problems (Ref. 9) and reacting flows (Ref. 4, 5, 6, 7). Define

$$\begin{aligned} \rho u &= r\,F(z) \\ \rho\, w &= H(z) \end{aligned} \tag{25}$$

The continuity equation (16) is reduced to

$$\frac{dH}{dz} + 2F(z) = 0 \tag{26}$$

The momentum equations can be similarly reduced by letting

$$\begin{aligned} \rho\,(r,\ z) &= \rho\,(z) \\ T(r,z) &= T(z) \end{aligned} \tag{27}$$

Equations (17) and (18) assume the following form:

$$\frac{1}{\rho}F^2 + H\,\frac{d}{dz}\,(F/\rho) - \frac{1}{Re}\,\frac{d}{dz}\,\mu\frac{d}{dz}\,(F/\rho) = \text{constant} \tag{28}$$

$$\frac{1}{Re}\left[2\mu\frac{d}{dz}\,(F/\rho) + \frac{4}{3}\,\mu\frac{d}{dz}\,(H/\rho) - \frac{4}{3}\,\mu(F/\rho)\right] - H\frac{d}{dz}\,(H/\rho) = \frac{\partial p}{\partial z} \tag{29}$$

The species conservation equations and the energy equation can be similarly simplified by letting

$$\left.\begin{aligned} \varkappa_i(r,z) &= \varkappa_i(z) \\ h(r,z) &= h(z) \\ T_\ell(r,z) &= T_\ell\,(z) \end{aligned}\right\} \tag{30}$$

$$H(z)\frac{d\alpha_i}{dz} = \omega_i + \frac{1}{ReSc}\frac{d}{dz}\rho D\frac{d\alpha_i}{dz} \tag{31}$$

$$H(z)\frac{dh}{dz} = \frac{1}{ReSc}\frac{d}{dz}\left[\left(k\frac{dT}{dz}\right) + \frac{Pr}{Sc}\Sigma\,\rho D h_i\frac{d\alpha_i}{dz}\right] \tag{32}$$

$$\frac{1}{Pr_\ell}\frac{d}{dz}k_\ell\frac{dT_\ell}{dz} = \theta_\ell \tag{33}$$

$$\frac{1}{ReSc_\ell}\frac{d}{dz}\rho_\ell D_\ell\frac{d\alpha_i}{dz} = \Omega_i \tag{34}$$

Because gas oxidant is being introduced to flow downstream and the vaporizing gas fuel is moving upstream, there exists a stagnation plane at some distance ℓ^* from the liquid surface. Fuel must diffuse against convection for $z' > 0$ and oxidant likewise for $z' < 0$. Both reactants cross the stagnation plane $z' = 0$ by diffusion only. The velocity profile is symmetric with respect to the stagnation plane. This requires that the flow for $0 < z' < -\ell^*$ be the mirror image of $z' < 0$. The solution for such a flow field is identical with the well known inviscid flow where $u' \approx r'$ or

$$u = r \tag{35}$$

Using equations (27) and (35), the continuity equation (16) can be integrated to give

$$\rho w = -\int_0^z 2\rho\,dz \tag{36}$$

It is convenient to introduce a new dimensionless variable η such that

$$\eta = \int_0^z \rho\,dz \tag{37}$$

Using equations (35) and (36), equation (31) can be expressed in terms of η as

$$-2\eta \frac{d\varkappa_i}{d\eta} = \frac{1}{\rho}\,\omega_i + \frac{1}{Re\,Se}\,\frac{d}{d\eta}(\rho D)\,\rho\,\frac{d\varkappa_i}{d\eta} \tag{38}$$

The energy equation (32) can be expressed in terms of the gas temperature T by assuming the specific heat of species i $C_{pi} = C_p$ = constant.

$$H(z)\frac{dT}{dz} = \frac{1}{Re\,Pr}\,\frac{d}{dz}\left(k\frac{dT}{dz}\right) - \sum_i \omega_i h^\circ_i \tag{39}$$

Using equations (35) and (36), equation (39) is reduced to

$$-2\eta\,\frac{dT}{d\eta} = \frac{1}{Re\,Pr}\,\frac{d}{d\eta}(\rho k)\frac{dT}{d\eta} - \frac{1}{\rho}\sum \omega_i h^\circ_i \tag{40}$$

In the region where equations (35) and (36) are valid, local pressure variation is negligible. The equation of state can be reduced to

$$\rho = \frac{1}{T} \tag{41}$$

when $\sum \varkappa_i M_i / \sum \varkappa^\circ_i M_i$ is approximately equal to unity. It is further assumed that

$$\left.\begin{aligned} \rho D \quad &= T \\ k \quad &= T \end{aligned}\right\} \tag{42}$$

The governing equations (38) and (40) are reduced to

$$-2\eta\,\frac{d\varkappa_i}{d\eta} = \frac{1}{\rho}\omega_i + \frac{1}{ReSc}\,\frac{d^2\varkappa_i}{d\eta^2} \tag{43}$$

$$-2\eta\,\frac{dT}{d\eta} = -\frac{1}{\rho}\sum \omega_i h^\circ_i + \frac{1}{RePr}\,\frac{d^2T}{d\eta^2} \tag{44}$$

Assuming Pr = Sc and define

$$\zeta = \frac{\eta}{\sqrt{Re\,Pr}}$$

equations (43) and (44) are

$$\frac{d^2\varkappa_i}{d\zeta^2} + 2\zeta\,\frac{d\varkappa_i}{d\zeta} = -\frac{1}{\rho}\,\omega_i \tag{45}$$

$$\frac{d^2T}{d\zeta^2} + 2\zeta \frac{dT}{d\zeta} = \frac{1}{\rho} \Sigma \omega_i h^\circ_i \tag{46}$$

Reaction Kinetics

Define quantitives pertaining to the fuel and oxidizer with subscripts f and o. For an Arrhenius type reaction, ω'_f can be written as

$$\omega'_f = -b \varkappa_f \varkappa_o \exp - \frac{E}{RT'} \tag{47}$$

where ω'_f is the rate of fuel consumption; $\varkappa_f$ and $\varkappa_o$ are the fuel and oxidizer mass concentration; E is the activation energy and b is the frequency factor. Similarly, ω'_o can be written as

$$\omega'_o = -\nu' b \varkappa_f \varkappa_o \exp - \frac{E}{RT'} \tag{48}$$

where ν' is the ratio of the stoichiometric coefficients.

The energy term $-\Sigma \omega_i h^\circ_i$ is

$$-\Sigma \omega_i h^\circ_i = - b \varkappa_f \varkappa_o e^{-E/RT'} \left[\sum_{\substack{\text{over} \\ \text{products}}} \omega_i h^\circ_i - \nu_f h^\circ_o - \nu_f h^\circ_f \right]$$

Define $Q' = \nu_o h^\circ_o + \nu_f h^\circ_f - \sum_{\substack{\text{over} \\ \text{products}}} \nu_i h^\circ_i$

$$- \Sigma \omega_i h^\circ_i = b \varkappa_f \varkappa_o e^{-E/RT'} Q' \tag{49}$$

Define

$$D_1 = \frac{b r_o}{\rho_o u_o}$$

$$\theta = \frac{E}{RT_o}$$

$$Q = \frac{Q'}{C_p T_o}$$

equations (47), (48), and (49) are

$$\left.\begin{aligned} \omega_f &= D_1 \varkappa_o \varkappa_f e^{-\theta/T} \\ \omega_o &= \nu D_1 \varkappa_o \varkappa_f e^{-\theta/T} \\ -\Sigma \omega_i h^\circ_i &= D_1 Q \varkappa_o \varkappa_f e^{-\theta/T} \end{aligned}\right\} \tag{50}$$

The governing equations (45) and (46) can be written as

$$\frac{d^2\varkappa_o}{d\zeta^2} + 2\zeta \frac{d\varkappa_o}{d\zeta} = \frac{-1}{\rho} D_1 \varkappa_o \varkappa_f e^{-\theta/T} \tag{51}$$

$$\frac{d^2\varkappa_f}{d\zeta^2} + 2\zeta \frac{d\varkappa_f}{d\zeta} = -\frac{\nu}{\rho} D_1 \varkappa_o \varkappa_f e^{-\theta/T} \tag{52}$$

and

$$\frac{d^2T}{d\zeta^2} + 2\zeta \frac{dT}{d\zeta} = \frac{1}{\rho} D_1 Q \varkappa_o \varkappa_f e^{-\theta/T} \tag{53}$$

Boundary Conditions

The boundary conditions for $z' = \infty$ are

$$\left.\begin{aligned} &T'(z' = \infty) = T_o \\ &\varkappa_o(z' = \infty) = \varkappa_\infty^o = \text{constant} \\ &\varkappa_f(z' = \infty) = 0 \end{aligned}\right\} \tag{54}$$

Considering the case where the liquid fuel is always being maintained at a constant temperature T_ℓ, the boundary conditions at $z = -\ell^*$ are

$$T'(z = -\ell^*) = T_\ell \tag{55}$$

Vapor concentration of the fuel on the liquid surface is described in terms of the Clausius-Clapeyron relations

$$\frac{p_f}{p_f^o}(z' = -\ell^*) = \exp -\left[\left(\frac{L}{RT_\ell} - \frac{L}{RT_o}\right)\right] \tag{56}$$

where L is the latent heat of vaporization and is assumed to be a constant.

$$\varkappa_f = \frac{\rho'_f}{\rho} = \frac{M_f}{\sum \varkappa_i M_i} \frac{\rho_f}{\rho_o} \exp -\left[\frac{L}{RT_o}\left(\frac{T_o}{T_\ell} - 1\right)\right] = \alpha \exp -\left[\frac{L}{RT_o}\left(\frac{T_o}{T_\ell} - 1\right)\right] \tag{57}$$

α is defined as

$$\alpha = \frac{M}{\sum \varkappa_i M_i} \frac{p_{fo}}{p_o}$$

The problem being investigated is the ignition due to vapor phase reactions. This leads to the assumption that reaction between oxidizer and liquid fuel on the liquid surface is negligible. The net oxidizer flow in the axial direction is $\rho' \varkappa_o (w' + W'_o)$. The above assumption leads to the condition that

$$\rho' \varkappa_o (w' + W'_o) = 0 \qquad \text{at } z' = -\ell^*$$

or

$$\rho' \varkappa_o w' - \rho' D' \frac{\partial \varkappa_o}{\partial z} = 0 \text{ at } z' = -\ell^* \tag{58}$$

To summarize, the boundary conditions expressed in terms of non-dimensionalized variables are as follows:

$$\left.\begin{aligned} \zeta = \infty : \quad & T = 1 \\ & \varkappa_o = \varkappa_o^o = \text{constant} \\ & \varkappa_f = 0 \end{aligned}\right\} \tag{59}$$

Define

$$-\zeta^* = \frac{\int_o^{-\ell^*} \rho \, dz}{\sqrt{Re\ Sc}}$$

$$\left.\begin{aligned} \zeta = -\zeta^* : \quad & T = \frac{T_\ell}{T_o} = \tau \\ & \varkappa_f = \alpha \exp - \frac{L}{RT_o} \left(\frac{1}{\tau} - 1\right) = f(\tau) \\ & \varkappa_o = 1 - f(\tau) \end{aligned}\right\} \tag{60}$$

ζ^* is obtained by solving

$$- 2\zeta^* \varkappa_o + \frac{d\varkappa_o}{d\zeta} = 0 \tag{61}$$

Vapor Phase Ignition

Ignition of liquid hydrazine and diluted (with nitrogen) nitrogen tetroxide have been previously studied under this research program. The experiments were conducted by introducing a stream of nitrogen tetroxide/nitrogen gas mixtures to flow over a dish of liquid hydrazine in a direction normal to the liquid surface. Minimum mass concentrations of nitrogen tetroxide in a nitrogen tetroxide/nitrogen gas mixture that induced ignition when it was led to flow over liquid hydrazine were measured. These experiments were conducted for hydrazine temperatures varying from its melting point to boiling point. Effects of flow velocity and burner pressure were also evaluated.

Figure 12 is an ignition threshold measurement with the solid line dividing the region of ignition and no-ignition. For hydrazine temperature below $\approx 315^{\circ}K$, the vapor pressure of hydrazine is not high enough to sustain a vapor phase ignition. Nitrogen tetroxide mixture diffuses towards liquid surface and preignition reactions mainly occur between nitrogen tetroxide and liquid hydrazine. Reaction products formed and also dissolved in the liquid fuel produce very noticeable foaming and bubbling as evidenced by photographic results (Fig. 13). The preignition reaction mechanism is governed by the rate of oxidizer diffusion and is thus relatively insensitive to hydrazine temperature as shown by experimental results.

For hydrazine temperatures above $\approx 315^{\circ}K$, the vapor pressure of hydrazine appears to be high enough to sustain a vapor phase ignition. The logarithm of the ignition threshold concentration decreases linearly with the inverse of the hydrazine temperature.

In order to define the hydrazine temperature ranges where vapor phase ignition is important, the set of governing equations (51), (52), and (53) have to be solved for various hydrazine temperatures. Variation of maximum gas mixture temperature for different first Damkohler number D_1 defines ignition and quenching regions (22, 23). Similar techniques can also be extended to investigate the effect of liquid temperature in addition to D_1 and thus defines liquid temperature where vapor phase ignition occurs.

An alternate and simpler approach to analyze the heat of reaction term Ω.

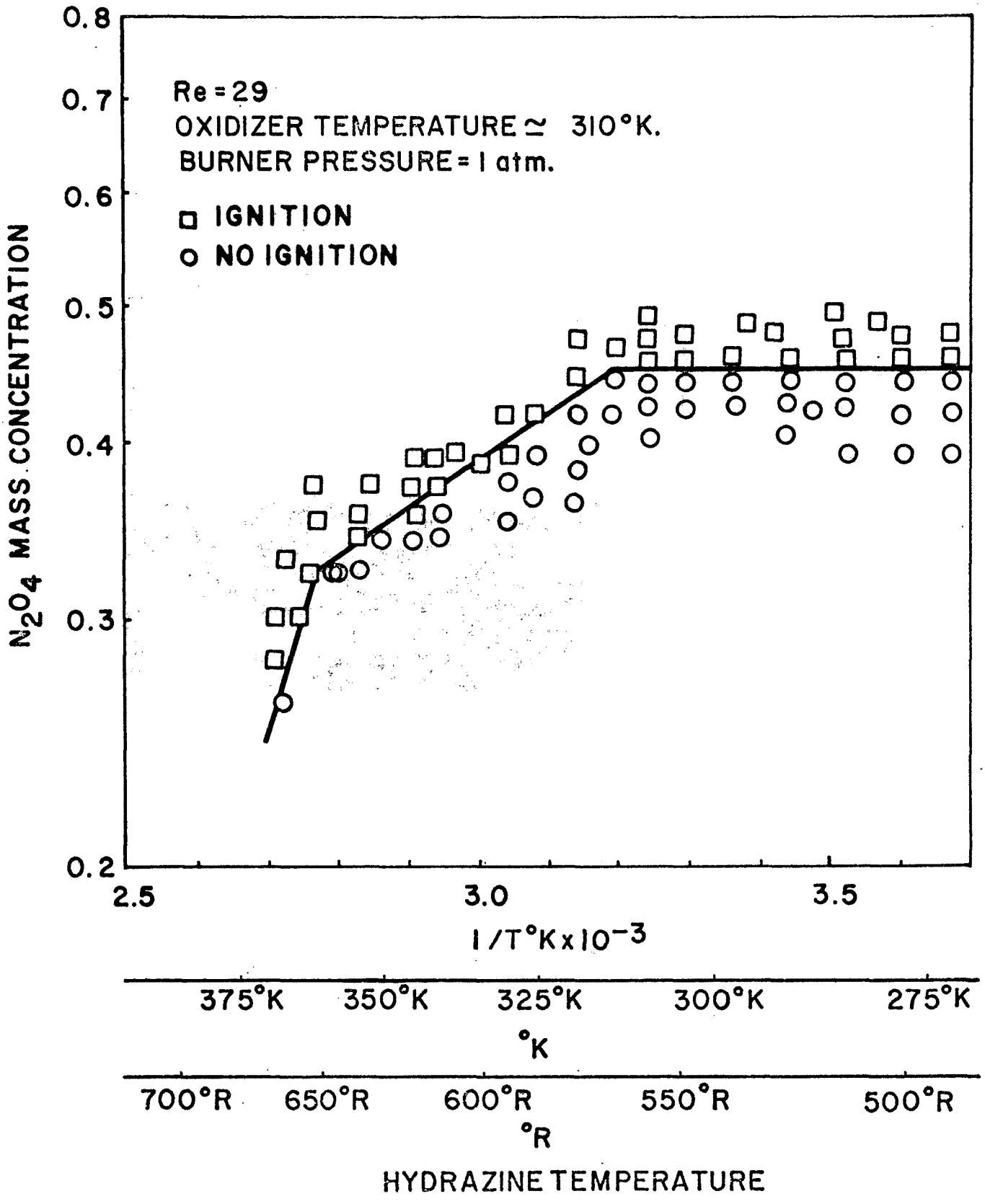

Figure 12. Ignition Threshold

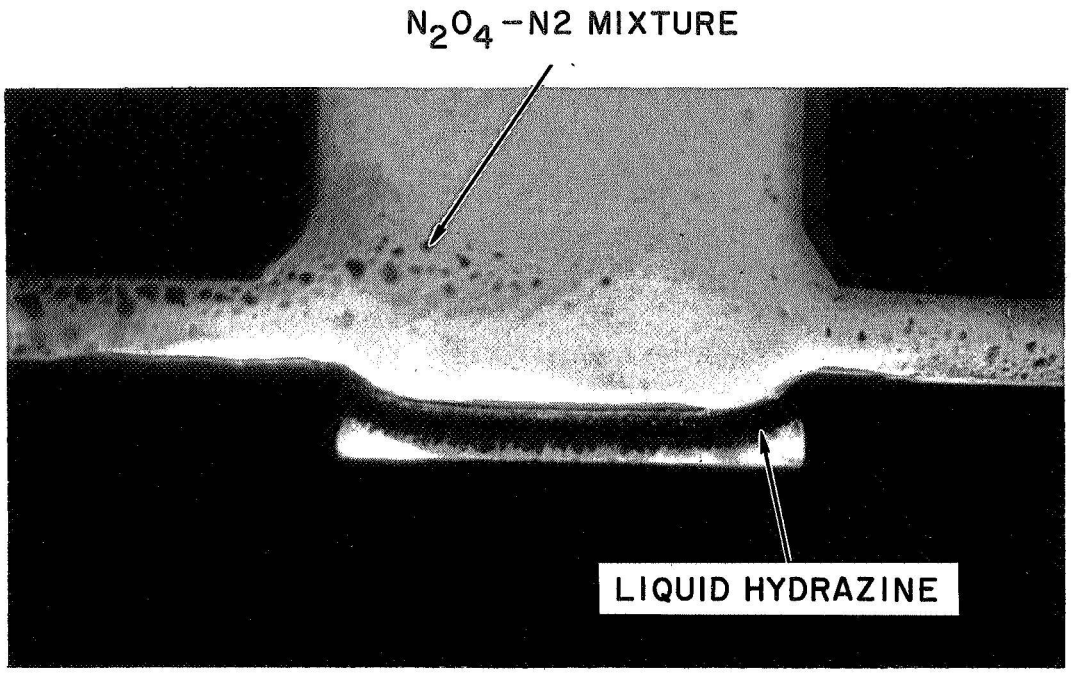

Figure 13. Foaming and Bubbling During Preignition Reactions

$$\Omega = -\sum \omega h_i^{\circ} = D_1 Q \kappa_o \kappa_f e^{\theta/T} \tag{62}$$

By appropriately defining κ_o, κ_f and θ, the location of maximum reaction $\bar{\zeta}$ can be obtained by solving $\partial\Omega/\partial\zeta \mid_{\zeta=\bar{\zeta}} = 0$. Variation of $\Omega(\zeta^*, \bar{\zeta}, \tau)$ for different liquid temperatures τ can give us information regarding vapor phase ignition.

Prior to ignition the fuel and oxidizer concentrations and the local gas temperatures correspond very closely to that of nonreactive flow. The solutions to the nonreactive flows can be easily obtained by solving the homogeneous equations of (51), (52), and (53). Denote $\bar{\kappa}_f$, $\bar{\kappa}_o$, and $\bar{T}$ as the fuel and oxidizer concentrations and the gas temperature for nonreactive flows,

$$\bar{\kappa}_f = f(\tau)\,[1-\mathrm{Erf}\,(\zeta, \zeta^*)] \tag{63}$$

$$\bar{\kappa}_o = 1-f(\tau)\,[1-\mathrm{Erf}\,(\zeta, \zeta^*)] \tag{64}$$

$$\bar{T} = (1-\tau)\,\mathrm{Erf}\,(\zeta, \zeta^*) + \tau \tag{65}$$

$$\mathrm{Erf}\,(\zeta,\zeta^*) = \frac{\mathrm{erf}\,(\zeta^*) + \mathrm{erf}(\zeta)}{\mathrm{erf}(\zeta^*) + 1}$$

and

$$\mathrm{erf}(\zeta) = \frac{1}{2\sqrt{\pi}} \int_0^{\zeta} e^{-t^2}\, dt$$

ζ^* is defined by equation (61) and can similarly be approximated by

$$\zeta^* e^{\zeta^{*2}} [\mathrm{erf}(\zeta^*) + 1] = \frac{1}{\sqrt{\pi}} \frac{f(\tau)}{1-f(\tau)} \tag{66}$$

Based on equations (63) - (65), the reaction rate prior to ignition, Eq. (62) can be approximated by

$$\Omega = D_1 Q f(\tau)\,[1-\mathrm{Erf}\,(\zeta, \zeta^*)]\,[1-f(\tau)(1-\mathrm{Erf}(\zeta, \zeta^*))] \exp\left[-\frac{\theta}{(1-\tau)\,\mathrm{Erf}\,(\zeta, \zeta^*) + \tau}\right] \tag{67}$$

$$x \exp\left[-\frac{\theta}{(1-\tau)\ \mathrm{Erf}\ (\zeta,\zeta^*)+\tau}\right] \tag{67}$$

The location of maximum reaction $\bar{\zeta}$ is obtained by solving $\frac{\partial \Omega}{\partial \bar{\zeta}} \Big| \zeta=\bar{\zeta} = 0$. and is expressed as

$$[1-\mathrm{Erf}\ (\bar{\zeta},\zeta^*)]\quad 2\ f(\tau) - \frac{1-f(\tau)\ [1-\mathrm{Erf}(\bar{\zeta},\zeta^*)]}{(1-\tau)\mathrm{Erf}(\bar{\zeta},\zeta^*)+\tau} = 1 \tag{68}$$

The rate of reaction prior to ignition at $\zeta = \bar{\zeta}$ is

$$\Omega(\zeta^*,\bar{\zeta},\tau) = D_1\ Q f(\tau)\ [1-\mathrm{Erf}\ (\bar{\zeta},\zeta^*)][1-f(\tau)(1-\mathrm{Erf}\ (\bar{\zeta},\zeta^*)]\quad \exp\left[-\frac{\theta}{(1-\tau)\mathrm{Erf}(\bar{\zeta},\zeta^*)+\tau}\right] \tag{69}$$

The problem is now reduced to the solutions of equations (66), (68), and (69), and for the three unknown quantities, ζ^*, $\bar{\zeta}$, and $\Omega(\zeta^*, \bar{\zeta}, \tau)$ as a function of τ, liquid temperature τ at which vapor phase ignition predominates can be defined. Numerical solutions of equations (66), (68), and (69) have not yet been attempted.

Bubble Formation in the $N_2O_{4(g)}$-$N_2H_{4(\ell)}$ Reaction

In an idealized picture of a gas such as N_2O_4 reacting at the surface of a liquid, such as N_2H_4, a smooth composition profile can be postulated between the liquid surface and some remote boundary in the gas. In particular, if the liquid temperature is well below the boiling point and the conditions being examined involve the relatively low temperature reactions leading to ignition, one would not expect bubble formation in the liquid phase. It is possible, however, to postulate bubble formation by considering only slight departures from the pure diffusion idealized model generally used.

One factor which could lead to bubble formation at or near the liquid surface would be the result of solution of some of the vapor phase oxidant in the liquid. The result of dissolving some oxidant in the liquid could be a bi-propellant liquid phase reaction near the surface. If a gas were produced by the reaction then bubbles would be observed. A low temperature reaction between hydrazine and N_2O_4 has been observed which produces ammonium nitrate and various gas products which could account for bubble formation. One would expect that the rate of bubble formation (or number of bubbles) might decrease as the liquid temperature increased. Although liquid temperature rise increases the rate of gas forming reactions, the greater partial pressure of

liquid vapor inhibits diffusion of the gas phase oxidant. The bubble formation also increases with partial pressure of oxidant at constant liquid temperature.

An equally plausible mechanism for bubble formation involves the surface reactions directly, particularly where solids (partially or completely soluble in the liquid) are formed as well as gases. The surface reactions produce solids such as ammonium nitrate which dissolves in the liquid slowly but which also traps gas formed in the same reaction. Reactions continue below the surface and involve the dissolved nitrates as well as the trapped gas. The evolution of gas by this mechanism increases with increased oxidant gas partial pressure.

Based on the stagnation flow field, the ignition phenomenon of liquid hydrazine has been recorded using motion pictures. From the pictures it would seem that the change from bubble formation to gas phase reaction might be associated with the liquid temperature which in turn governs the rate of fuel evaporation.

Surface reaction, bubbles, and foaming could be anticipated when the liquid fuel is at a low temperature. Reactions of the type

$$6\ N_2H_4 + 5\ N_2O_4 = 5\ NH_4NO_3 + 3\ N_2O + 3N_2 + 2\ H_2O$$

and

$$N_2H_4 + 2\ NO_2 = NH_4NO_3 + N_2O$$

often takes place. The NH_4NO_3 dissolves and reacts

$$NH_4NO_3 + N_2H_4 = N_2H_5NO_3 + NH_3$$ producing bubbles and foam.

Similarly if $N_2H_5NO_3$ is formed then

$$6\ N_2H_5NO_3 + 2\ NO_2 = N_2O + 3\ N_2 + 6\ NH_4NO_3 + 3\ H_2O$$

could liberate gas.

CONCLUSIONS

Quantitative analysis of the distribution of products due to gas phase reactions of unsymmetrical dimethylhydrazine/nitrogen dioxide and monomethylhydrazine/nitrogen dioxide at low concentrations ($\approx$ 1-6 mole %) and low temperature (25°C) gave N_2O and N_2 as the main gaseous products when the system was fuel rich and NO when the system was oxidizer rich. With an excess of monomethylhydrazine, monomethylhydrazinium nitrate was found to be the main solid intermediate. With an excess of nitrogen dioxide, ammonium nitrate was found to be the main solid intermediate. This was similar to that of hydrazine/nitrogen dioxide reactions where hydrazinium nitrate and ammonium nitrate were respectively the main solid intermediates. In the case of unsymmetrical dimethylhydrazine, both fuel rich and oxidizer rich conditions gave ammonium nitrate. Quantitative results from these preignition chemistry studies can also be used as inputs to certain mathematical space start model (Ref. 14). The reason for this is that any clarification of detonable and sensitizing substances, together with the associated preignition heat release and gas formation, will help predict chamber pressurization and the chemical species present in the chamber at ignition.

An ignition burner based on the principle of stagnation flow was used to conduct ignition studies of liquid diborane and oxygen difluoride. The experiment was not very successful because of difficulties encountered in maintaining sufficient amount of liquid diborane in the diborane cup. Detonation waves were observed where pure oxygen difluoride was introduced to flow over liquid diborane.

The experimental technique developed during this program of introducing the oxidizer gas to flow over liquid fuel has great advantages in ignition studies. The randomness and the uncertainties of fluid dynamics are removed and each of the transport rate processes leading to ignition can be studied individually so as to integrate combustion theory with that of chemical kinetics. Based on this technique, experimental parameters which are easily controlled are (i) fuel temperature, (ii) oxidizer temperature, (iii) oxidizer concentration, (iv) burner pressure, and (v) oxidizer flow velocity. This experimental technique is presently being used to study the ignition of polymeric materials. (Ref. 24)

To understand the ignition phenomena in more detail, an analytical study has been carried out based on the stagnation flow field. The purpose of this study is to define propellant temperature ranges where vapor phase reaction is dominant. Based on the similarity flow field, the governing partial equations were reduced to a set of ordinary differential equations. Realizing the fact that prior to ignition, the species concentrations and gas temperatures do not vary much from the nonreactive flows, the nonreactive solutions were used to describe the rate of reaction. When the hydrazine vapor concentration, given off by the liquid, is not high enough to sustain a vapor phase ignition, reactions could occur between nitrogen tetroxide and liquid hydrazine. The dissolved solid products produced by the preignition reactions contaminate the liquid fuel to the extent of changing its ignition characteristics significantly from that of a "clean" fuel. Determining the range of pressure and temperature conditions within which the vapor/liquid or vapor/vapor reactions predominate were important.

REFERENCES

1. Kappl, J. J.; Knox, R.M.: Altitude Ignition of Hypergolic Bipropellant Rockets. The Marquardt Corp.

2. Bernard, M.L.J.; and Dufour, J: On the Existence of Detonation Conditions in the Combustion of Some Nitric Acid Propellants. 8th Intl Symposium on Combustion, pp 1074.

3. Stevens, M.R.; Fisher, H.D.; Weiss, H.G.; Breen, B.P.: Effect of Additives on the Ignition Delay Time of Hypergolic Propellants." Dynamic Science Final Report NAS7-438, March 1967.

4. Stevens, M.R.; Fisher, H.D.; Weiss, H.G.; Breen, B.P.: Effect of Additives on the Ignition Delay Time of Hypergolic Propellants, Western Combustion Conference, WSC1-67-22.

5. Lawver, B.R.; and Breen, B.P. "Hypergolic Stream Impingement Phenomena Nitrogen Tetroxide/Hydrazine. Dynamic Science NAS7-467 NASA/Lewis, CR-72444, October 1968.

6. Weiss, H.G.; Johnson, B.; Fisher, H.D.,; and Gerstein, M.: Modifications of the Hydrazine-Nitrogen Tetroxide Ignition Delay. AIAA Journal, Vol. 2, No. 12, pp 2222 (Dec. 1964).

7. Skinner, B.G.; Hedley, W.H.; Snyder, A.D.: Mechanism and Chemical Inhibition of the Hydrazine-Nitrogen Tetroxide Reaction. ASD-TDR-62-1041, Monsanto Research Corp. (Dec. 1962).

8. Mayer, S. W.; Taylor, D.; Schieler, L.: Preignition Products from Storable Propellants at Simulated High-Altitude Conditions.

9. Symposium on Hypergolic Vacuum Ignition Phenomena. Manned Spacecraft Center, Houston, Texas, Nov. 15-16, 1967.

10. Perlee, H. E.; Christos, T.; Miron, Y.; James, H.D.: Preignition Phenomena in Small A-50/NTO Pulsed Rocket Engines. AIAA 3rd Prop. Jt. Specialist Conference, No. 67-415 (July 1967).

11. Seamans, T.F. and Dawson, B. E.: Hypergolic Ignition at Reduced Pressures. Tech. Rpt. HFRPL-TR-67-129. Thiokol Chemical Corporation, Reaction Motors Division (June 1967).

12. Zung, L.B.; Tkachenko, E.A.; Breen, B.P.: A Basic Study of the Ignition of Hypergolic Liquid Propellants. Dynamic Science Rpt. SN-80-Mod 3-F, NAS7-438, July 1968.

13. NASA/OART Space Storable Propulsion Technology Review, Lewis Research Center, Cleveland, Ohio, June 13-14, 1968.

14. Mills, T. R.; Tkachenko, E.A.; Lawver, E.A.; Breen, B.P.: Transients Influencing Rocket Engine Ignition and Popping. Final Rept. SN-95D Dynamic Science Contract NAS7-467,

15. Zung, L. B.; Breen, B.P.; Kushida, R.: A Basic Study of Ignition of Hypergolic Liquid Propellants. Western States Section/The Combustion Institute. Paper No. 68-43.

16. Potter, A.E.; Butler, J.N.: A Novel Combustion Measurement Based on the Extinguishment of Diffusion Flames. ARS J. Vol. 54, pp 54-56, Jan. 1959.

17. Potter, A.E.; Heimel, S.; Butler, J.N.: Apparent Flame Strength, A Measure of Maximum Reaction Rate in Diffusion Flames. 8th Symposium (Intl) on Combustion, pp 1027-1034, Williams and Wilkins, 1962.

18. Anagoston, E.; and Potter, A.E.: Flame Strength of Propane-Oxygen Flames at Low Pressures in Turbulent Flames. 9th Symposium (Intl) on Combustion, pp 1-6, Academic Press, 1963.

19. Pandya, T.P. and Weinberg, F.J.: The Structure of Flat, Counterflow Diffusion Flames. Proc. Roy. Soc. (London), A279, pp 544-561, 1964.

20. Kushida, R.: Theory of Laminar Flames in Stagnation Flows. Western States Combustion Institute, 1967.

21. Spalding, D.B.: Theory of Mixing and Chemical Reaction in the Opposed-Jet Diffusion Flame. ARS J. Vol. 31, pp 763, 1961.

22. Jain, V.K. and Mukunda, H.S.: On the Ignition and Extinction Problems in Forced Convection System. Vol. II, pp 491, 1968.

23. Fendell, F.E.: Ignition and Extinction in Combustion of Initially Unmixed Reactants. J. Fluid Mech. Vol. 21, part 2, pp 281-303, 1965.

24. Zung, L.B.: Fundamental Ignition Study for Material Fire Safety Improvement, Contract NASW-1921. 1969.

APPENDIX A

INFRARED SPECTRUM

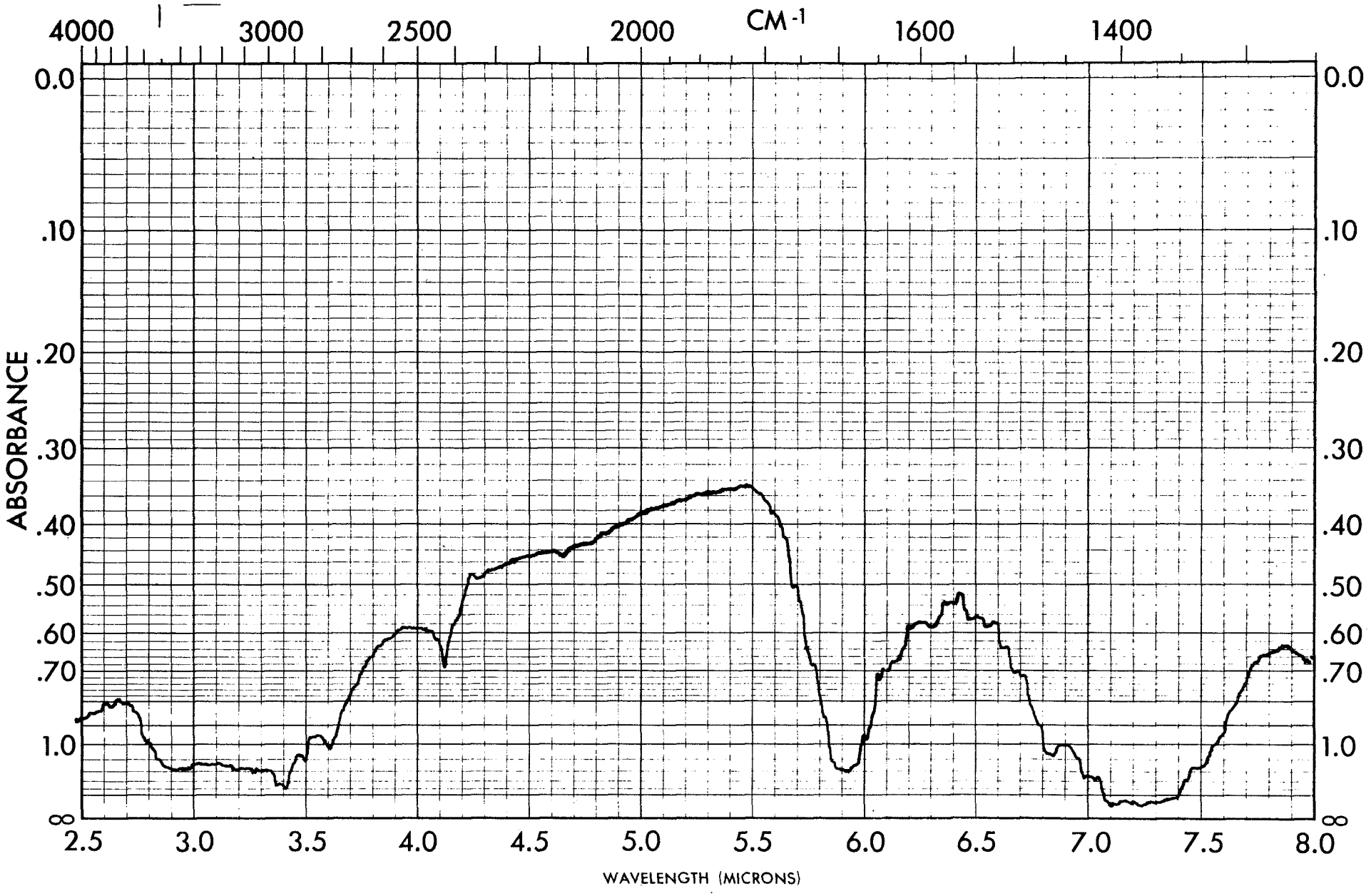

Figure 14. Infrared Spectrum - Solid #2.

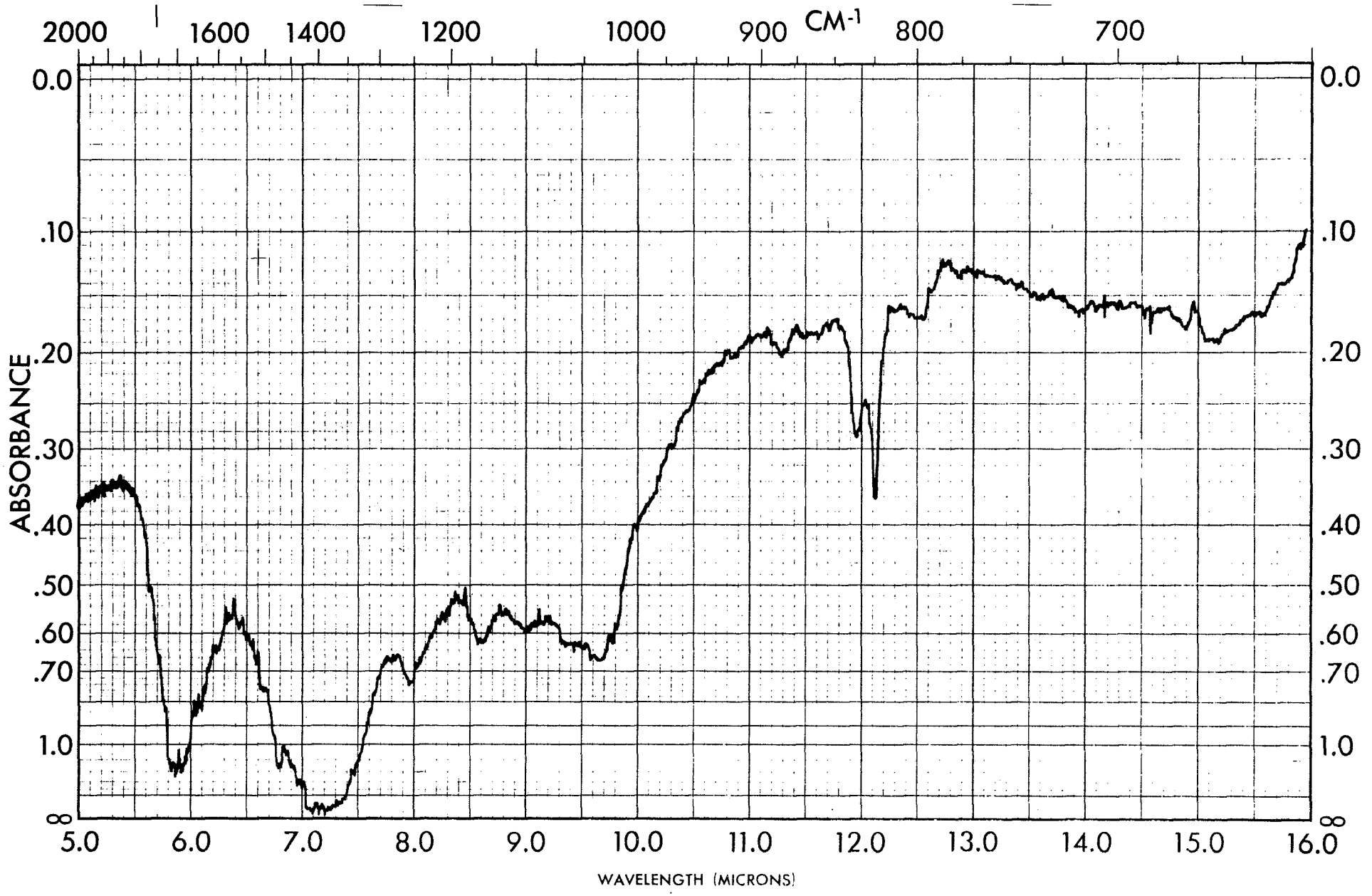

Figure 15. Infrared Spectrum - Solid #2

PRINTED IN U.S.A.

WHEN REORDERING SPECIFY CHART NO. 18920 BECKMAN INSTRUMENTS, INC., FULLERTON, CALIFORNIA, U.S.A.

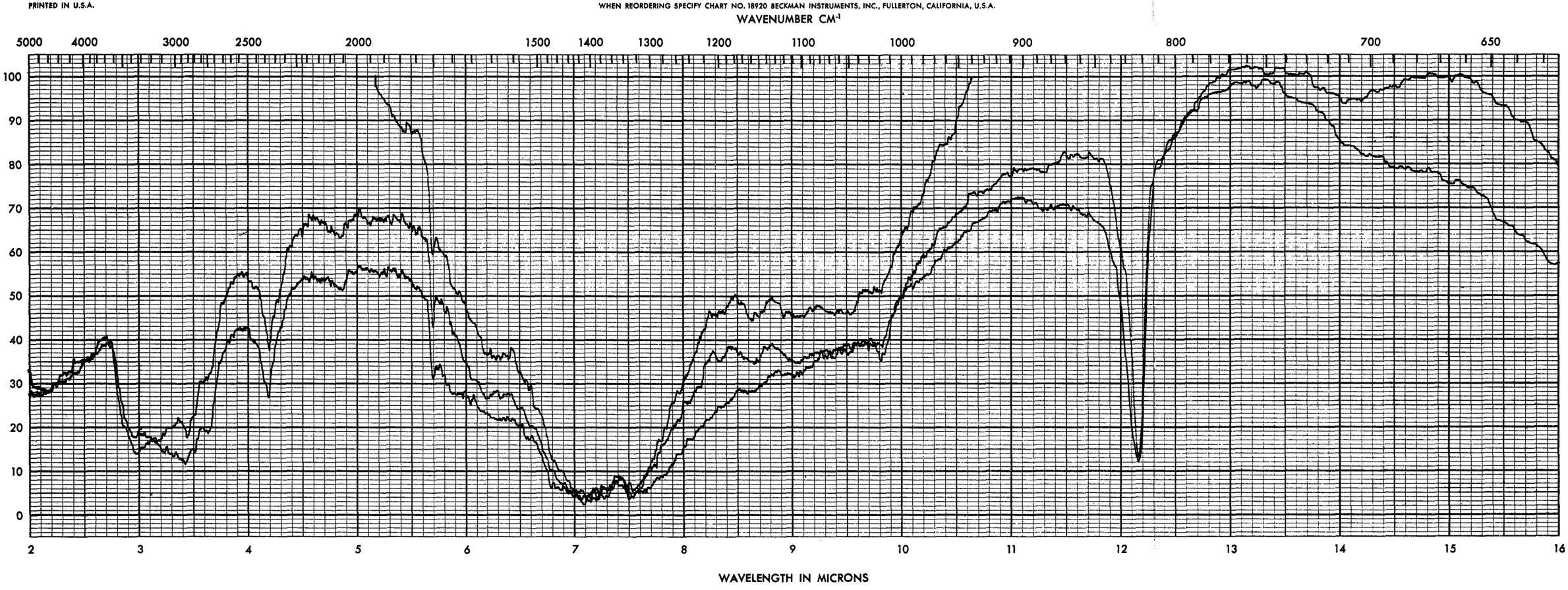

Figure 16. Infrared Spectrum - Solid #3.

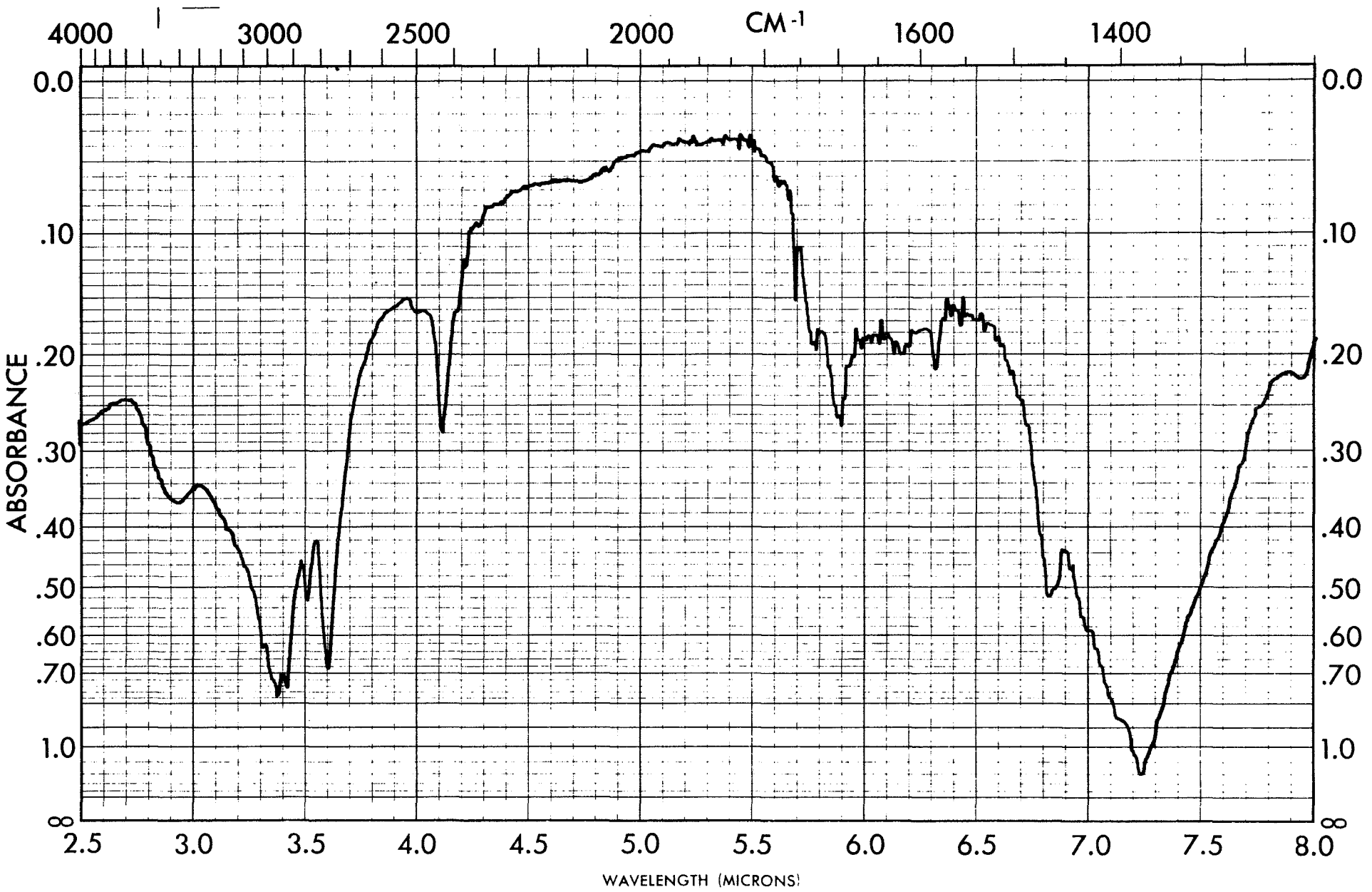

Figure 17. Infrared Spectrum - Solid #4.

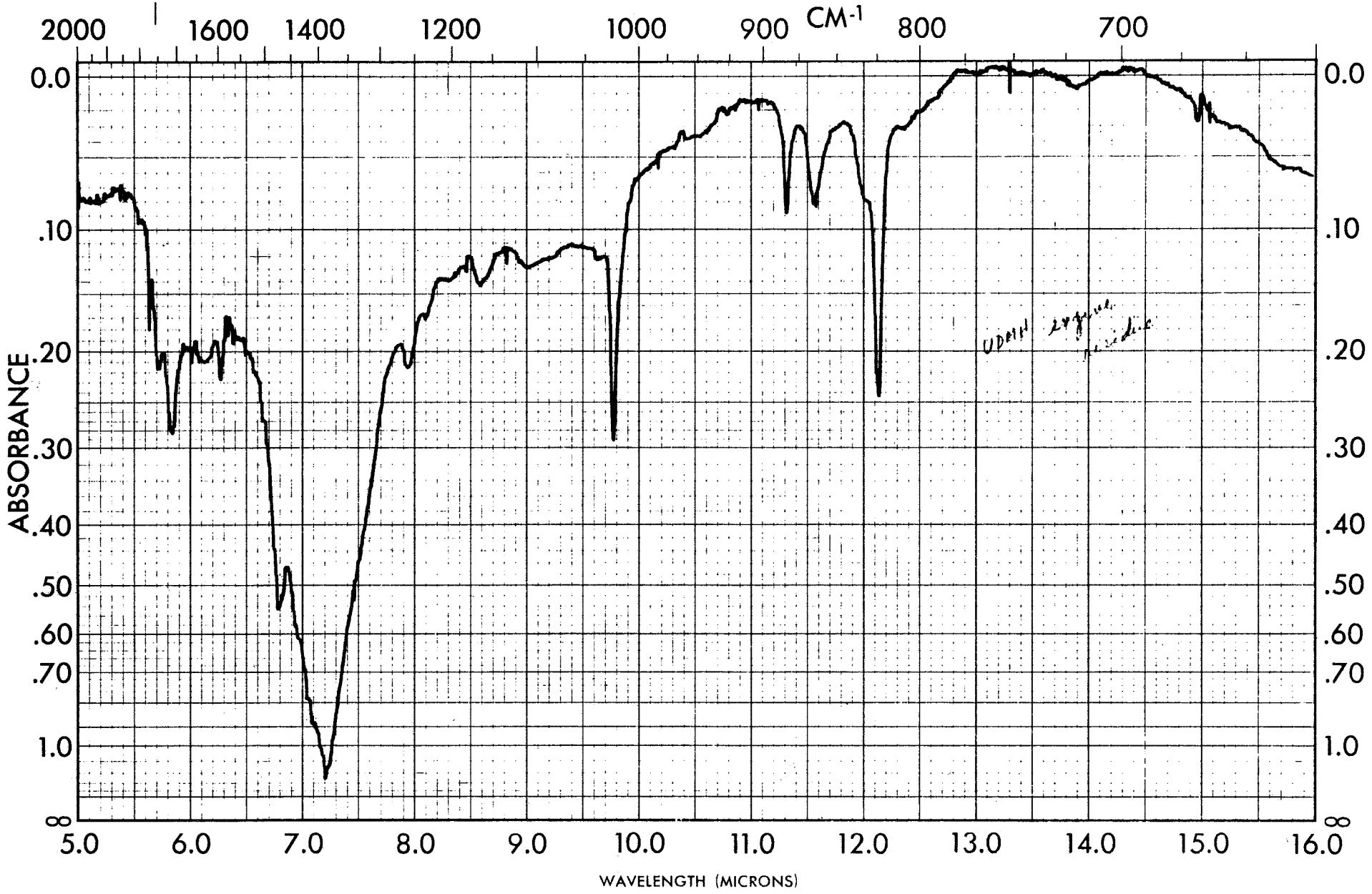

Figure 18. Infrared Spectrum - Solid #10.

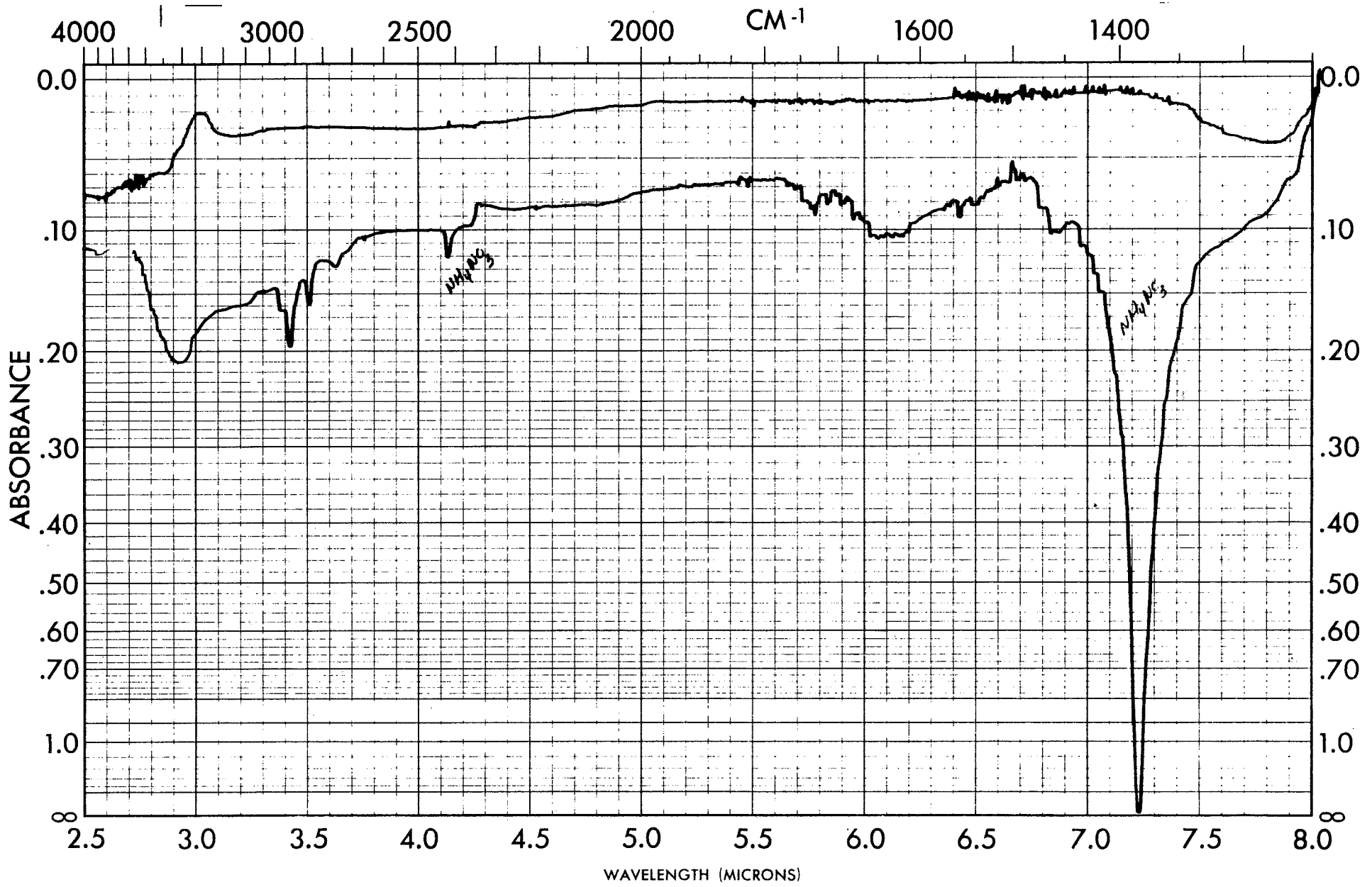

Figure 19. Infrared Spectrum - Solid #7.

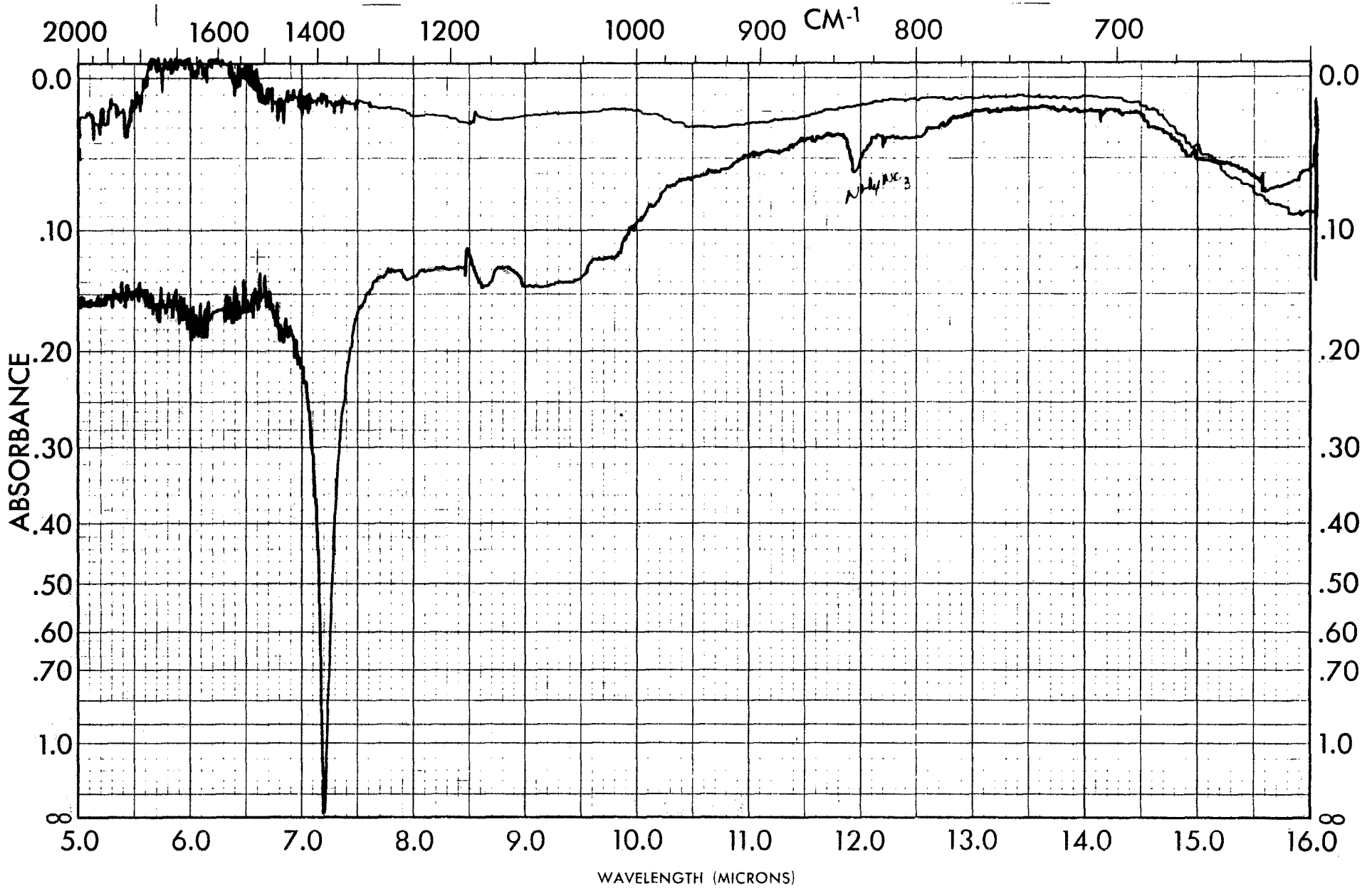

Figure 20. Infrared Spectrum - Solid #7.

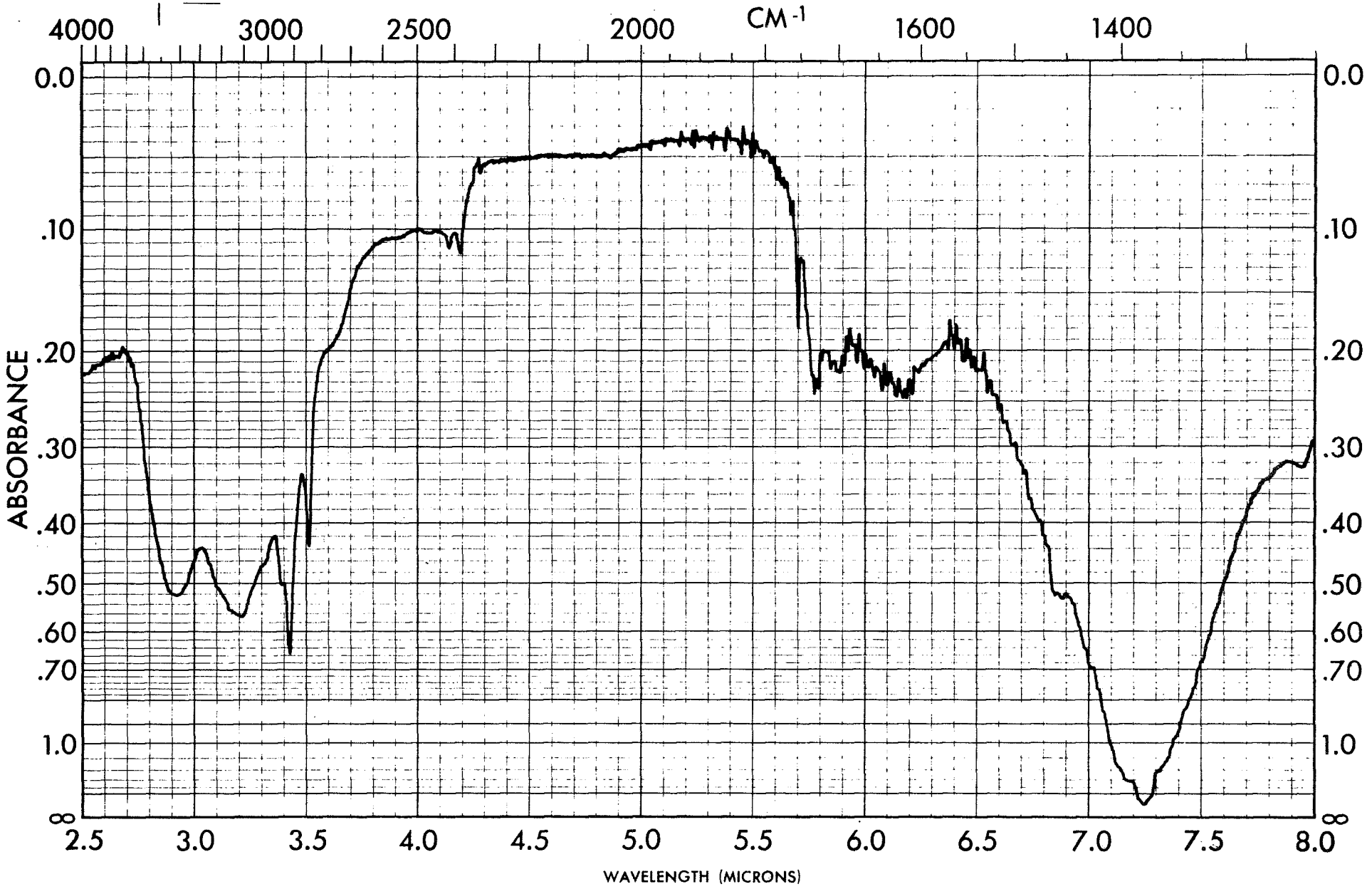

Figure 21. Infrared Spectrum - Solid #4.

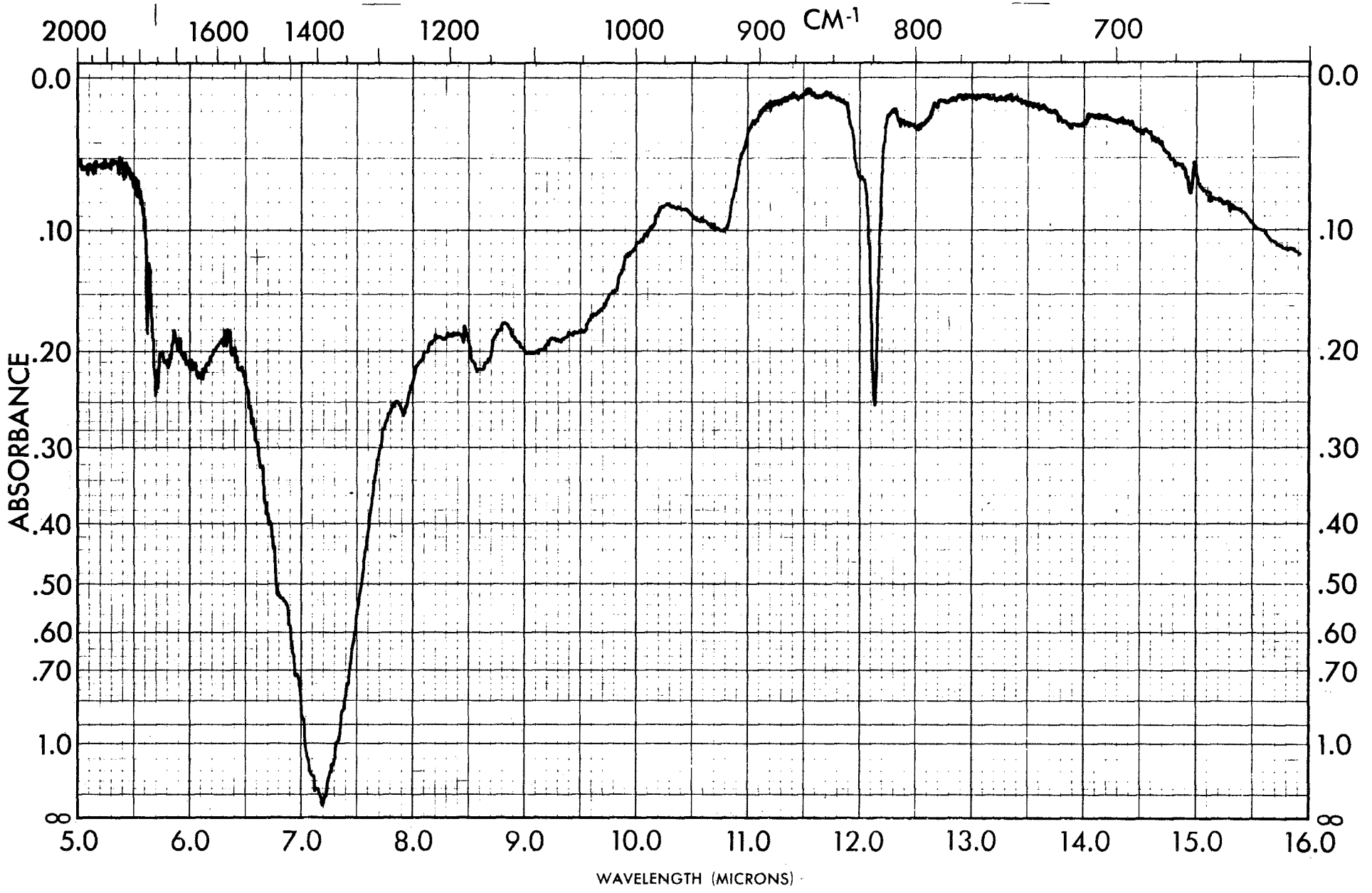

Figure 22. Infrared Spectrum - Solid #4.

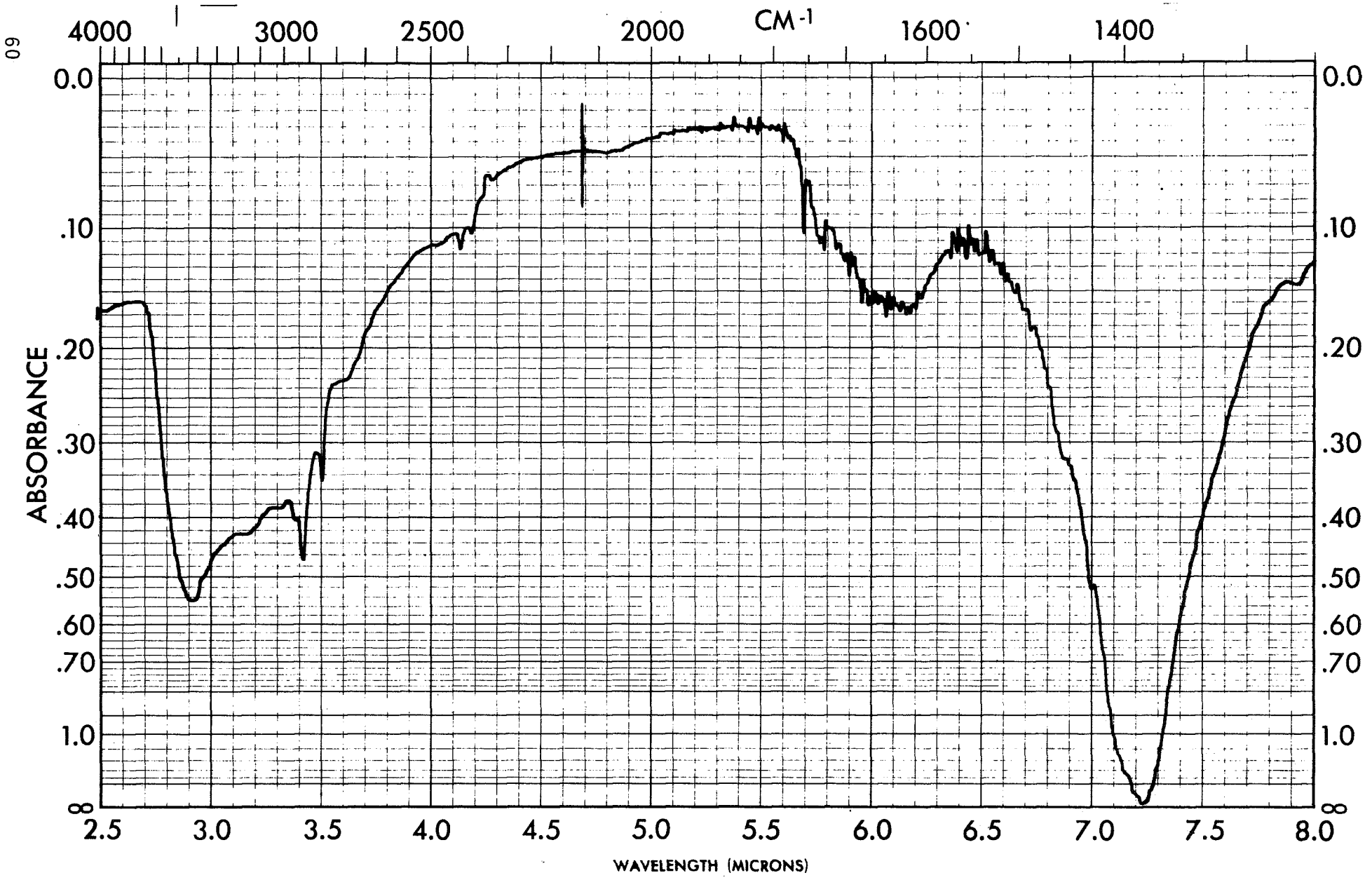

Figure 23. Infrared Spectrum - Solid #5

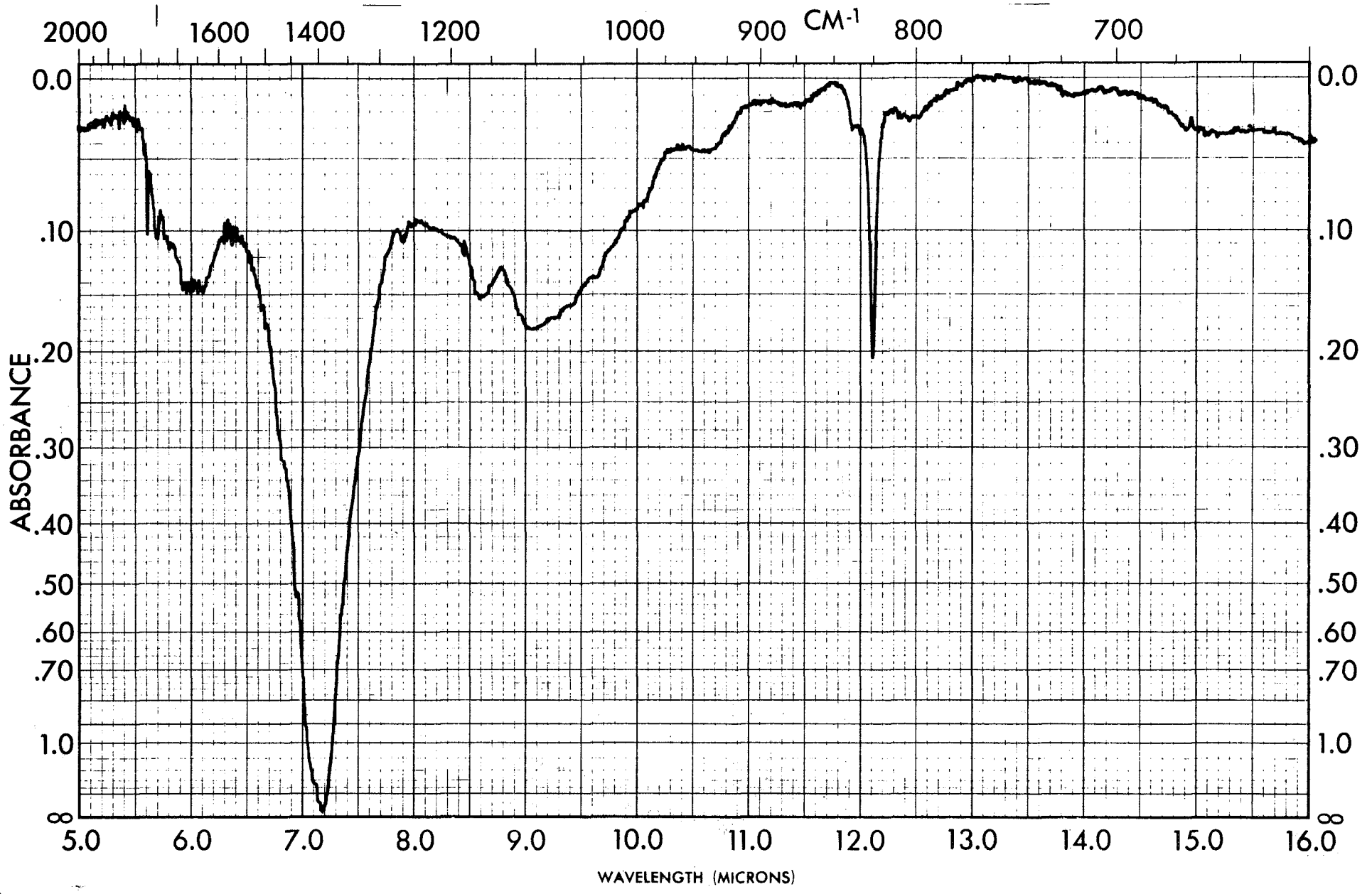

Figure 24. Infrared Spectrum - Solid #5.

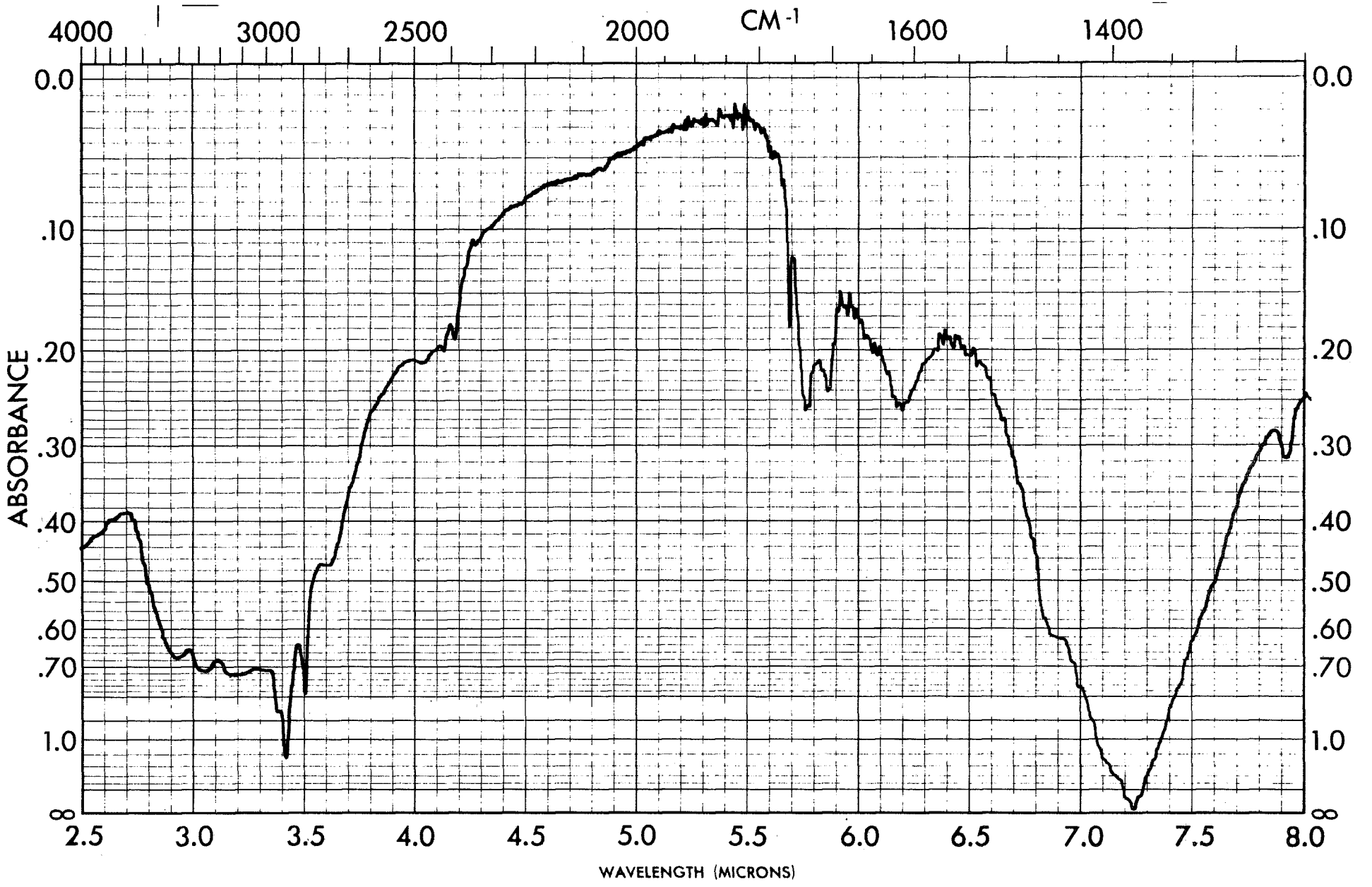

Figure 23. Infrared Spectrum - Solid #6.

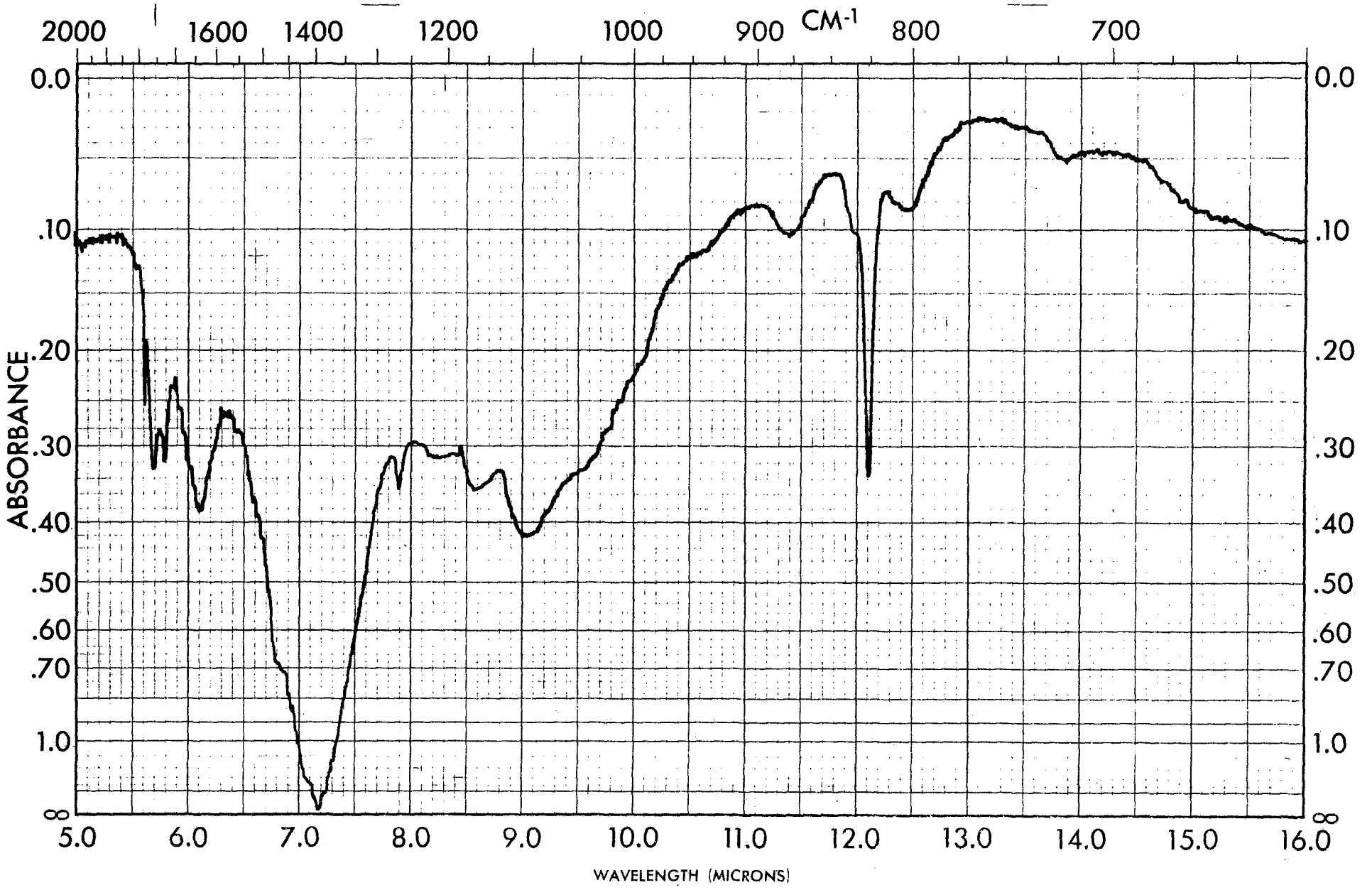

Figure 26. Infrared Spectrum - Solid #6.

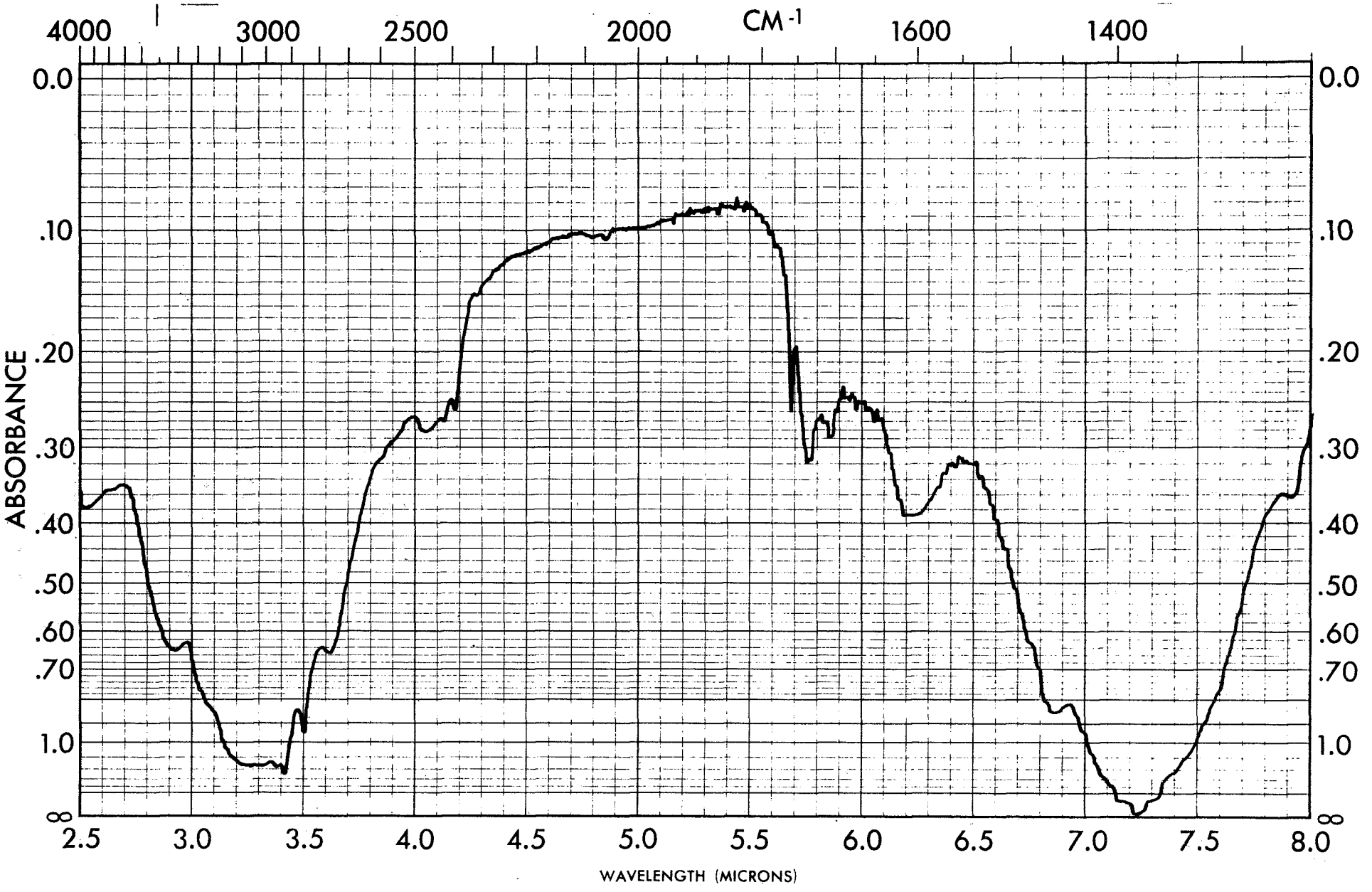

Figure 27. Infrared Spectrum - Solid #8

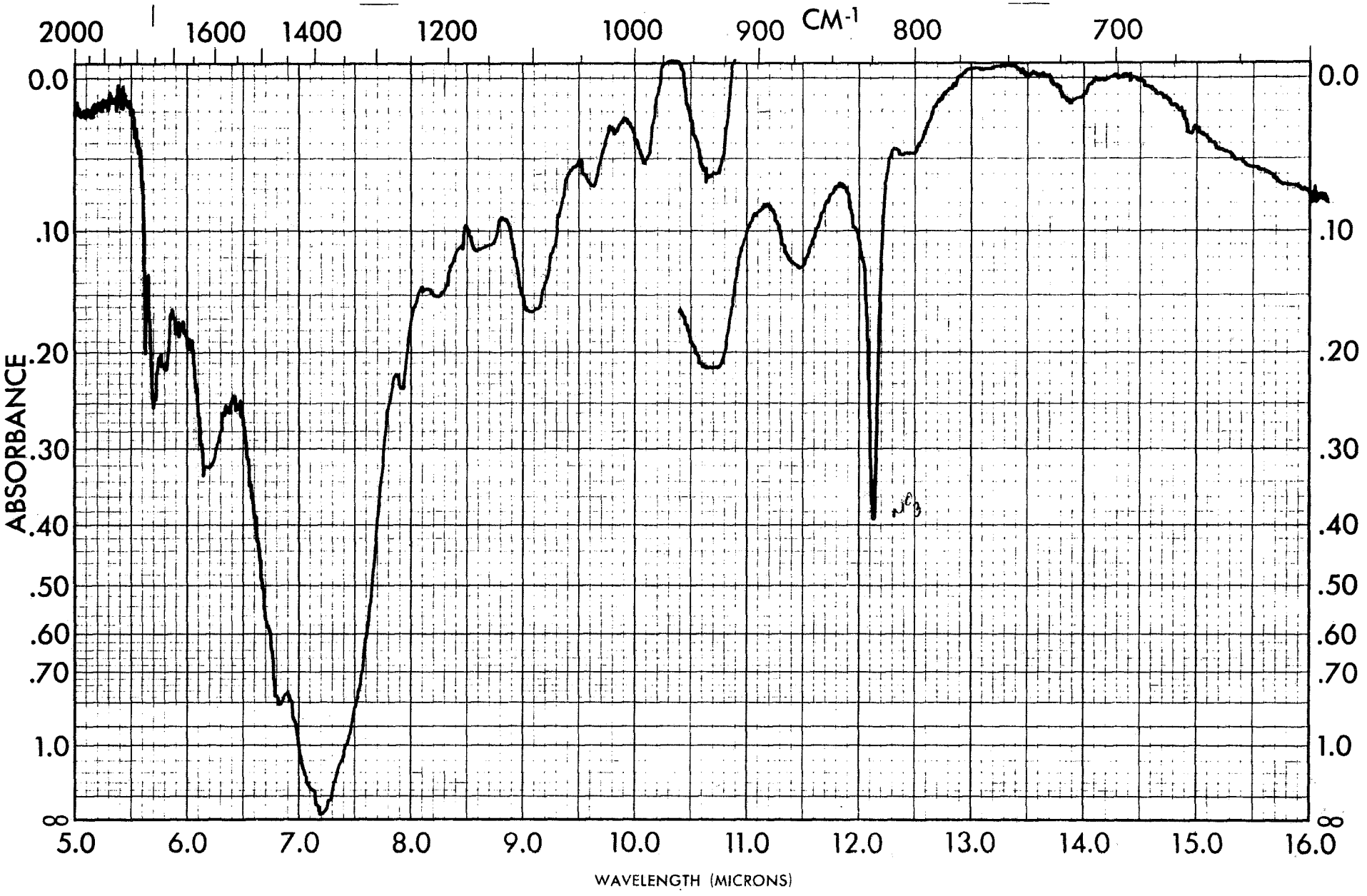

Figure 28. Infrared Spectrum - Solid #8.

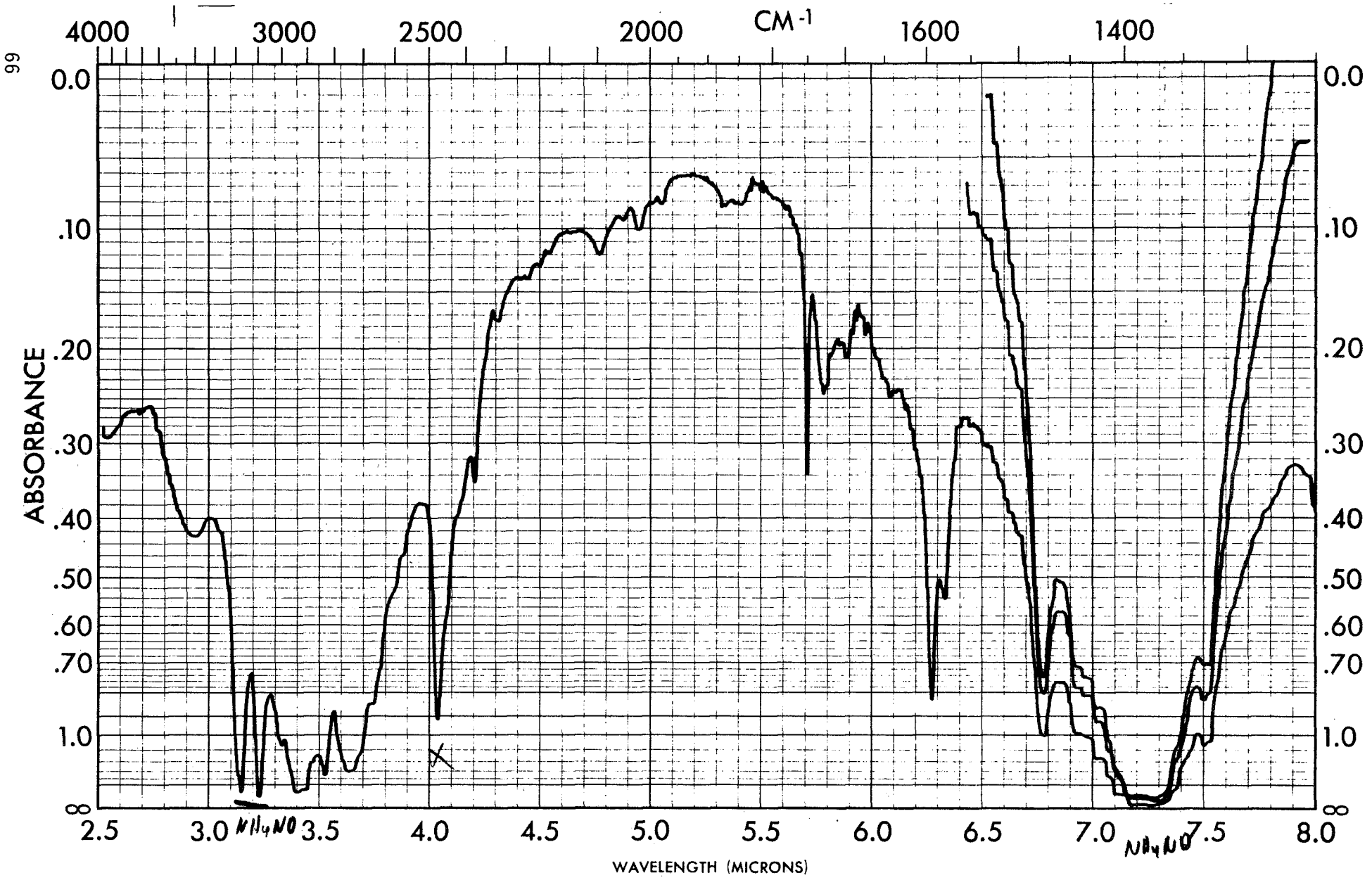

Figure 29. Infrared Spectrum - Solid #9.

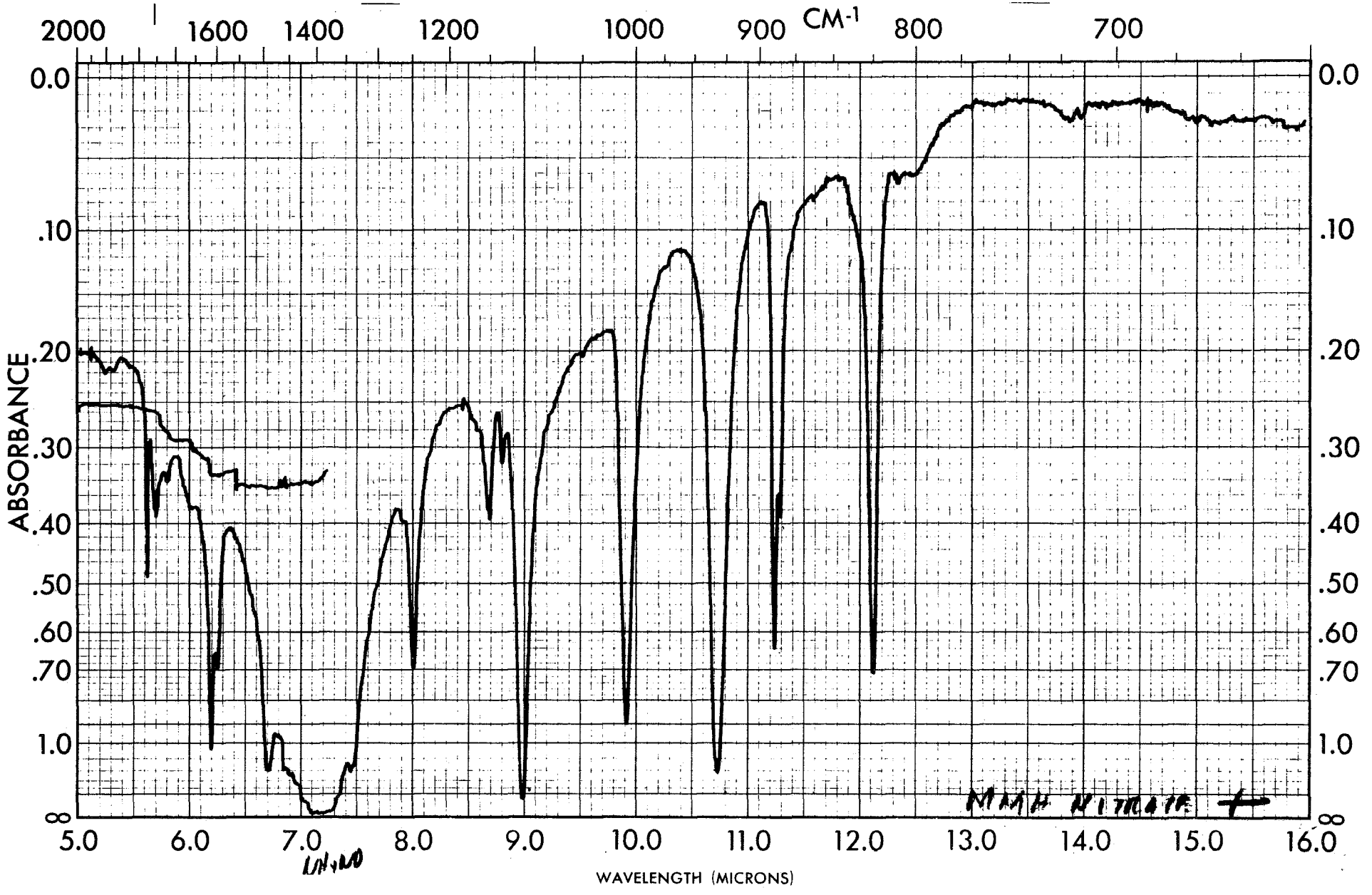

Figure 30. Infrared Spectrum - Solid #9.

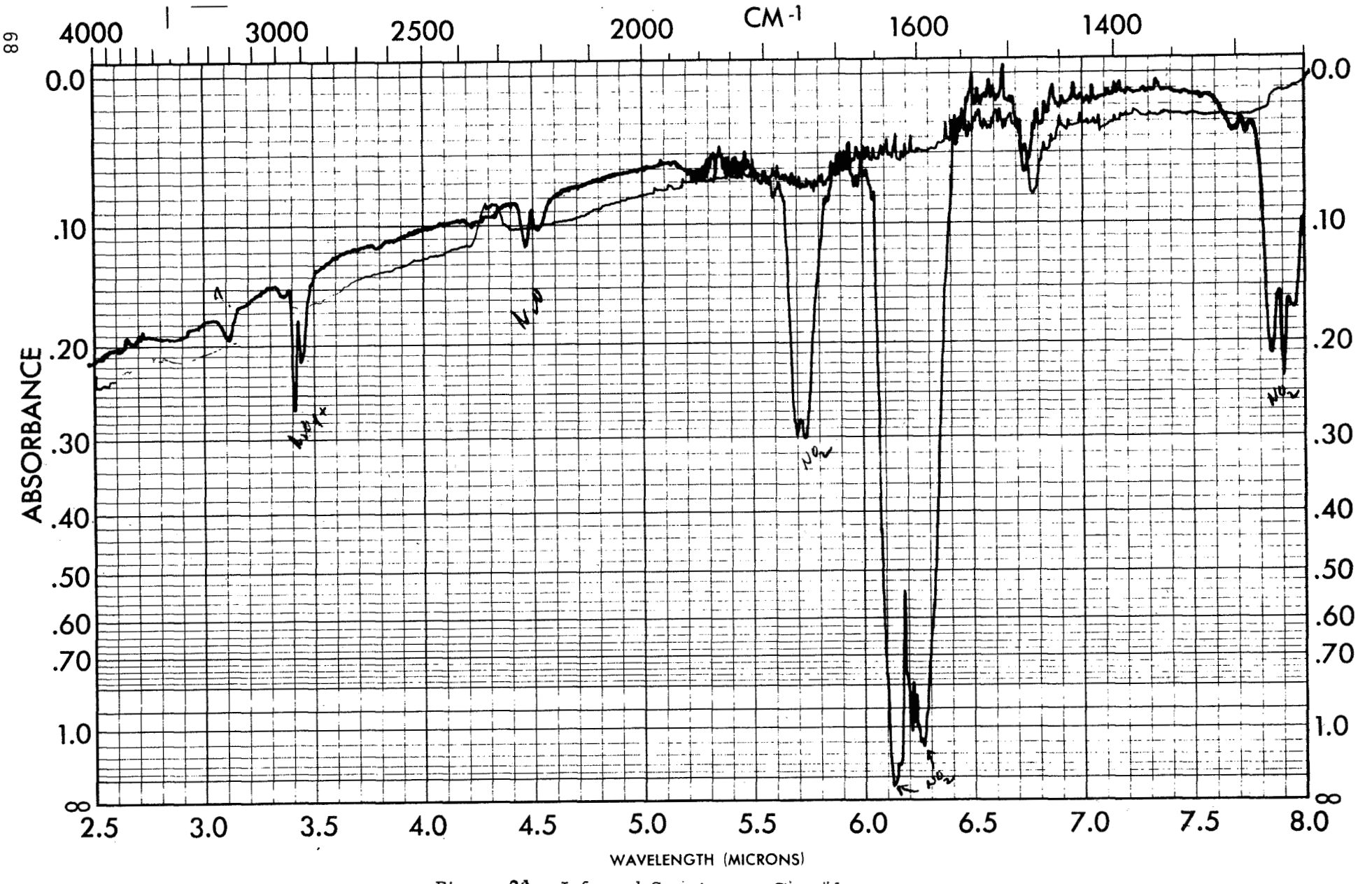

Figure 31. Infrared Spectrum - Gas #1.

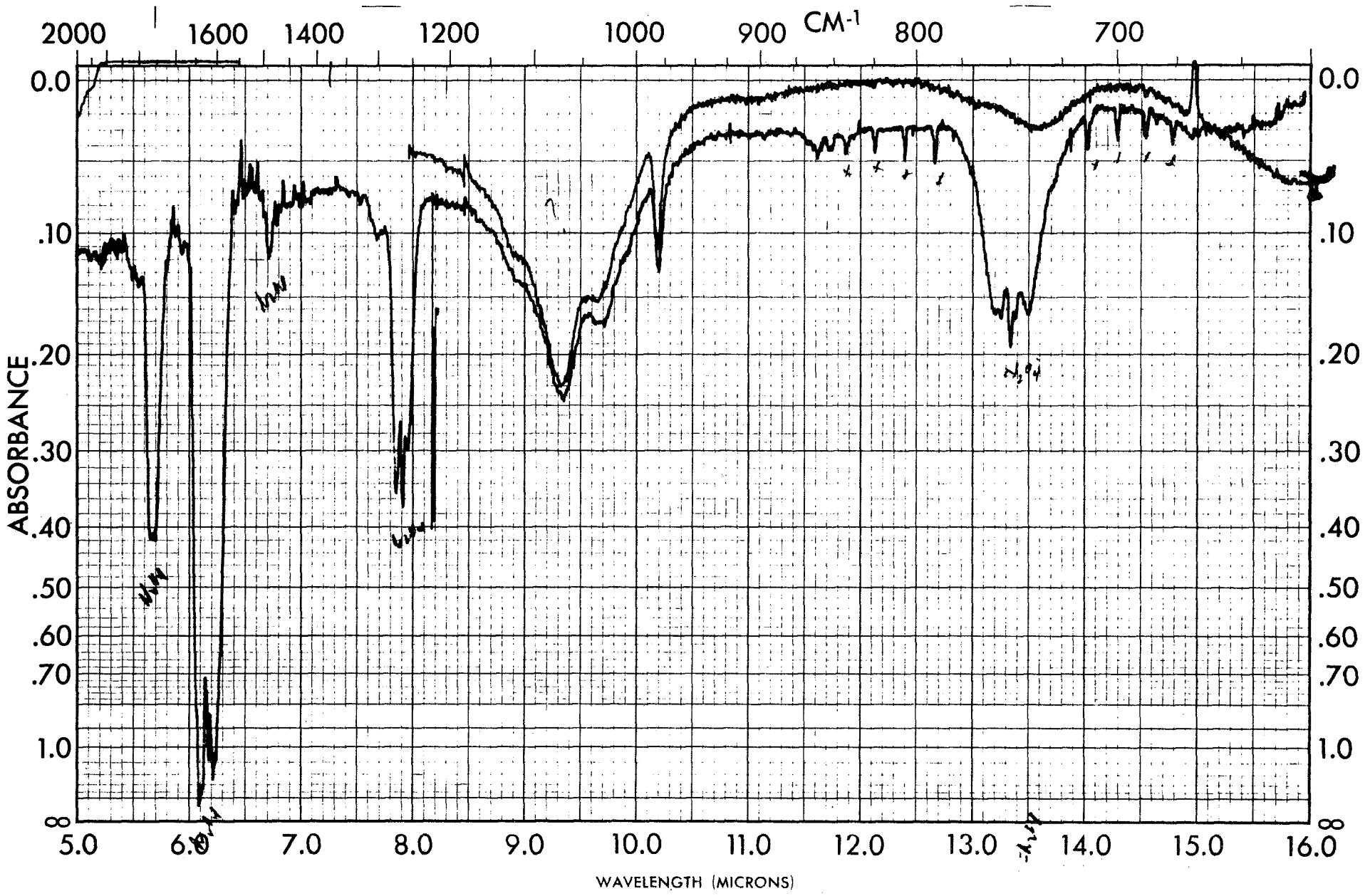

Figure 32. Infrared Spectrum - Gas #1.

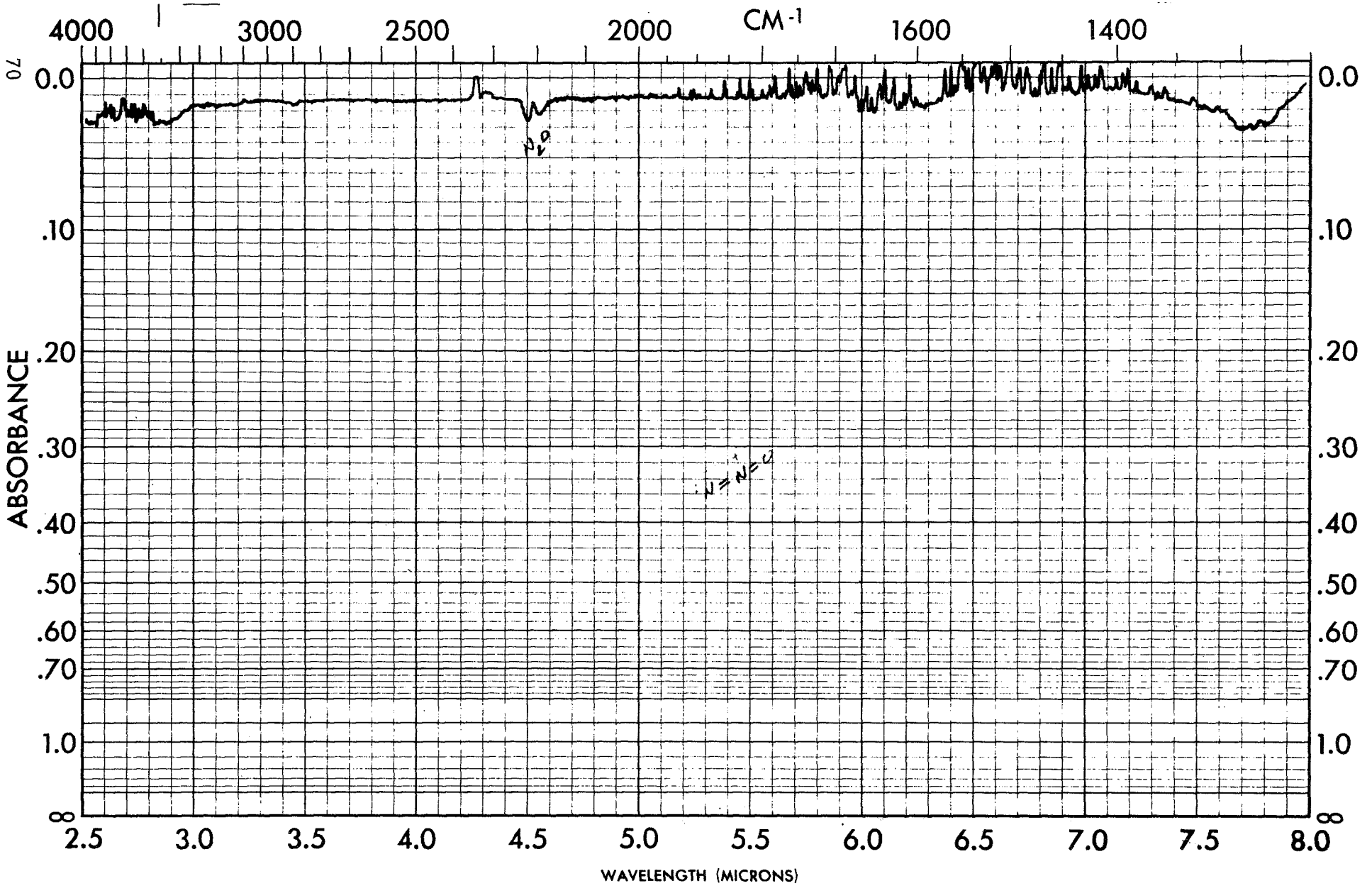

Figure 38. Infrared Spectrum - Gas #2.

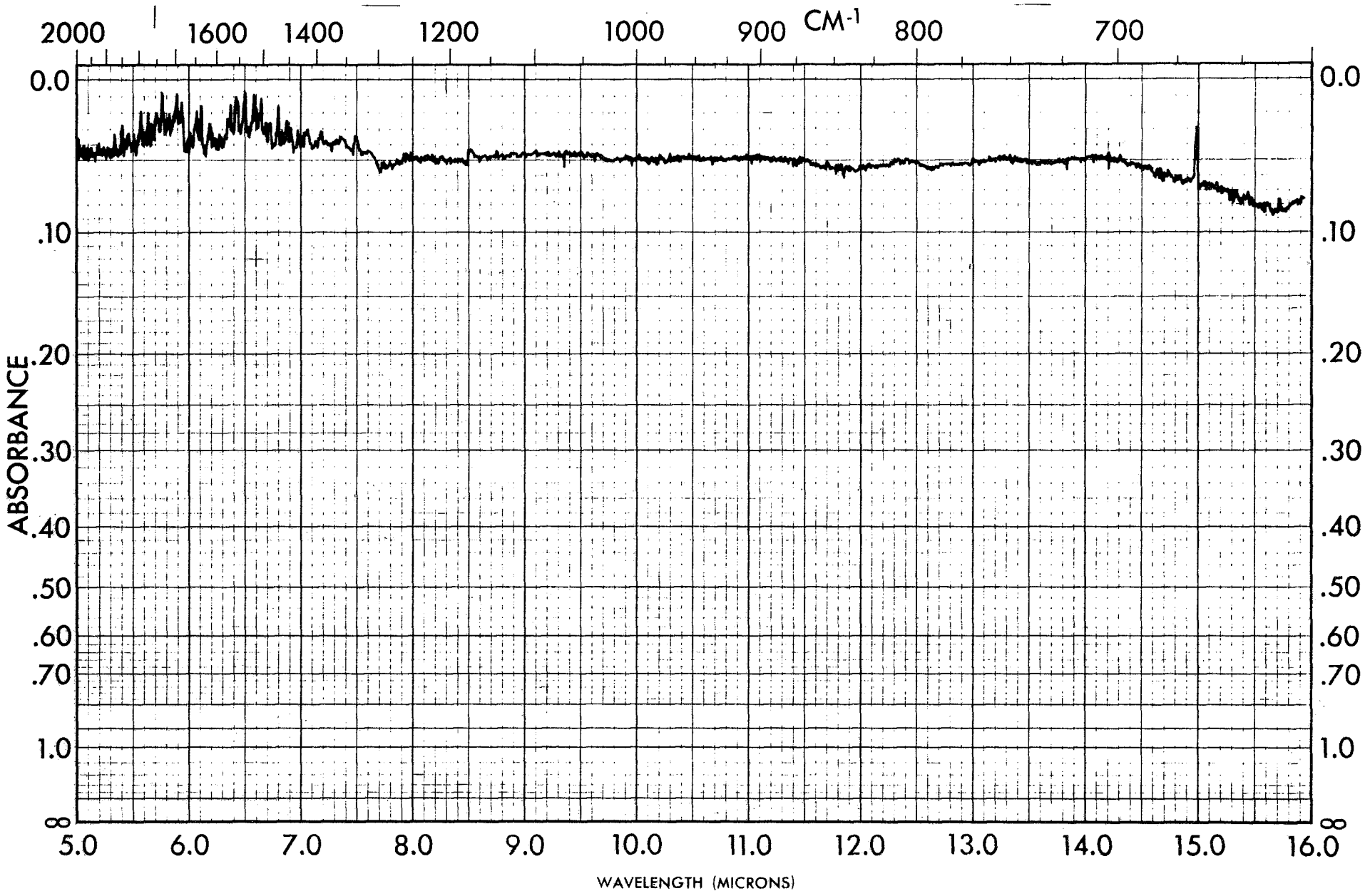

Figure 34. Infrared Spectrum - Gas #2.

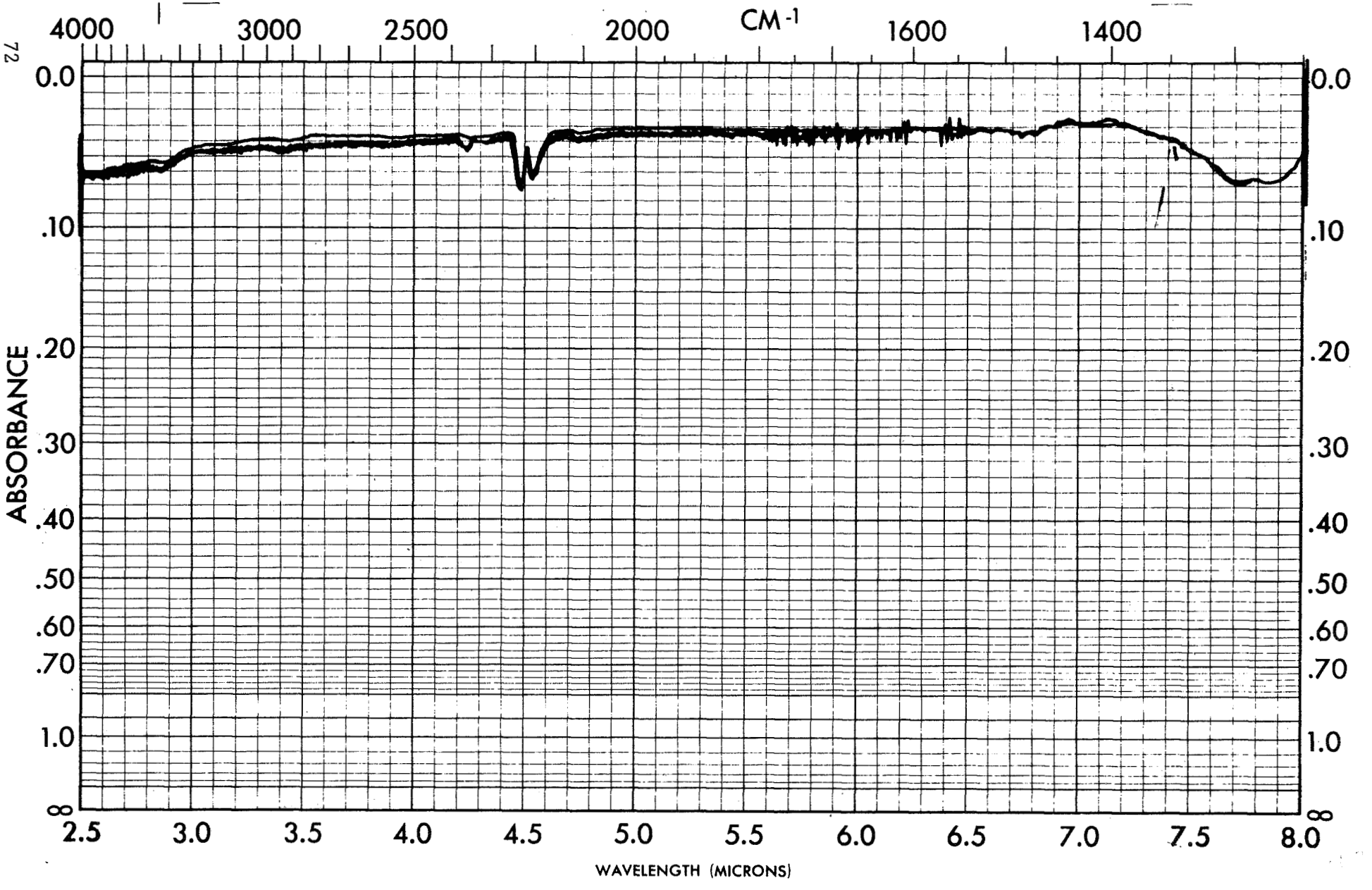

Figure 33. Infrared Spectrum - Gas #7.

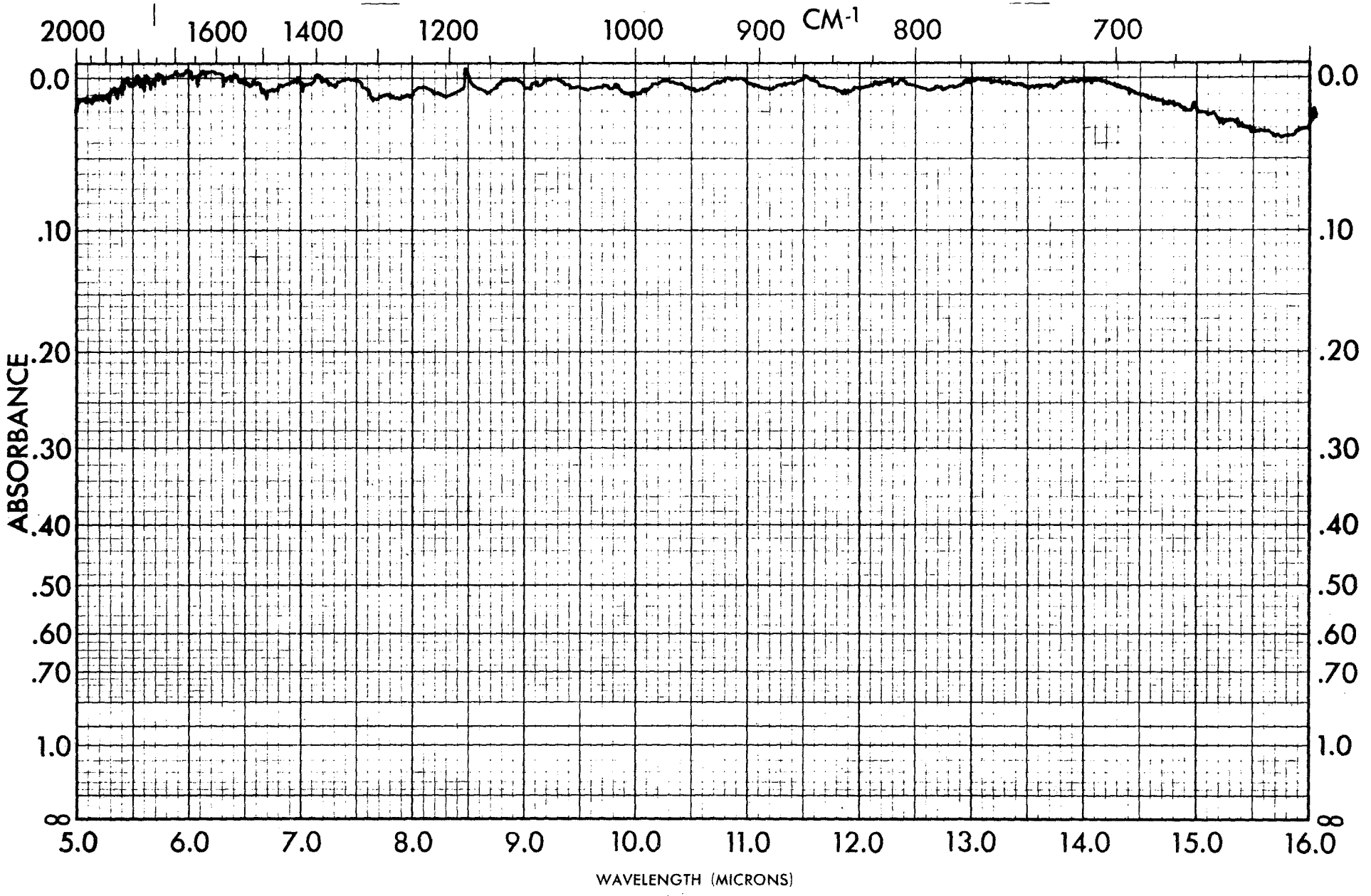

Figure 36. Infrared Spectrum - Gas #7.

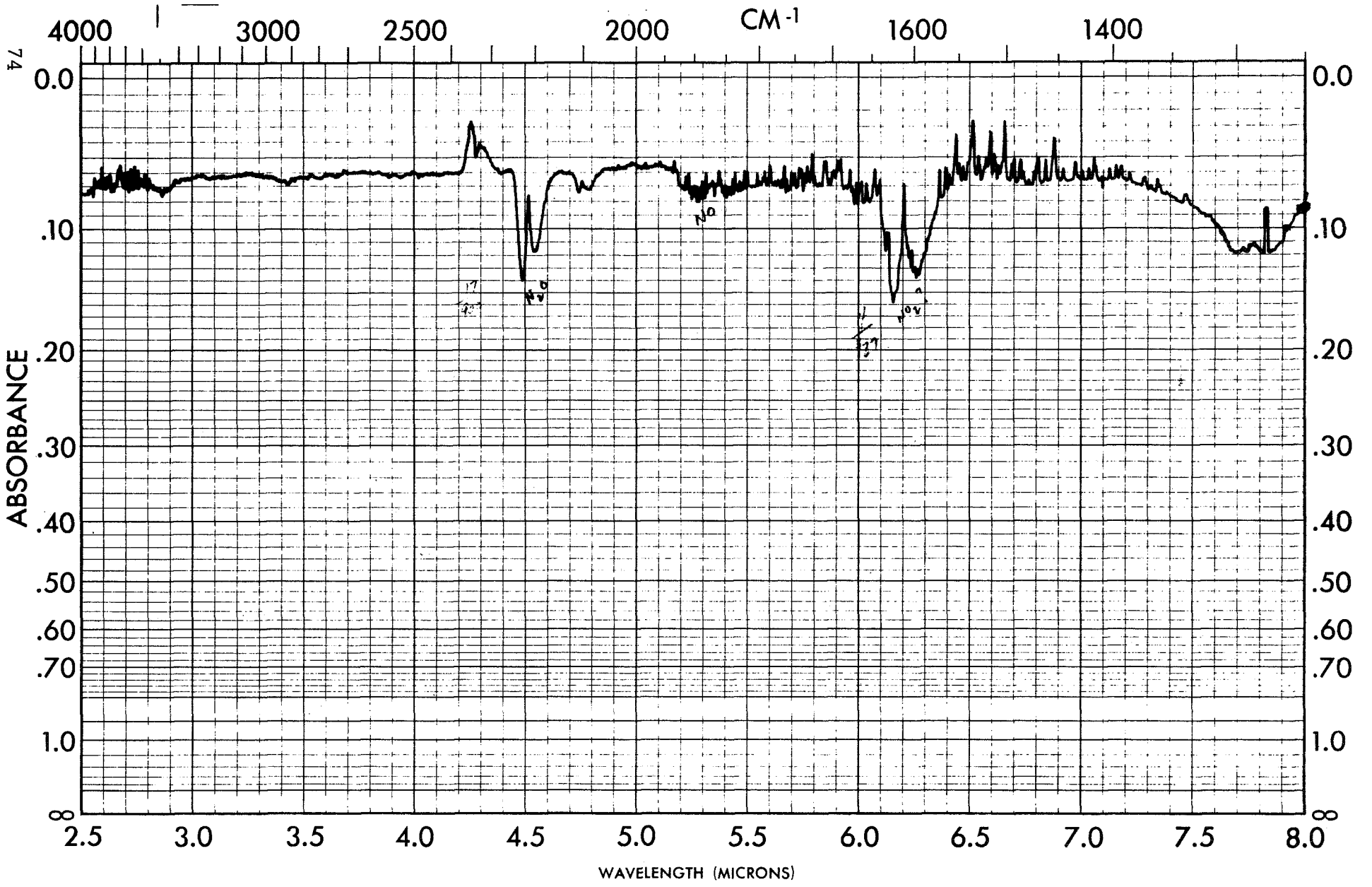

Figure 37. Infrared Spectrum - Gas #3.

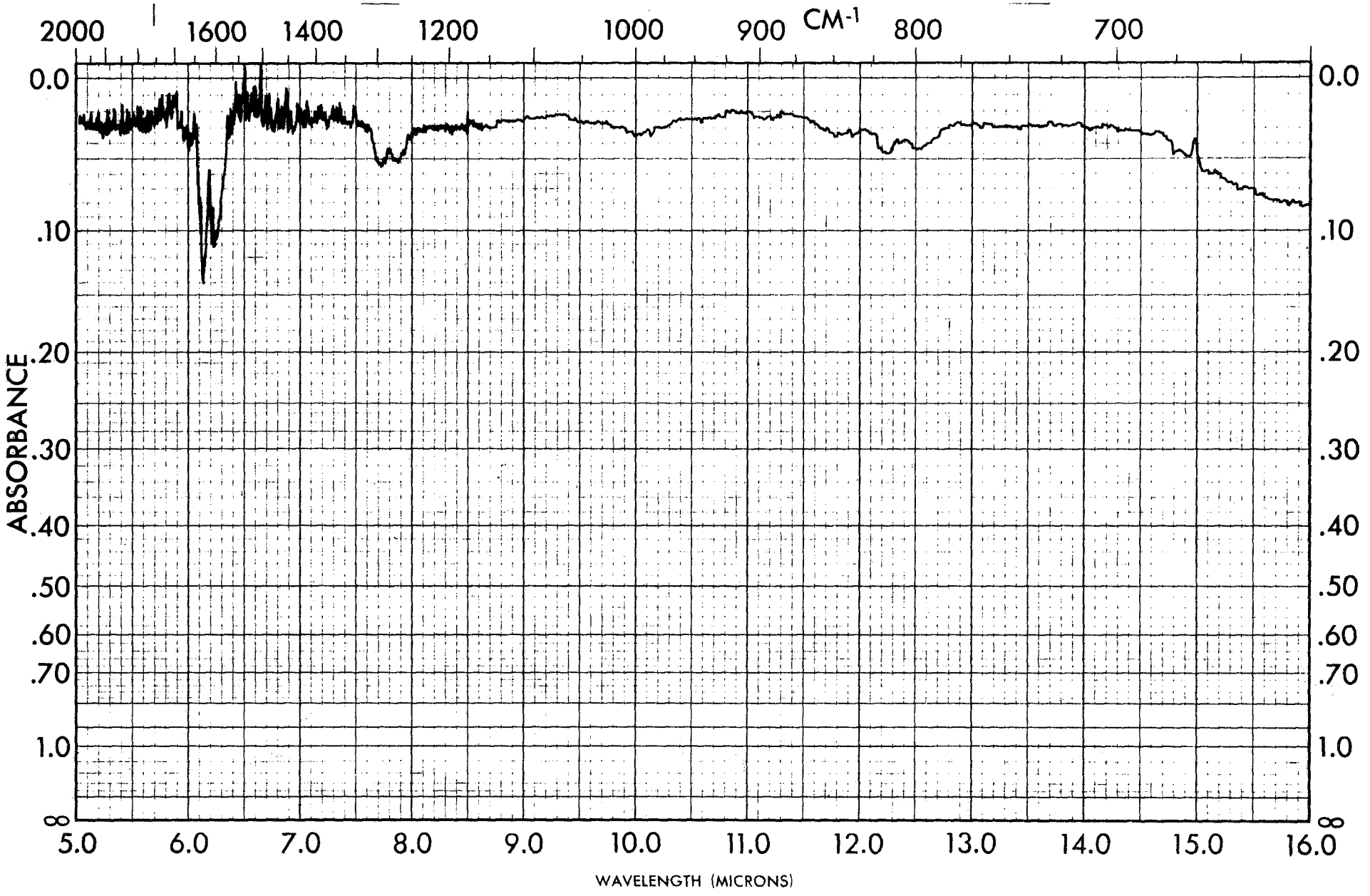

Figure 38. Infrared Spectrum - Gas #3.

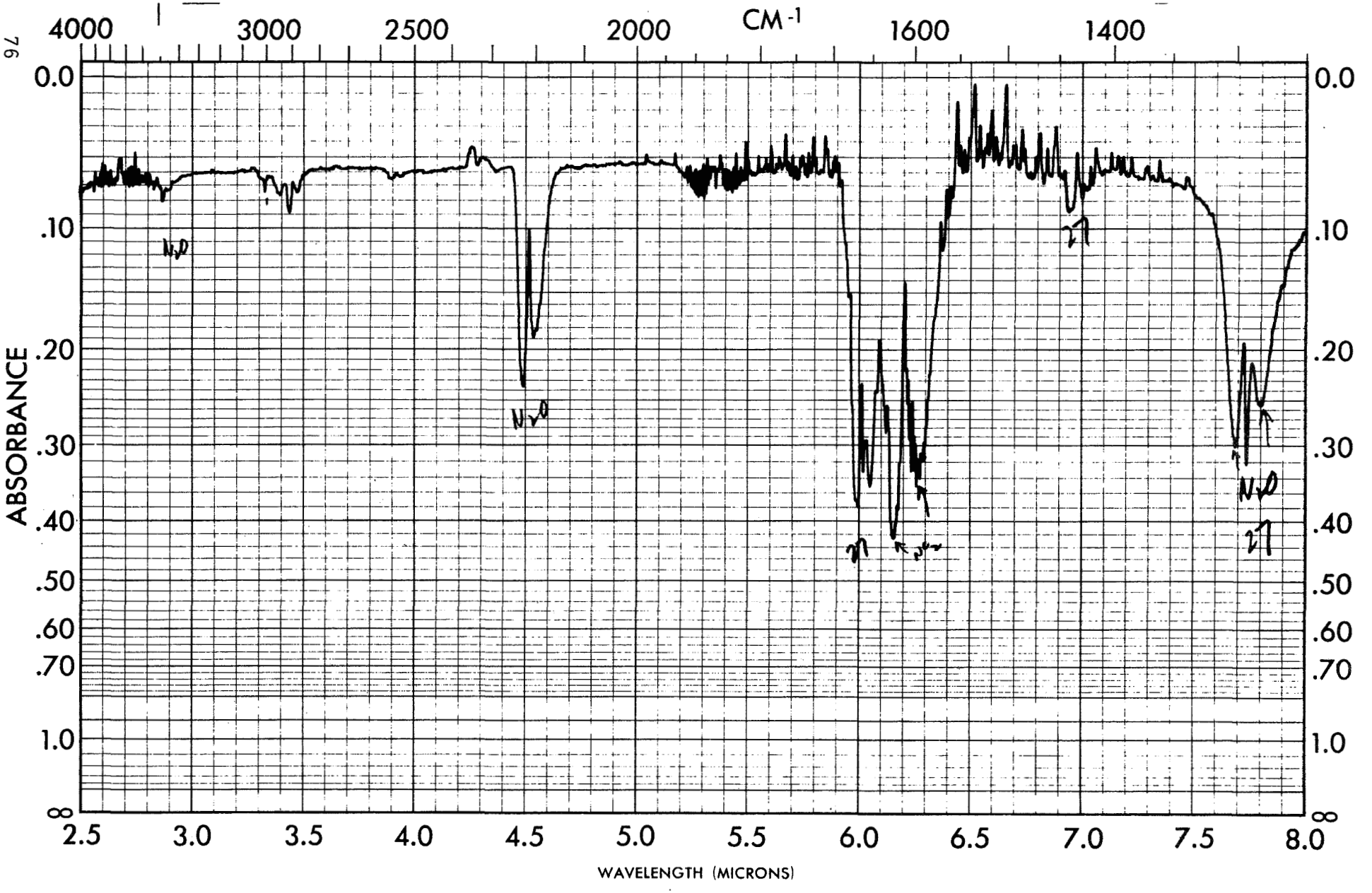

Figure 39. Infrared Spectrum - Gas #4.

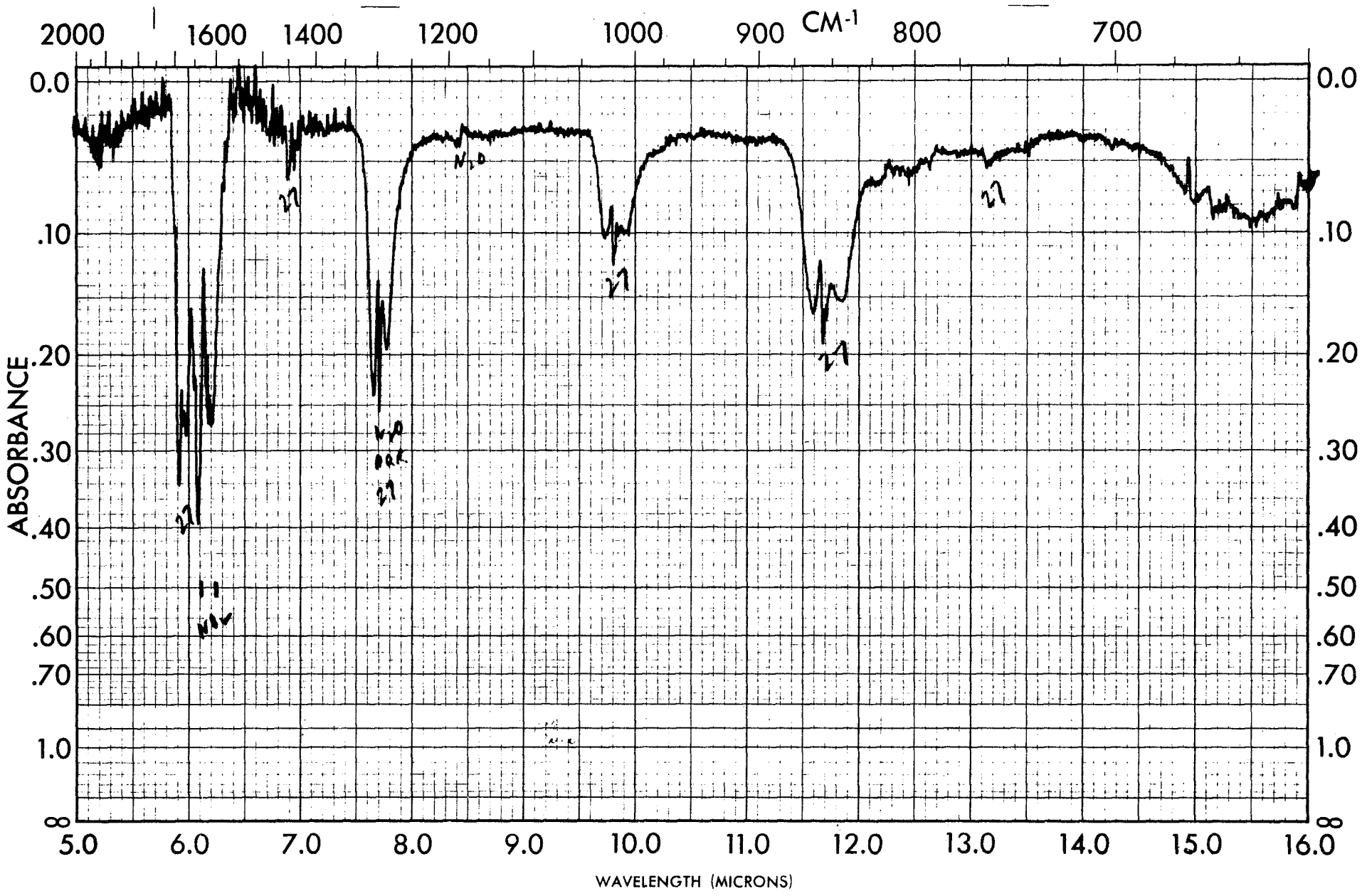

Figure 40. Infrared Spectrum - Gas #4.

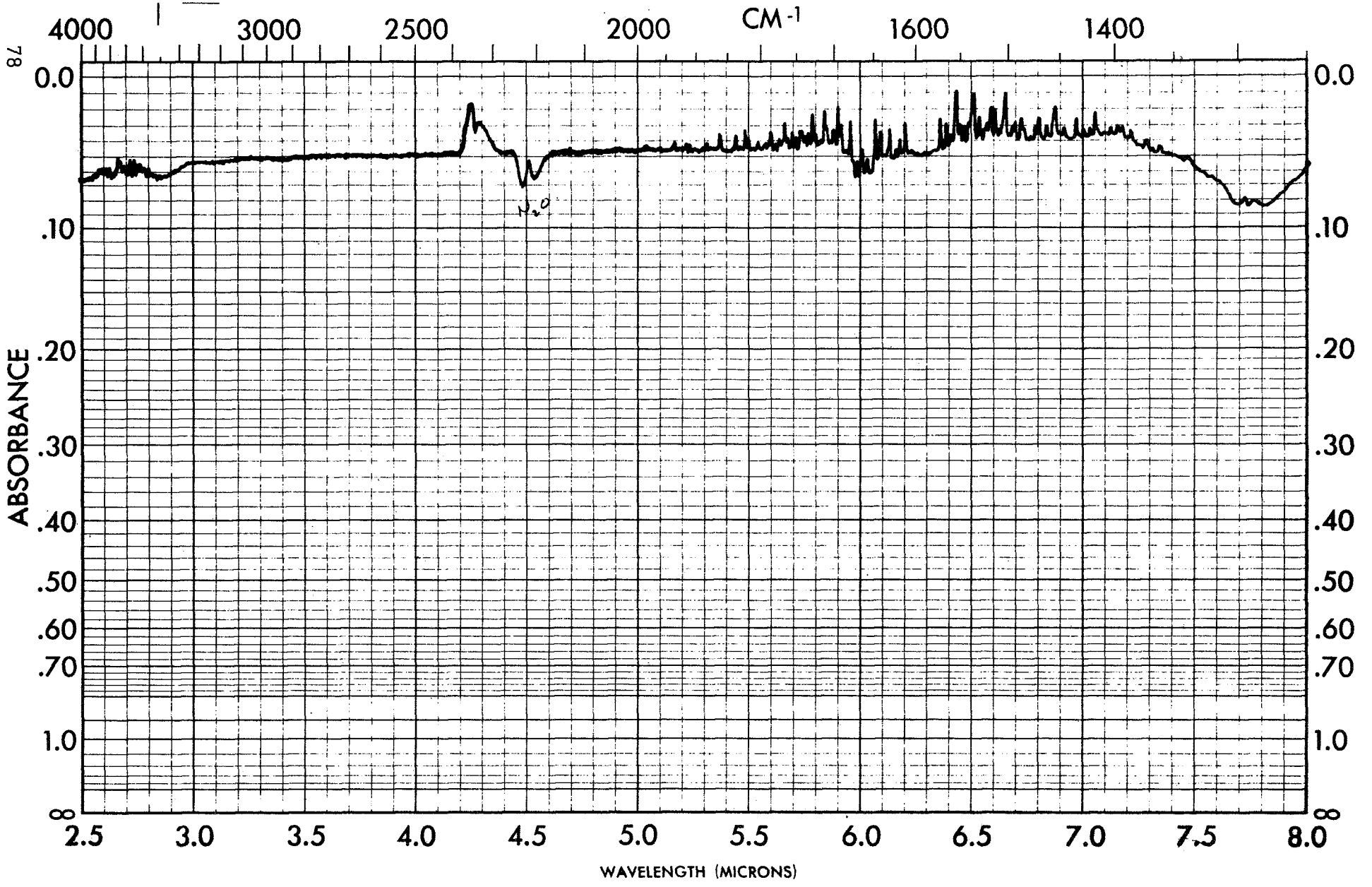

Figure 41. Infrared Spectrum - Gas #5.

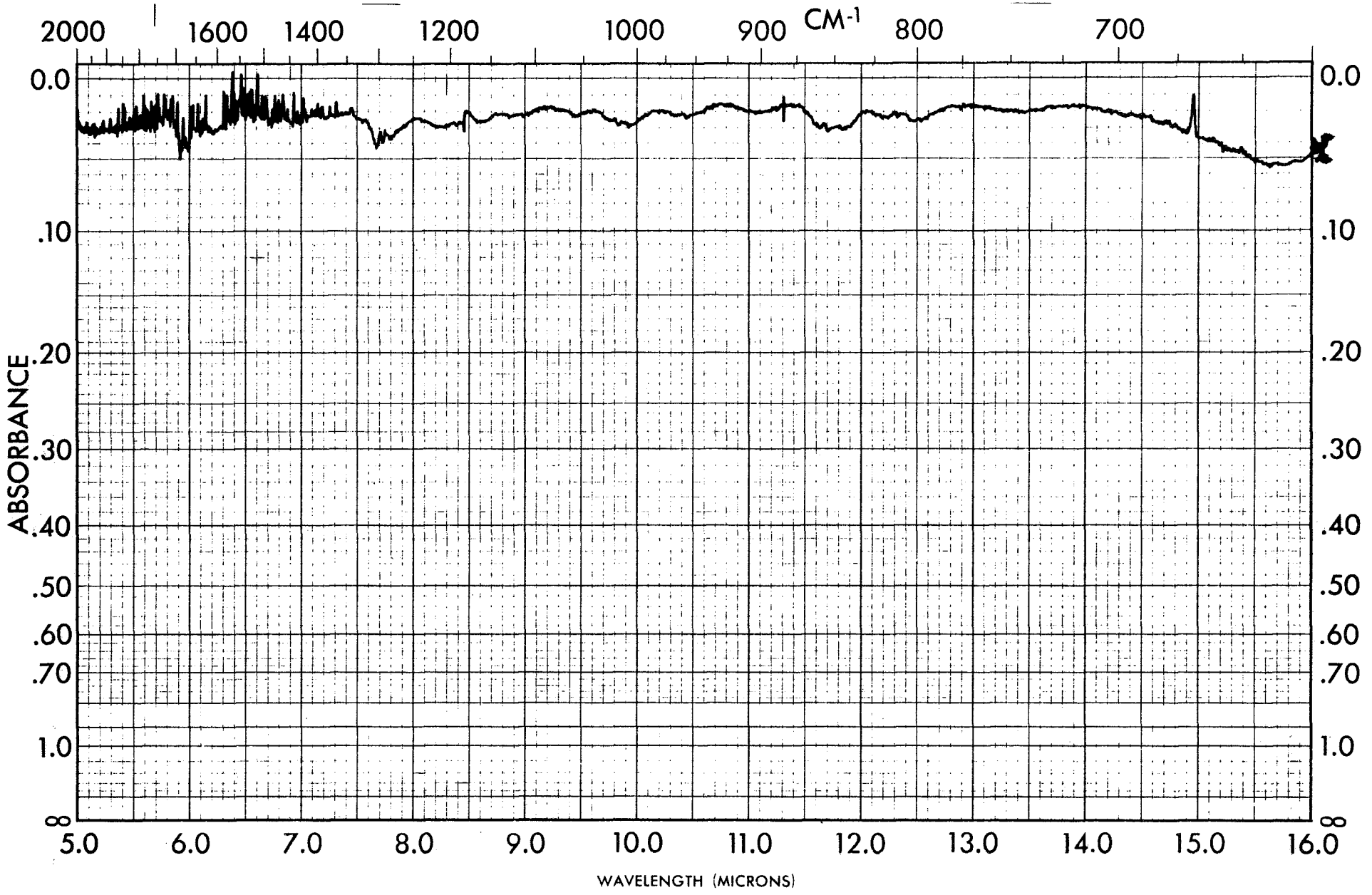

Figure 42. Infrared Spectrum - Gas #5.

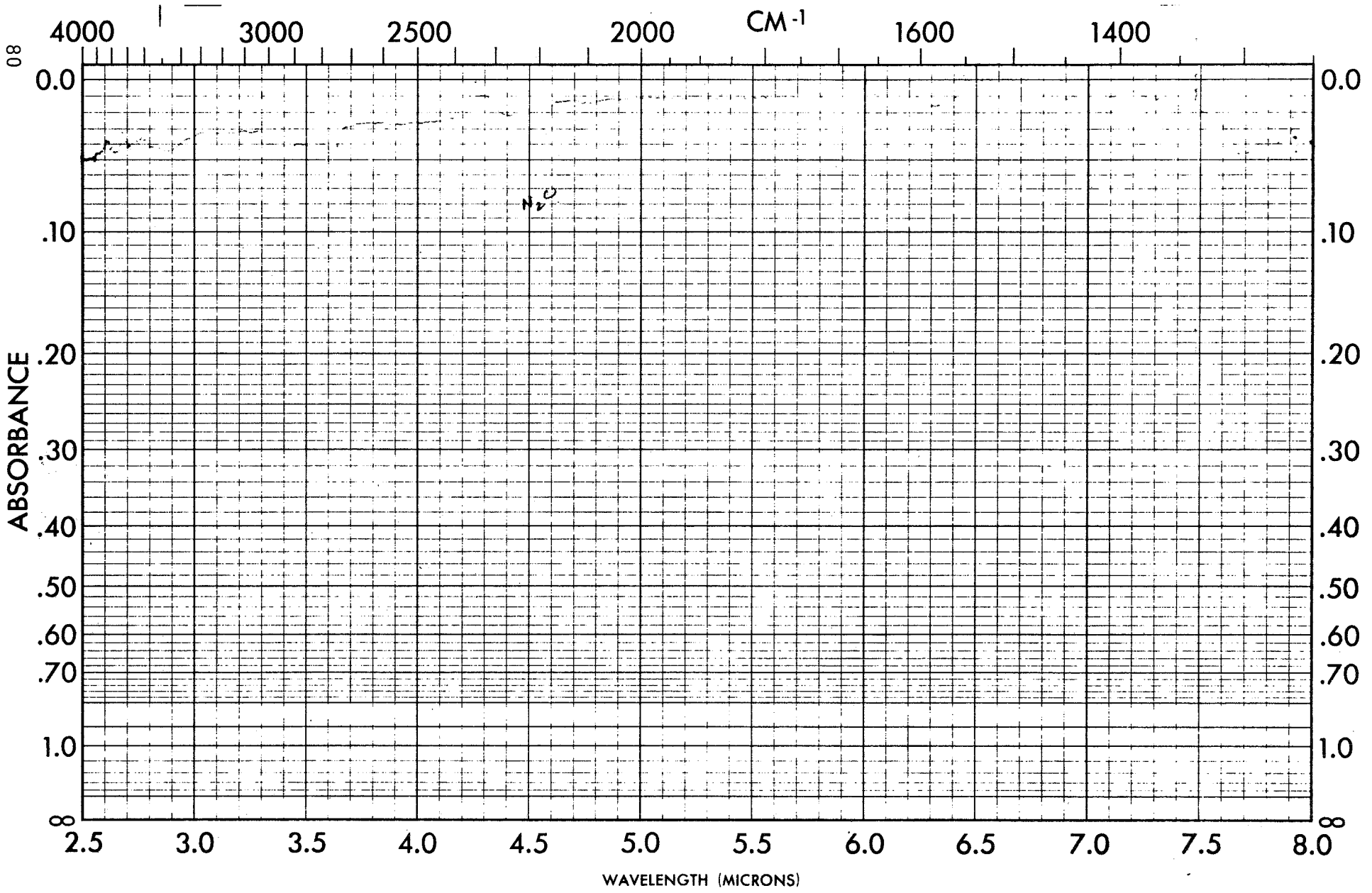

Figure 43. Infrared Spectrum - Gas #8.

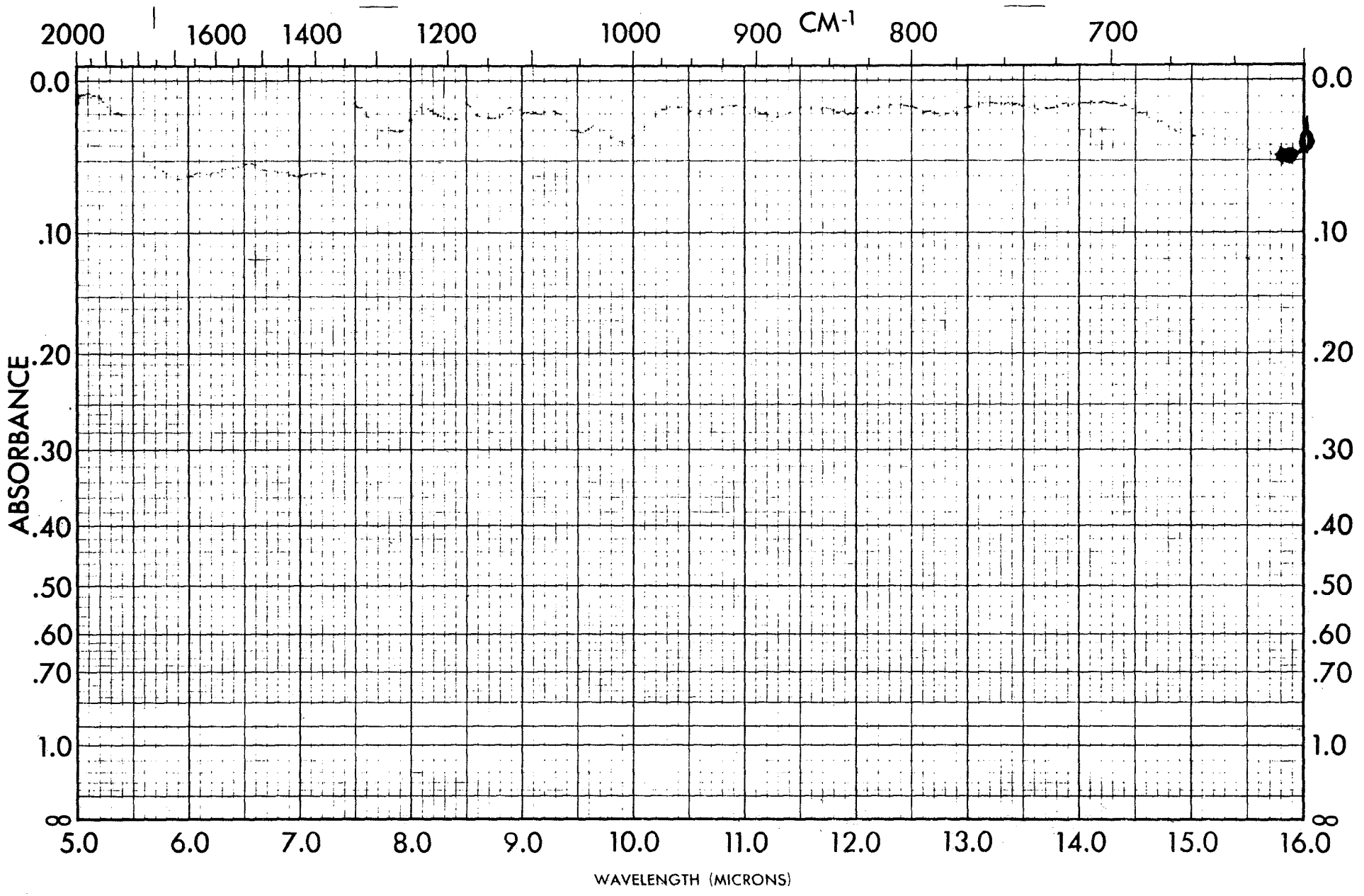

Figure 44. Infrared Spectrum - Gas #8.

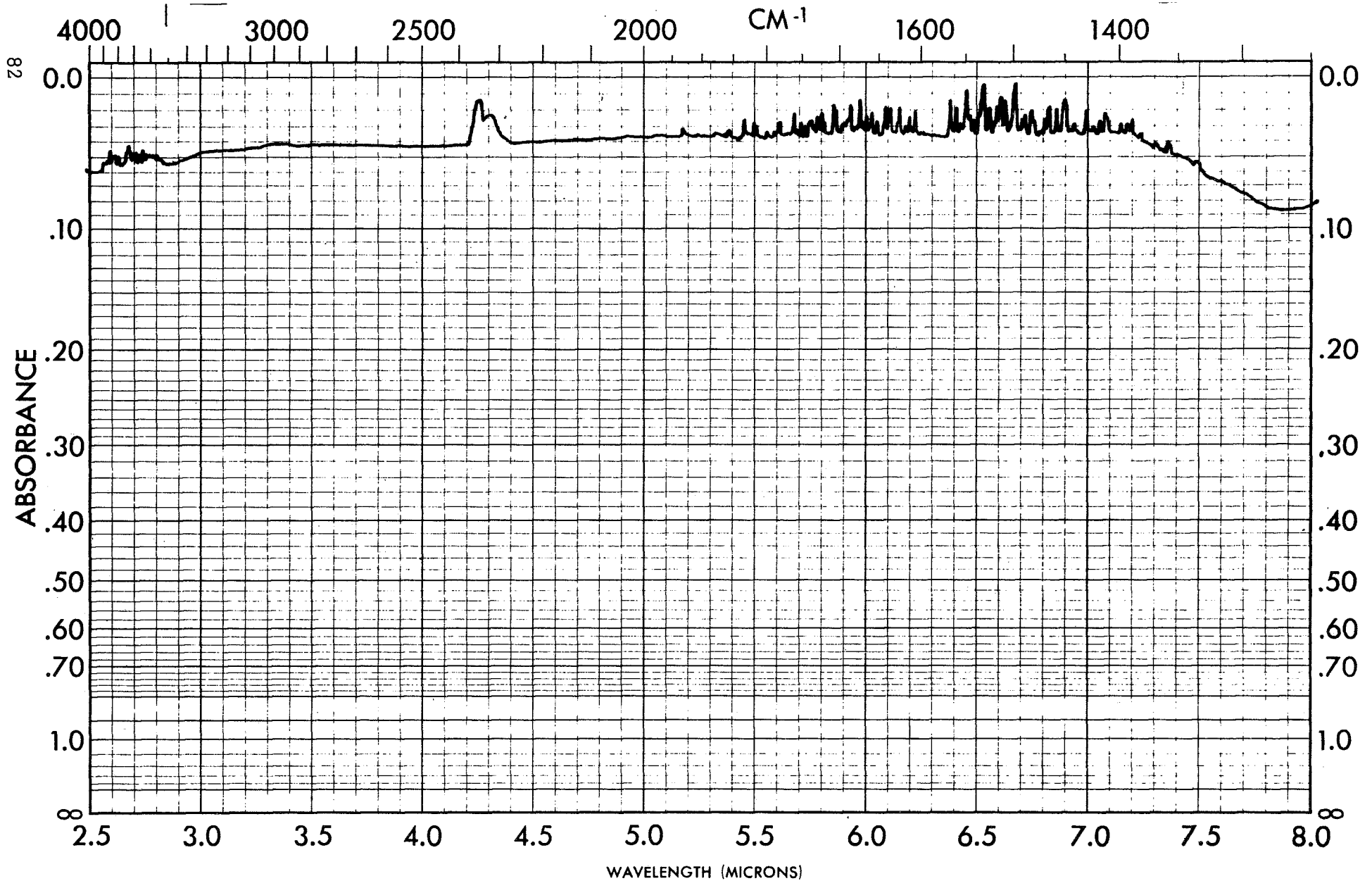

Figure 45. Infrared Spectrum - Gas #6.

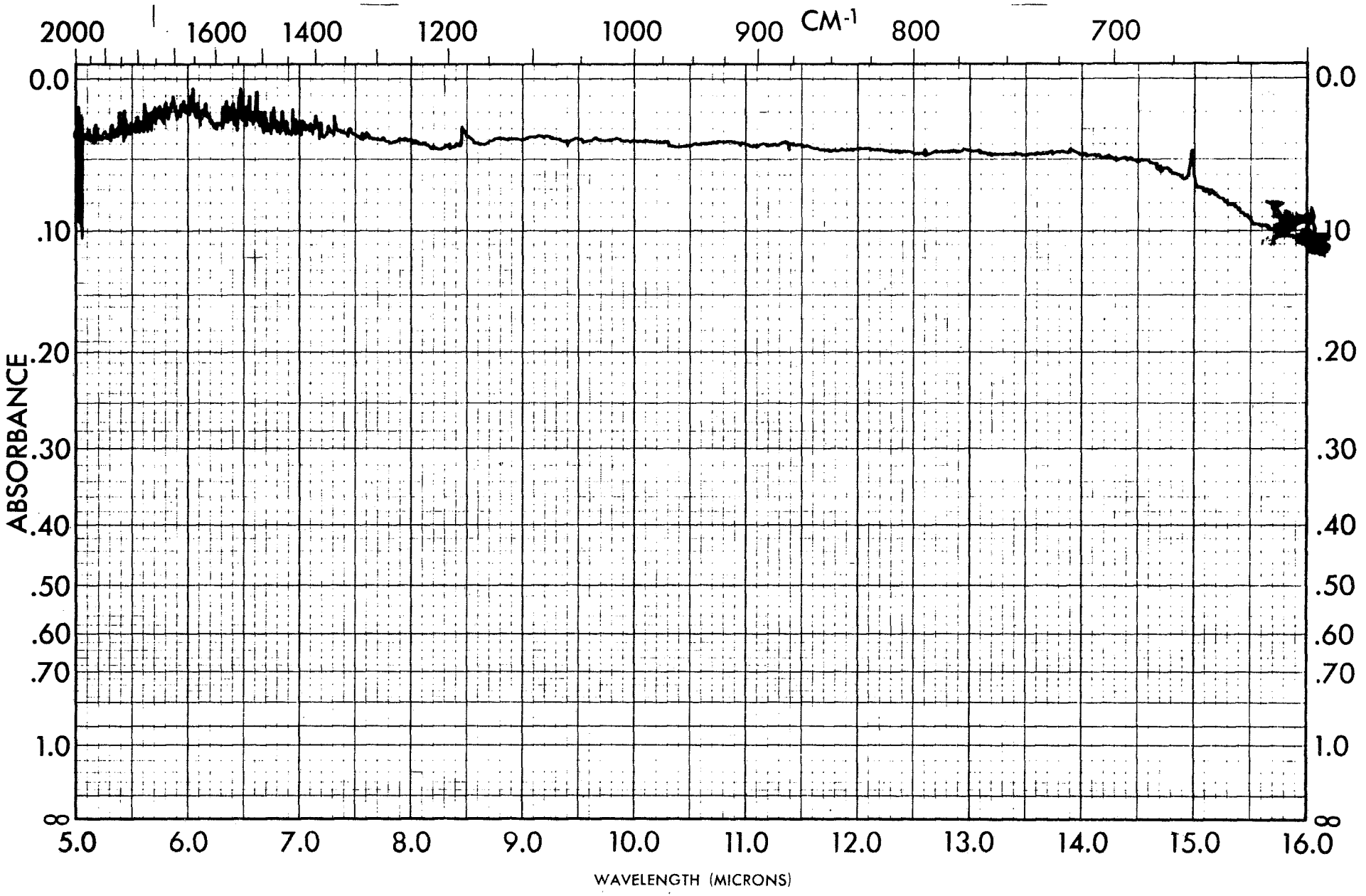

Figure 46. Infrared Spectrum - Gas #6.

APPENDIX B
DISTRIBUTION LIST
NAS 7-438 - SN-80-F

Chief, Liquid Propellant Experimental Engineering, RPX
NASA
Washington, D.C. 20546 4*

Director, Launch Vehicles and Propulsion, SV
NASA
Washington, D.C. 20546

Director, Advanced Manned Missions, MT
NASA
Washington, D.C. 20546

Director, Mission Analysis Division
NASA Ames Research Center
Moffett Field, California 24035

Jet Propulsion Laboratory
4800 Oak Drove Drive
Pasadena, California 91103
Attn: Dr. Raymond Kushida 2

NASA Pasadena Office
4800 Oak Grove Drive
Pasadena, California 91103
Attn: Contracting Officer
Attn: Office of Technical Information and Patent Matters

Scientific and Technical Information Facility
Attn: NASA Representative Code CRT
P.O.Box 33
College Park, Maryland 25

Marshall Space Flight Center
Huntsville, Alabama, 35812
Attn: Mr. Keith Chandler

Ames Research Center
Moffett Field, California 94035
Attn: Mr. Harold Hornby 2

Goddard Space Flight Center
Greenbelt, Maryland 20771
Attn: Merland L. Moseson 2
Attn: D. Grant, Code 620

Jet Propulsion Laboratory
California Institute of Technology
4800 Oak Grove Drive
Pasadena, California 91103
Attn: Henry Burlage, Jr. 2
Propulsion Division

Langley Research Center
Langley Station
Hampton, Virginia 23365
Attn: Dr. Floyd L. Thompson 2
Director

Lewis Research Center
21000 Brookpark Road
Cleveland, Ohio 44135
Attn: Dr. Abe Silverstein 2
Director

Lewis Research Center
21000 Brookpark Road
Cleveland, Ohio 44135
Attn: R. J. Rollbuhler 2
Mail Stop 21-5
Attn: M. C. Burrows

Marshall Space Flight Center
Huntsville, Alabama 35812
Attn: Hans G. Paul, Code R-P+VED
Attn: Werner Voss, R-P & VE-PM 2

Manned Spacecraft Center
Houston, Texas 77001
Attn: Dr. Robert R. Gilruth 3
Director
Attn: G. Thibodaux
Attn: B. J. Rosenbaum, E P 4

John F. Kennedy Space Center
NASA
Cocoa Beach, Florida 32931
Attn: Dr. Kurt H. Debus 2

*One copy unless otherwise designated

NASA Test Facility
Propulsion Engineering Office
White Sands, New Mexico
Attn: I. D. Smith
Staff Chemist

Aeronautical Systems Division
Air Force Systems Command
Wright-Patterson Air Force Base
Dayton, Ohio 45433
Attn: D. L. Schmidt
Code ASRCNC-2

Air Force Missile Development
Center
Holloman Air Force Base
New Mexico 88330
Attn: Maj. R. E. Bracken
Code MDGRT

Air Force Missile Test Center
Patrick Air Force Base, Florida
Attn: L. J. Ullian

Air Force Systems Division
Air Force Unit Post Office
Los Angeles 45, California 90045
Attn: Col. Clark, Tech. Data Center

AFFTC (FTBPP-2)
Edwards AFB, California 93523
Attn: Myrtle C. Jones 2

Arnold Engineering Development Center
Arnold Air Force Station
Tullahoma, Tenn. 37388
Attn: Dr. H. K. Doetsch

Bureau of Naval Weapons
Department of the Navy
Washington, D. C. 20546
Attn: J. Kay, RTMS-41

Defense Documentation Center Hqs.
Cameron Station, Bldg. 5
5010 Duke Street
Alexandria, Virginia 22314
Attn: TISIA

Headquarters, U.S. Air Force
Washington 25, D.C. 20546
Attn: Col. C. K. Stambaugh, AFRST

Picatinny Arsenal
Dover, New Jersey 07801
Attn: I. Forsten, Chief
Liquid Propulsion Lab
SMUPA-DL

Air Force Rocket Propulsion Lab.
Research and Technology Div.
Air Force Systems Command
Edwards, Calif. 93523 3
Attn: Mr. H. Main, RPPR
Attn: Maj. W.S. Moe "
Attn: Capt. C. J. Abbe "

U.S.Atomic Energy Commision
Technical Information Services
Box 62
Oak Ridge, Tenn. 37830
Attn: A. P. Huber, Oak Ridge Gaseous
Diffusion Plant
(ORGDP) P.O.Box P

U. S. Army Missile Command
Redstone Arsenal
Alabama 35809
Attn: Dr. Walter Wharton

U.S. Naval Ordnance Test Station
China Lake, Calif. 93557
Attn: Code 4562, Chief, Missile
Propulsion Division

Chemical Propulsion Information
Agency
8621 Georgia Avenue
Silver Spring, Maryland 20910
Attn: P. Martin

Explosives Research Center
Bureau of Mines
4800 Forbes Avenue
Pittsburgh, Pa.
Attn: Robert W. Van Dolah

Air Force Office of Scientific
Research
1400 Wilson Blvd.
Arlington, Virginia 22209
Attn: Dr. B. T. Wolfson

Aerojet-General Corporation
P.O.Box 296
Azusa, California 91703
Attn: L. F. Kohrs

Aerojet-General Corporation
P.O.Box 1947
Technical Library, Bldg. 2015
Dept. 2410
Sacramento, California 95809
Attn: R. Stiff

Aeronutronic Division
Philco Corporation
Ford Road
Newport Beach, California 92663
Attn: Mr. N. Stern

Aerospace Corporation
2400 East El Segundo Blvd.
P.O.Box 95085
Los Angeles, California 90045
Attn: Mr. M. J. Russi

Air Research Mfg. Co.
9851 Sepulveda Blvd.
Los Angeles, Calif. 90045
Attn: Mr. C. S. Coe

Arthur D. Little, Inc.
20 Acorn Park
Cambridge, Mass. 02140
Attn: E. Karl Bastress

Astropower Laboratory
Douglas Aircraft Company
2121 Paularino
Newport Beach, California 92663
Attn: Dr. George Moc
Director, Research

Astrosystems Invernational, Inc.
1275 Bloomfield Avenue
Fairfield, New Jersey 07007
Attn: A. Mendenhall

Atlantic Research Corporation
Edsall Road and Shirley Highway
Alexandria, Virginia 22314
Attn: R. Friedman

Beech Aircraft Corporation
Boulder Division
Box 631
Boulder, Colorado 80302
Attn: J. H. Rodgers

Bell Aerosystems Company
P.O.Box 1
Buffalo, New York 14240
Attn: J. Flanagan

Bendix Systems Division
Bendix Corporation
3300 Plymouth Road
Ann Arbor, Michigan 48105
Attn: John M. Brueger

Boeing Company
P.O.Box 3707
Seattle, Washington 98124
Attn: J. D. Alexander

Missile Division
Chrysler Corporation
P.O.Box 2628
Detroit, Michigan 48231
Attn: John Gates

Wright Aeronautical Division
Curtiss-Wright Corporation
Wood-Ridge, New Jersey 07075
Attn: G. Kelley

Missile and Space Systems Division
Douglas Aircraft Company, Inc.
3000 Ocean Park Blvd.
Santa Monica, Calif. 90406
Attn: R. W. Hallet, Chief Engineer
Advanced Space Technology

Aircraft Missiles Division
Fairchild Hiller Corporation
Hagerstown, Maryland 21740
Attn: J. S. Kerr

General Dynamics Convair Division
5001 Kearny Villa Road
P.O.Box 1628
San Diego, Calif. 92112
Attn: E. R. Peterson, V.P.,
Research and Engineering

Missile and Space Systems Center
General Electric Company
Valley Forge Space Technology Center
P.O.Box 8555
Philadelphia, Pa.
Attn: F. Mezger

Advanced Engine & Technology Dept.
General Electric Company
Cincinnati, Ohio 45215
Attn: D. Suichu

Grumman Aircraft Engineering Corp.
Bethpage, Long Island
New York 11714
Attn: Joseph Gavin

Honeywell, Inc.
Aerospace Division
2600 Ridgway Road
Minneapolis, Minn.
Attn: Mr. Gordon Harms

Hughes Aircraft Co.
Aerospace Group
Centinela and Teale Streets
Culver City, Calif.
Attn: E. H. Meier, V. P.
Research and Dev. Div.

Walter Kidde and Company, Inc.
Aerospace Operations
567 Main Street
Belleville, New Jersey
Attn: Mr. R.J.Hanville
Director of Research Engr.

Ling-Temco-Vought Corporation
Astronautics
P.O.Box 5907
Dallas, Texas 75222
Attn: Garland Whisenhunt

Lockheed Missiles and Space Co.
Attn: Technical Information Center
P.O.Box 504
Sunnyvale, California 94088
Attn: Y. C. Lee

Lockheed Propulsion Company
P.O.Box 111
Redlands, California 92374
Attn: H. L. Thackwell

The Marquardt Corporation
16555 Saticoy Street
Van Nuys, Calif. 91409
Attn: Warren P. Boardman, Jr.

Baltimore Division
Martin Marietta Corporation
Baltimore, Maryland 21203
Attn: John Calathes (3214)

Denver Division
Martin Marietta Corporation
P.O.Box 179
Denver, Colorado 80201
Attn: J. D. Goodlette (A-241)
A. J. Kullas

Orlando Division
Martin Marietta Corp.
Box 5837
Orlando, Florida
Attn: Mr. J. Ferm

McDonnell Aircraft Corporation
P.O.Box 516
Municipal Airport
St. Louis, Missouri 63166
Attn: R. A. Herzmark

Rocket Research Corporation
520 South Portland Street
Seattle, Washington 98108
Attn: Foy McCullough, Jr.

Space and Information Systems Div.
North American Rockwell
12214 Lakewood Blvd.
Downey, California 90241

Rocketdyne (Library)
North American Rockwell
6633 Canoga Avenue
Canoga Park, California 91304
Attn: E. B. Monteath

Northrop Space Laboratories
3401 West Broadway
Hawthorne, California 90250
Attn: Dr. William Howard

Astro-Electronics Division
Radio Corporation of America
Princeton, New Jersey 08540
Attn: Y. Brill

Reaction Motors Division
Thiodol Chemical Corporation
Denville, New Jersey 07832
Attn: Arthur Sherman
Mr. Robert Gere

Republic Aviation Corporation
Farmingdale Long Island, New York
Attn: Dr. William O'Donnell

Space General Corporation
9200 East Flair Avenue
El Monte, California 91734
Attn: C. E. Roth

Stanford Research Institute
333 Ravenswood Avenue
Menlo Park, California 94025
Attn: Lionel Dickinson

TRW Systems
One Space Park
Redondo Beach, Calif. 90278
Attn: Mr. D. Lee

Tapco Division
TRW, Incorporated
23555 Euclid Avenue
Cleveland, Ohio 44117
Attn: P. T. Angell

Thiokol Chemical Corporation
Huntsville Division
Huntsville, Alabama 35807
Attn: John Goodloe

United Technology Center
587 Methilda Avenue
P.O. Box 358
Sunnyvale, California 94088
Attn: B. Adelman

Florida Research and Development
Pratt and Whitney Aircraft
United Aircraft Corporation
P.O.Box 2691
West Palm Beach, Florida 33402
Attn: R. J. Coar

Vickers Inc.
Box 302
Troy, Michigan

Sunstrand Aviation
2421 11th Street
Rockford, Illinois 61101
Attn: Mr. R. W. Reynolds

Hamilton Standard Division
Windsor Locks, Conn. 06096
United Aircraft Corp.
Attn: Mr. R. Hatch

Denver Research Institute
University Park
Denver, Colorado 80210
Attn: Mr. William McLain

Mathematical Applications Group, Inc.
180 South Broadway
White Plains, N. Y. 10605
Attn: Dr. S. Z. Burstein

Ohio State University
Dept. of Aeronautical Eng.
Columbus, Ohio 43210
Attn: Mr. R. Edse

Pennsylvania State University
Mechanical Engineering Dept.
207 Mech. Eng. Blvd.
University Park, Pa. 16802
Attn: Mr. G. M. Faeth

University of Southern California
Department of Mechanical Engineering
University Park
Los Angeles, California 90007
Attn: Dr. M. Gerstein

Princeton University
Forrestal Campus
Guggenheim Laboratory
Princeton, New Jersey 08540
Attn: Dr. D. Harrje

University of Wisconsin
Mechanical Engineering Dept.
1513 University Avenue
Madison, Wisconsin 53705
Attn: Dr. P. S. Myers

University of Michigan
Aerospace Engineering
Ann Arbor, Michigan 48104
Attn: Dr. J. A. Nichols

University of California
Dept. of Chemical Eng.
6161 Etcheuerry Hall
Berkeley, Calif. 94720
Attn: Dr. A. K. Oppenheim

University of California
Dept. of Chemical Eng.
6161 Etcheurry Hall
Berkeley, California 94720
Attn: Dr. R. F. Sawyer

Purdue University
School of Mech. Eng.
Lafayette, Indiana 47907
Attn: Dr. J. R. Osborn

Sacramento State College
Engineering Division
60000 J. Street
Sacramento, California 95819
Attn: Dr. E. H. Reardon

Massachusetts Institute of Technology
Department of Mechanical Engineering
Cambridge, Mass. 02139
Attn: Dr. T. Y. Toong

Illinois Institute of Technology
Rm. 200, M. H.
3300 S. Federal Street
Chicago, Illinois 60616
Attn: Dr. T. P. Torda

Polytechnic Institute of Brooklyn
Graduate Center
Route 110
Farmingdale, New York
Attn: Dr. V. D. Agosta

Georgia Institute of Technology
Atlanta, Georgia 30332
Attn: Dr. B. T. Zinn

New York University
Department of Chemical Engineering
New York City, New York
Attn: Dr. L. Dauerman

University of Santa Clara
Department of Mechanical Engineering
Santa Clara, Calif. 95053
Attn: Dr. M. Saad